Geophys. J. Int. (2002) **150,** 321–361

Young tracks of hotspots and current plate velocities

Alice E. Gripp[1,*] and Richard G. Gordon[2]

[1] *Department of Geological Sciences, University of Oregon, Eugene, OR* 97401, *USA*
[2] *Department of Earth Science* MS-126, *Rice University, Houston, TX* 77005, *USA. E-mail: rgg@rice.edu*

Accepted 2001 October 5. Received 2001 October 5; in original form 2000 December 20

SUMMARY

Plate motions relative to the hotspots over the past 4 to 7 Myr are investigated with a goal of determining the shortest time interval over which reliable volcanic propagation rates and segment trends can be estimated. The rate and trend uncertainties are objectively determined from the dispersion of volcano age and of volcano location and are used to test the mutual consistency of the trends and rates. Ten hotspot data sets are constructed from overlapping time intervals with various durations and starting times. Our preferred hotspot data set, HS3, consists of two volcanic propagation rates and eleven segment trends from four plates. It averages plate motion over the past ≈5.8 Myr, which is almost twice the length of time (3.2 Myr) over which the NUVEL-1A global set of relative plate angular velocities is estimated. HS3-NUVEL1A, our preferred set of angular velocities of 15 plates relative to the hotspots, was constructed from the HS3 data set while constraining the relative plate angular velocities to consistency with NUVEL-1A. No hotspots are in significant relative motion, but the 95 per cent confidence limit on motion is typically ±20 to ±40 km Myr^{-1} and ranges up to ±145 km Myr^{-1}. The uncertainties of the new angular velocities of plates relative to the hotspots are smaller than those of previously published HS2-NUVEL1 (Gripp & Gordon 1990), while being averaged over a shorter and much more uniform time interval. Nine of the fourteen HS2-NUVEL1 angular velocities lie outside the 95 per cent confidence region of the corresponding HS3-NUVEL1A angular velocity, while all fourteen of the HS3-NUVEL1A angular velocities lie inside the 95 per cent confidence region of the corresponding HS2-NUVEL1 angular velocity. The HS2-NUVEL1 Pacific Plate angular velocity lies inside the 95 per cent confidence region of the HS3-NUVEL1A Pacific Plate angular velocity, but the 0 to 3 Ma Pacific Plate angular velocity of Wessel & Kroenke (1997) lies far outside the confidence region. We show that the change in trend of the Hawaiian hotspot over the past 2 to 3 Myr has no counterpart on other chains and therefore provides no basis for inferring a change in Pacific Plate motion relative to global hotspots. The current angular velocity of the Pacific Plate can be shown to differ from the average over the past 47 Myr in rate but not in orientation, with the current rotation being about 50 per cent faster (1.06 ± 0.10 deg Myr^{-1}) than the average (0.70 deg Myr^{-1}) since the 47-Myr-old bend in the Hawaiian–Emperor chain.

Key words: Galapagos, Hawaii, hotspots, Pacific Plate, plate tectonics, volcanoes.

INTRODUCTION

A global set of current angular velocities of the plates relative to the hotspots is a benchmark for motion between hotspots, the interaction between spreading ridges and hotspots, recent changes in plate velocity relative to the hotspots, plate-driving forces and a terrestrial reference frame tied to the deeper Earth through surface observations. For prior global estimates of current plate angular velocities relative to the hotspots, uncertainties in the segment trends and rates of volcanic propagation, though carefully considered, had been subjectively estimated and the age span of incorporated volcanoes varied considerably (Minster *et al.* 1974; Chase 1978; Minster & Jordan 1978; Gripp & Gordon 1990). Here we present a method for objectively estimating the uncertainty of the segment trends and incorporate them into our estimates of plate angular velocity. We tabulate ages of young hotspot volcanoes based as much as possible on consistent horizons, estimate the time it takes the bulk of a hotspot volcano to grow and check the consistency between volcano ages and plate speed.

*Now at: Santa Barbara Orchid Estate, 1250 Orchid Drive, Santa Barbara, CA 93111, USA. E-mail: sboe@sborchid.com

Our investigation is aimed at answering the following questions:

(1) What is the best estimate of the current angular velocities of the plates relative to the hotspots?

(2) What is the best estimate of the uncertainties in the current angular velocities of plates relative to the hotspots? How do these uncertainties compare with prior estimates?

(3) How can one objectively estimate the uncertainties of the trends of hotspot tracks? Are these uncertainties consistent with those estimated before? In particular, are the uncertainties previously assumed for trends on slow-moving plates realistic?

(4) Over how short a time interval can one use hotspot tracks and still obtain usefully accurate plate motions? What's the best time interval to use?

(5) Are previously published estimates of current plate velocities relative to the hotspots consistent with the data now available?

(6) Does the current angular velocity of the Pacific Plate relative to the hotspots differ significantly from that averaged over the past ≈47 Myr, i.e. the time interval represented by the entire Hawaiian ridge (Sharp & Clague 1999)?

(7) Are the patterns of plate rms velocities consistent with those found before?

(8) Do ages obtained from the tops of hotspot volcanoes accurately reflect the age at which most of the volcano formed?

The question of possible and appropriate time span is important for several reasons. NUVEL-1A, the global set of current relative plate angular velocities used herein, averages plate motion over a time span no longer than ≈3.2 Myr, the time interval over which nearly all of its spreading rates were determined (DeMets *et al.* 1990, 1994). There is convincing evidence that the motion of the Pacific Plate, which carries most of the useful hotspot tracks, changed direction by 8° and increased in rate by about 20 per cent relative to the Antarctic Plate at ≈6 to ≈8 Ma. At the same time it also changed direction by 20° to 25° relative to the North American Plate (Cande *et al.* 1995; Atwater & Stock 1998). In contrast, prior global hotspot data sets incorporated observations from some tracks spanning 10 to 30 Myr or longer. Thus, a new global hotspot data set spanning less than 6 to 8 Myr is needed.

Toward that end, we have determined a new set of angular velocities of the plates relative to hotspots that are consistent with the NUVEL-1A angular velocities. The new set of angular velocities, which we refer to as HS3-NUVEL1A, are based on a data set, HS3, of hotspot segment trends and volcanic propagation rates that average plate motion relative to the hotspots over the past ≈5.8 Myr. We chose this interval in part because it is the longest interval that is most likely to exclude the most recent major change in Pacific–Antarctic relative plate motion, which may have occurred as recently as 5.9 Ma (Cande *et al.* 1995).

Herein we use units of millions of years (Myr) and kilometers (km) because they are appropriate to hotspot volcanoes. A predicted trend or rate is one estimated from a set of angular velocities constructed from data that exclude that trend or rate. In contrast, a calculated trend or rate is one estimated from a set of angular velocities constructed from data that include that trend or rate. We consider 'hotspots' to be surface features. When we use the phrase 'motion between hotspots', it refers only to motion between loci of volcanism. No implications are intended about relative motion of their sublithospheric sources.

In evaluating statistical differences, herein we use the 95 per cent confidence level, which is equivalent to a 5 per cent level of significance, as the confidence level is one (or 100 per cent) minus the significance level. In some cases, a result may lie just outside or inside the 95 per cent confidence limit and in other cases well outside or inside the limit. To convey additional information about how widely or narrowly a null hypothesis passed or failed, we also quote, usually parenthetically, the value of p, which is the probability of obtaining data as different or more different from the null hypothesis as the data we use. Barring bad luck, the smaller the value of p, the less likely that the null hypothesis is true.

METHODS AND RESULTS

We analyse hotspot data, uncertainties and model assumptions at four levels. First, we assign an age and a location to the volcanoes at the young end of each promising hotspot track—those with young islands or well-studied seamounts (tracks used in HS3-NUVEL1A are listed in Table 1 and Appendix A; see Gripp (1994) for a list of other hotspots considered but discarded). Second, for segments with enough young volcanoes, we estimate segment trends and volcanic propagation rates by least-squares. Third, we estimate a global set of angular velocities of the plates relative to the hotspots, while fixing relative plate angular velocities to those of NUVEL-1A (DeMets *et al.* 1990, 1994). Fourth, we compare results for hotspot data averaged over ten overlapping time intervals with various starting times and durations.

Level one: volcano age and location

Our first-tier analysis consists of assigning volcano age and volcano location (Table 1), which are needed to estimate segment trend or volcanic propagation rate. We require that the volcano formed off-ridge (for Galapagos we use only the near-ridge, not the on-ridge, part of the track to measure trend), that a submarine volcano has been sampled (not just known from bathymetry) and that the volcano is young. To qualify as young, all rocks sampled from an edifice must be young and if the effective elastic thickness has been estimated for the underlying lithosphere, the thickness must be consistent with the edifice having a young age.

Volcano location

Unlike spreading centres, where young eruptions and intrusions occur within 1 to 5 km of the spreading centre axis (Macdonald 1986), hotspot volcanism is less localized. For example, Loihi, Kilauea and Mauna Loa, which are the three Hawaiian volcanoes in their main phase of construction, are separated by 60 km along trend (Table 1, Appendix A). Within the past 30 000 yr, volcanism has occurred over a 375 km length of the Hawaiian Ridge. Thus the 0 Ma isochron for Hawaii is an undulating, subhorizontal surface (Moore 1987), which cannot be drawn as a single line or point on a map. Even a single volcano is hardly a point because one volcano may be 100 km wide and have several rift zones and many vents.

To keep the analysis simple, however, we assign a single geographic point to each volcano. For volcanoes with summit calderas, which include ≈30 per cent of all volcanoes, we take the location of each volcano to be the centre of its summit caldera or the intersection of its rift zones. For ≈10 per cent of the volcanoes, usually those that are older and eroded, there is indirect evidence for the location of a summit caldera. For the remaining volcanoes (≈60 per cent) we use the geographic centre or summit.

Volcano age

Although a typical hotspot volcano erupts subaerially for at least several million years (Appendix A), the length of time it takes for a

Table 1. Data from individual volcanoes.

Volcano	Location, N°, E°	Age $\pm 1\sigma$, Myr old	Description and age basis
Easter-Sala y Gomez (Nazca)			*Age ≡ Oldest, Moderately Reliable Age from the 'Main Group'*
Ahu Volcanic Field	−26.58, −110.94[a]	Active	2700-km^2 tholeiitic submarine lava field made up of ridges and seamounts; degree of sample alteration ranges from fresh glass to mm-thin Fe-Mn oxide crusts (Stoffers *et al.* 1994; Haase *et al.* 1996)
Umu Volcanic Field	−26.96, −111.05[b]	Active	1700-km^2 tholeiitic submarine lava field made up of ridges; degree of sample alteration ranges from fresh to thin crusts (Stoffers *et al.* 1994; Fretzdorff *et al.* 1996)
Tupa Volcanic Field	−27.90, −110.50[c]	Active?	Small, tholeiitic volcanic field (or seamount); samples are covered by Fe-Mn crusts similar to those on Ahu and Umu (Stoffers *et al.* 1994; Haase & Devey 1996)
Pukao Seamount	−26.95, −110.26[d]	$<0.63 \pm 0.18$	Ar-Ar plateau age (O'Connor *et al.* 1995) from the Volcanic Field Group, which seems to predate the Main Group (Haase *et al.* 1997)
Moai Seamount	−27.10, −109.68[d]	0.23 ± 0.08	Ar-Ar plateau age (O'Connor *et al.* 1995) from the Main Group (Haase *et al.* 1997)
Tereveka volcano	−27.09, −109.38[e]	0.25 ± 0.05	Fissure volcano (Baker *et al.* 1974); hawaiite from the oldest series of the main shield dated by K-Ar (Clark 1975)
Rano Kau volcano	−27.19, −109.44[e]	0.98 ± 0.19	Strato-volcano (Baker *et al.* 1974); K-Ar date on feldspar separates from a basalt at the base of a sea cliff (Clark 1975)
Poike volcano	−27.11, −109.26[e]	0.69 ± 0.13	Whole-rock, K-Ar date on an olivine basalt from the deepest outcrop of the volcano (Kaneoka & Katsui 1985), which belongs to the Main Group (Haase *et al.* 1997); Clark (1975) reports an age of 2.61 ± 0.28 Ma for a similarly located sample
Sala y Gomez Island	−26.46, −105.46[f]	2.00 ± 0.07	Dredged hawaiite dated by K-Ar (Clark 1975) of unknown group; the tiny island comprises two eroded mugearite flows (Fisher & Norris 1960) one of which has a K-Ar date of 1.38 ± 0.04 Ma (Clark 1975)
Galapagos (Nazca)			*Age ≡ Oldest Moderately Reliable Age Estimate*
Isla Darwin (Culpepper)	1.65, −92.00[g]	0.41 ± 0.16	Rock dated by K-Ar (White *et al.* 1993); island itself is a tiny eroded summit of this volcano (McBirney & Williams 1969)
Isla Wolf (Wenman)	1.37, −91.82[g]	1.60 ± 0.07	Rock dated by K-Ar (White *et al.* 1993); island itself is a tiny eroded summit of this volcano (McBirney & Williams 1969)
Roca Redonda	0.27, −91.62[h]	Active	Active fumaroles occur on this small eroded remnant of an alkalic-lava-filled crater (Standish *et al.* 1998)
Ecuador Volcano (Cape Berkeley)	−0.02, −91.56[i]	0.092 ± 0.035	Normally polarized sample dated by K-Ar (Cox & Dalrymple 1966) from this eroded volcano (McBirney & Williams 1969); although extinct, its composition, unstable isotopic ratios, and trace elements are most similar to those of the active volcanoes of Roca Redonda and Cerro Azul (Standish *et al.* 1998)
Fernandina Island (Narborough)	−0.36, −91.54[j]	Active	Historic eruptions on the tholeiitic shield (Richards 1962; McBirney & Williams 1969)
Cerro Azul volcano	−0.92, −91.42[j]	Active	Historic eruptions on this shield volcano (Naumann & Geist 2000)
Volcan Wolf	0.02, −91.36[j]	Active	Historic eruptions on this shield volcano (Richards 1962)
Volcan Darwin	−0.19, −91.29[j]	Active	Very fresh lava flows on this shield volcano (Richards 1962)
Sierra Negra vol.	−0.81, −91.12[j]	Active	Historic eruptions on this shield volcano (Reynolds *et al.* 1995)
Alcedo volcano	−0.42, −91.12[j]	Active	Historic eruptions on this shield volcano (Geist *et al.* 1994)
Pinta Island (Abingdon)	0.59, −90.75[g]	≈0.78	Normally magnetized transitional shield volcano modified by normally magnetized late fissure eruptions (Cullen & McBirney 1987); shield rock gives an age of 0.89 ± 0.24 Ma (White *et al.* 1993)
San Salvador Isl. (James, Santiago)	−0.22, −90.77[k]	0.78	Alkalic shield partially covered by younger flows; all lava flows are normally magnetized and the oldest K-Ar date is 0.79 ± 0.12 Ma (Swanson *et al.* 1974)
Rabida Island (Jervis)	−0.41, −90.70[k]	0.99–1.07	Tholeiitic shield volcano; normally magnetized (Jaramillo?) shield is overlain by reversely magnetized rocks; average date from the scattered, stratigraphically inconsistent K-Ar dates is 1.0 Ma (Swanson *et al.* 1974)
Pinzon Island (Duncan)	−0.61, −90.66[k]	1.40 ± 0.08	Rock dated by K-Ar (White *et al.* 1993) from this tholeiitic volcano (Swanson *et al.* 1974)
Marchena Island (Bindloe)	0.35, −90.46[g]	0.56 ± 0.04	Basalt fragment in tephra from the transitional shield volcano (Vicenzi *et al.* 1990) dated by K-Ar (White *et al.* 1993)
Santa Maria Island (Charles, Floreana)	−1.29, −90.45[k]	1.52 ± 0.08	Alkalic basanatoid from the alkalic shield (Bow 1979) dated by K-Ar (White *et al.* 1993)
Santa Cruz Island (Indefatigable)	−0.64, −90.36[k]	2.1 ± 0.5	K-Ar date of rock from the tholeiitic platform series (the oldest rocks on the island), after which follow the eruption of a shield made of M0RB-like tholeiitic basalts and alkalic basalts (Bow 1979; date from J. Dymond, pers. comm.)
Santa Fe Island (Barrington)	−0.81, −90.08[k]	2.82 ± 0.05	Weighted average K-Ar date on a basalt (Bailey 1976) from the transitional volcano (Geist *et al.* 1985; White *et al.* 1993)
Genovesa Island (Tower)	0.33, −89.96[g]	0.0	Rock with no detectable radiogenic Ar (White *et al.* 1993); island is tholeiitic (White *et al.* 1993) and consists of a shield cut by younger fissure eruptions (McBirney & Williams 1969)

Table 1. (*Continued.*)

Volcano	Location, N°, E°	Age $\pm 1\sigma$, Myr old	Description and age basis
Espanola Island (Hood)	−1.38, −89.70[k]	3.40 ± 0.36	Eroded alkalic shield volcano (Hall 1983); basalt dated by K-Ar (Bailey 1976)
San Christobal Island (Chatham)	−0.91, −89.52[k]	2.35 ± 0.03	K-Ar date on an alkaline rock (White *et al.* 1993) from the normally polarized alkalic flood basalts that underlie a shield and fissure eruptions composed of alkalic basalts, OIB tholeiitic basalts, MORB-like tholeiitic basalts, and all of their differentiates (Geist *et al.* 1986) of reversed and normal polarity (Cox 1971); however this K-Ar date is inconsistent with magnetic time scale of Hilgen (1991a)
Unnamed seamount	−1.19, −89.11[l]	5.8 ± 0.8	Ar-Ar plateau age from an aphyric highly vesicular moderately altered basalt (Sinton *et al.* 1996)
Hawaii (Pacific)			*Age ≡ Age of Shield-Postshield Transition*
Loihi Seamount	18.96, −155.26[m]	Active	Transitional between preshield and shield stages (Moore *et al.* 1982; Garcia *et al.* 1995)
Kilauea Volcano	19.42, −155.27[n]	Active	Shield stage (Stearns 1940)
Mauna Loa Volcano	19.48, −155.58[o]	Active	Shield stage (Stearns 1946)
Mauna Kea Volcano	19.82, −155.47[p]	0.237 ± 0.031	Basalt dated by K-Ar from the lowest exposures of the Hamakua Volcanics (older substage of the postshield stage) (Wolfe *et al.* 1997)
Hualalai Volcano	19.69, −155.87[p]	0.133 ± 0.005	Reef dated by $^{234}U/^{238}U$ (Ludwig *et al.* 1991) that is crossed by few tholeiitic flows from Hualalai (Moore & Clague 1988)
Kohala Volcano	20.08, −155.72[p]	0.261 ± 0.012	Mugearite with shield chemistry from uppermost Pololu Volcanics (shield stage) dated by K-Ar (McDougall & Swanson 1972) reinterpreted by (Spengler & Garcia 1988)
Mahukona Volcano	20.13, −156.24[q]	0.463 ± 0.004	Reef dated by $^{234}U/^{238}U$ (Ludwig *et al.* 1991) that probably formed at the end of shield building as fewer flows were able to cross the shoreline (Clague & Moore 1991a,b; Moore & Clague 1992)
Haleakala Volcano (East Maui)	20.72, −156.22[r]	0.97 ± 0.04	Alkalic basalt dated by K-Ar from the uppermost part of the Honomanu Basalt (shield stage) (Chen *et al.* 1991)
Kahoolawe Volcano	20.54, −156.56[r]	0.99 ± 0.06	Tholeiitic basalt flow dated by K-Ar from the Kanapou Volcanics (shield and postshield), this date may be too young or the flow may a postshield flow (Fodor *et al.* 1992)
West Maui Volcano	20.88, −156.58[r]	1.33	Alkalic basalts near the top of the Wailuku Basalt (shield stage and caldera- filling lavas of the postshield stage) (Langenheim & Clague 1987); average K-Ar ages from 3 flows (McDougall 1964)
Lanai Volcano	20.79, −156.91[r]	1.24 ± 0.06	Youngest K-Ar date from the Lanai Basalt (shield stage) (Bonhommet *et al.* 1977)
East Molokai Volcano	21.14, −156.85[r]	1.53	Alkalic basalts from the upper part of the lower member of the East Molokai Volcanics; average of 2 K-Ar dates (McDougall 1964)
West Molokai Volcano	21.15, −157.12[r]	1.89	Tholeiitic flow near the top of the West Molokai Volcanics (shield and postshield) dated by K-Ar (McDougall 1964); this age was reconfirmed by Clague (1987) who measured K-Ar dates of 1.73 to 1.80 Ma on overlying hawaiite flows
Penguin Bank	21.03, −157.58[s]	Undated	Probable submarine Hawaiian volcano (Macdonald & Abbott 1970; Clague 1996)
Koolau Volcano	21.40, −157.76[r]	1.83 ± 0.25	Youngest K-Ar dates averaged from an outcrop of the Koolau Basalt (shield and postshield) (Doell & Dalrymple 1973)
Waianae Volcano	21.45, −158.15[r]	3.08 ± 0.02	Reversely polarized alkali basalt flow dated by K-Ar date from the Kamaileunu Member (later shield stage), although this date is inconsistent with its having erupted during the Kaena reversed event (Guillou *et al.* 2000)
Kaena Ridge	21.67, −158.50[s]	Undated	Probable submarine Hawaiian volcano (Clague 1996)
Haupu Volcano	21.93, −159.38[t]	Young	Once thought to be a flank caldera of Olokele (e.g. Langenheim & Clague 1987); it is now thought to be a separate volcano (Clague 1996)
Olokele Volcano	22.13, −159.51[r]	3.947 ± 0.046	Hawaiite dated by K-Ar from the top of the Waimea Canyon Basalt (shield and rare post shield stages) (Clague & Dalrymple 1988)
Niihau Volcano	21.94,−160.06[u]	4.89 ± 0.11	Tholeiitic flows and dikes from the Paniau Basalt (shield and postshield stages); date from an unpublished K-Ar isochron by G. B. Dalrymple (1983, referenced by Clague & Dalrymple 1987)
Kaula Island	21.66, −160.55[v]	Young	Small palagonitic tuff cone; accidental rock fragment of phonolite (likely from posterosional stage) yields a K-Ar data of 4.01 ± 0.9 Ma (Garcia *et al.* 1986)
Juan Fernandez (Nazca)			*Age ≡ Oldest K-Ar Date*
Friday seamount	−33.78, −81.71[w]	Young	Young alkalic basalts dredged from this seamount (Ken Farley, pers. comm, 1992)
Alejandro Selkirk Isl. (Mas Afuera)	−33.76, −80.77[x]	2.44 ± 0.14	Basalt (Stuessy *et al.* 1984) from the moderately eroded volcano (Baker *et al.* 1987)
Robinson Crusoe Isl. (Mas a Tierra)	−33.63, −78.86[x]	4.23 ± 0.16	Basalt (Stuessy *et al.* 1984) from the deeply dissected volcanic island (Baker *et al.* 1987)
Macdonald (Pacific)			*Age ≡ Oldest Moderately-Reliable Age Estimate*
Macdonald Seamount	−28.98, −140.25[y]	Active	Volcanic eruption and magma movement detected from T-waves (Norris & Johnson 1969); methane anomaly (Stoffers *et al.* 1989): a much older volcano was discovered on its flank after this data set was finalized (J. Reynolds and K. Jordahl, pers. comm., 1999)

Table 1. (*Continued.*)

Volcano	Location, N°, E°	Age $\pm 1\sigma$, Myr old	Description and age basis
Ra Seamount	−28.77, −141.08[y]	29.21 ± 0.61	Whole rock Ar-Ar plateau age on a rock (McNutt *et al.* 1997) dredged from this 1040-m deep guyot whose upper flank is covered with shallow-water indicators (Stoffers *et al.* 1989); features on summit are covered with thin Mn crusts (<2 mm thick) (Binard *et al.* 1992a)
Marotiri Rocks	−27.91, −143.43[z]	31.95 ± 0.82	Whole rock Ar-Ar plateau age on a rock dredged from this mixed age volcano, whose young volcanism gives a whole rock Ar-Ar plateau age of 3.78 ± 0.18 Ma (McNutt *et al.* 1997)
Rapa Island	−27.60, −144.34[aa]	Poorly dated	Dissected shield volcano (Chubb 1927); K-Ar dates range from 5.1 ± 0.2 to 5.3 ± 1.7 Ma (Krummenacher & Noetzlin 1966), but many of the dates from this paper have proved unreproducible
Marquesas (Pacific)			*Age = Oldest Moderately-Reliable K-Ar Date*
Unnamed seamount	−10.82, −138.43[bb]	0.76 ± 0.10	Ar-Ar plateau age on a potassic trachyandesite (Desonie *et al.* 1993)
Fatu Hiva Island	−10.47, −138.66[cc]	2.46 ± 0.12	Lava flow (K_2O = 0.77 wt. per cent) from the older of two concentric volcanoes, both of which contain only hypersthene and nepheline normative basalts (Brousse *et al.* 1990)
Motu Nao Island	−10.35, −138.44[dd]	1.27 ± 0.10	Ar-Ar plateau age on a potassic trachyandesite dredged from its SW flank (Desonie *et al.* 1993)
Motane Island	−9.99, −138.80[cc]	2.26 ± 0.11	Lava flow (K_2O = 1.17 wt. per cent) that belongs to a series that overlies an island wide unconformity (Brousse *et al.* 1990)
Tahuata Island	−9.96, −139.08[cc]	2.86 ± 0.14	Lava flow (K_2O = 0.85 wt. per cent) from the lower half of the volcano (Brousse *et al.* 1990)
Unnamed seamount	−9.90, −138.33[ee]	Undated	Unsampled seamount
Hiva Oa Island	−9.77, −139.04[ff]	2.74 ± 0.07	Basalt flow (K_2O = 1.28 wt. per cent) with normal polarity (Katao *et al.* 1988)
South H. F. Dumont D'urville Smt.	−9.81, −139.60[gg]	Undated	Unsampled seamount in the Marquesas ridge
Fatu Huka Island	−9.43, −138.92[cc]	2.65 ± 0.10	Alkalic basalt flow (K_2O = 1.27 wt. per cent) (Brousse *et al.* 1990; name based on silica and alkali content in Liotard & Barsczus 1983a)
North H. F. Dumont D'urville Smt.	−9.58, −139.78[gg]	3.13 ± 0.14	Alkali olivine basalt dated by Ar-Ar total fusion (Desonie *et al.* 1993)
Ua Pou Island	−9.39, −140.06[hh]	5.61 ± 0.06	Tholeiitic rock (K_2O = 0.78 wt. per cent) from the tholeiitic phase that spanned 5.61–4.46 Ma; alkalic rocks erupted from 2.88–1.78 Ma (Duncan *et al.* 1986)
Ua Huka Island	−8.93, −139.54[cc]	2.85 ± 0.02	Lava flow (K_2O = 1.44 wt. per cent) (Duncan & McDougall 1974)
Nuku Hiva Island	−8.90, −140.09[cc]	4.31 ± 0.02	Weighted average dates of a beach cobble (K_2O = 0.84 wt. per cent) (Duncan & McDougall 1974)
Hatu Iti Rocks (Motu Iti Rocks)	−8.68, −140.62[dd]	Young	Three rocks, the westernmost is 200 m high (Chubb, 1930)
Banc Clark	−8.07, −139.62[gg]	Undated	Unsampled bank in the Marquesas ridge
Banc J. Goguel	−7.91, −139.96[gg]	5.30 ± 0.30	Oceanite (K_2O = 0.48 wt. per cent) dredged from the 30-m-deep bank (Brousse *et al.* 1990)
Motu One Island (Coral Island)	−7.88, −140.39[dd]	Young?	3-m-high island (Aeronautical Chart Service 1951) of uncertain composition (Chubb 1930); because coral is rare in the Marquesas (Chubb 1930), if really is at least partly coral, it is likely that young basalt underlies it
Eiao Island	−8.01, −140.68[cc]	5.56 ± 0.05	Quartz tholeiite from 754-m level of a 800-m-deep drill hole, which contains quartz and olivine tholeiites (800–686 m); hawaiites, mugearites, and trachytes (686–415 m); and olivine tholeiites and alkalic basalts (415–0 m), which contains at 122 m an alkali basalt with an age of 5.22 ± 0.06 Ma (Caroff *et al.* 1995)
Hatutu Island	−7.91, −140.58[cc]	4.90 ± 0.20	Tholeiitic basalt (K_2O = 0.81 wt. per cent) flow (Brousse et al., 1990; name based on silica and alkali content in Liotard & Barsczus, 1983b)
Martin Vaz (South America)			*Age = Oldest Moderately-Reliable Age*
Ilha do Norte	−20.47, −28.85[ii]	Poorly dated	Largest island in Ilhas Martin Vaz; the only K-Ar dates consist of 67.0 ± 1.4 Ma on an ankaramite and <0.75 Ma on an hauynitite (Cordani 1970), the first of which is inconsistent with the island still being above sea level and the second of which may be more likely, but given the difficulties with the first, it remains unreliable as well
Unnamed seamount	−20.72, −29.20[jj]	Undated	2-km-deep, unsampled seamount on same ridge as the two main islands
Trindade Island	−20.51, −29.33[kk]	3.35 ± 0.29	Nephelinite dyke dated by K-Ar (Cordani 1970) from the Trindade Complex, the basal unit of the island (Almeida 1961)
Pitcairn (Pacific)			*Age = K-Ar Dates of the Approximate End of Shield Building*
Adams seamount	−25.38, −129.26[ll]	Young	Fresh lava, but summit is covered with coral and coral sands and it may have a trachyte dome on its summit (Stoffers *et al.* 1990; Binard *et al.* 1992b); the average isotopic ratios from this volcano lie nearer the isotopic ratios of the posterosional volcanism on Pitcairn than do those of Bounty (Woodhead & Devey 1993)

Table 1. (*Continued.*)

Volcano	Location, N°, E°	Age $\pm 1\sigma$, Myr old	Description and age basis
Bounty seamount	−25.18, −129.41[ll]	Active	Fresh lava and methane anomalies (Stoffers *et al.* 1990; Binard *et al.* 1992b)
Pitcairn Island	−25.07, −130.10[mm]	0.86 ± 0.01	Weighted average of 2 dates on an hawaiite near the top of the Tedside Volcanics (shield phase) (Duncan *et al.* 1974)
Henderson Island	−24.36, −128.33[nn]	Undated	Raised coral reef (Carter 1967)
Oeno atoll	−23.93, −130.75[nn]	Undated	Atoll (Carter 1967)
Temoe atoll	−23.35, −134.48[oo]	Undated	Atoll
Iles Gambier	−23.13, −134.93[oo]	5.66 ± 0.03	Lava flow from the top of Mt. Duff, which is a 430-m high remanent of this deeply dissected volcano (Guillou *et al.* 1994)
Samoa (Pacific)			*Age ≡ Oldest, Relatively Reliable K-Ar Date*
Rose Atoll	−14.55, −168.15[pp]	Undated	Atoll east of the Samoa
Rockne Volcano	−14.23, −169.05[qq]	Active	Fresh alkalic basalts dredged from this submarine volcano (Hart *et al.* 1999); it was, however, dredged after this data set was finalized, at which time it was known only as an unsampled seamount discovered by Johnson (1984)
Lata shield	−14.25, −169.46[rr]	Young	Main shield volcano on Tau Island (Stice & McCoy 1968)
A'ofa and Sila shields	−14.17, −169.64[rr]	Young	One or two shield volcanoes overlying pyroclastic cones on islands of Ofu and Olosega (Stice & McCoy 1968)
Pago Volcano	−14.29, −170.67[rr]	1.54 ± 0.02	Dyke from shield part of the Pago Volcanics on Tutuila (McDougall 1985)
PPT Seamount	−14.86, −170.64[ss]	Young	Seamount with young alkalic rocks (Poreda & Farley 1992)
Fagaloa Volcano	−13.92, −171.53[tt]	2.65 ± 0.07	Transitional basalt from shield part of the Fagaloa Volcanics on Upolu (Natland & Turner 1985)
Savai'i Island	−13.61, −172.48[uu]	Young	All sampled rocks are normally polarized (Keating 1985)
Wallis Islands	−13.27, −176.17[uu]	0.82 ± 0.03	Rock dredged offshore of this island (Duncan 1985); dates from one its islets (Nukufetau) span 0.08 to 0.50 Ma (excluding a date of 172 Ma, which is considered suspect because the rock is as fresh as and has a composition similar to the other samples) (Price *et al.* 1991); this young volcanism may overlie an older volcano (Duncan 1985), but this could still not account for the 172 Ma date because it is older than the underlying seafloor (Price *et al.* 1991)
Society (Pacific)			*Rate Age ≡ End of Shield Building*
Volcano 16	−18.28, −148.17[y]	Active?	Fresh lava flows on this 2750-m-deep seamount (Binard *et al.* 1991)
Seismic Volcano 1	−17.40, −148.83[vv]	Mixed	One of several low volcanoes in a region called Seismic Volcanoes; this one has both thickly Mn-coated low-K rocks and young alkalic rocks (Cheminee *et al.* 1989; Hekinian *et al.* 1991); 1985 earthquake swarms chronicled by Talandier & Okal (1987) coincided with this group of volcanoes (Cheminee *et al.* 1989)
Mehetia Island	−17.88, −148.07[y]	Active	Tiny island <2 km-wide with a very young, 400 m-high cone (Binard *et al.* 1993); earthquake swarm on submarine flank (Talandier & Okal 1984)
Seamount Turoi	−17.52, −148.95[y]	Mixed	900-m-high made of thickly Mn-coated low-K rocks and minor amounts of young alkalic volcanism (Hekinian *et al.* 1991; Binard *et al.* 1992a)
Volcano 17	−17.47, −147.97[y]	Active	Fresh alkalic rocks recovered from this seamount (Binard *et al.* 1991 N. Binard pers. comm., 1992)
Moua Pihaa Seamount	−18.33, −148.53[y]	Active	Earthquake swarms on this seamount (Talandier & Kuster 1976); basalts similar to ones on Mehetia (Brousse 1984)
Rocard Seamount	−17.65, −148.58[y]	Active	Earthquake swarms on this seamount (Talandier & Kuster 1976); popping trachytes and alkalic basalts (Cheminee *et al.* 1989; Hekinian *et al.* 1991)
Cyana Seamount	−17.93, −148.75[y]	Mixed	1800-m-high volcano with Fe- and Mn-coated pillows (Hekinian *et al.* 1991) and flanks smoothed by sediments, talus, and Mn crusts (Binard *et al.* 1992a); fresh trachytes recovered near its summit (Devey *et al.* 1990)
Teahitia Seamount	−17.57, −148.82[y]	Active	Earthquake swarms on this seamount (Talandier & Kuster 1976); hydrothermal activity (Hoffert *et al.* 1987); popping basanites (Hekinian *et al.* 1991)
Tahiti-Iti Volcano (Taiarapu)	−17.80, −149.19[ww]	0.39 ± 0.01	Flow with youngest K-Ar date (Duncan & McDougall 1976)
Tahiti-Nui Volcano	−17.63, −149.46[ww]	0.46	End of second shield-building episode dated by K-Ar (H. Guillou pers. comm., 1996)
Moorea Island	−17.52, −149.83[ww]	1.46 ± 0.02	End of subaerial volcanic activity dated by K-Ar (Guillou pers. comm, 1996)
Tetiaroa Atoll	−17.01, −149.56[xx]	Undated	Coral atoll of unknown origin
Maiao Island	−17.67, −150.64[xx]	1.67	Youngest K-Ar date from the greatest concentration of dates (Diraison *et al.* 1991 referencing R. A. Duncan pers. comm. 1988)
Huahine Island	−16.76, −151.00[xx]	2.6	Age of the end of the Gauss normal chron (Hilgen 1991a) because no reversely polarized rocks have been sampled and all but three samples (two of which are from late-stage trachytic intrusions) from (Duncan & McDougall 1976) and Roperch & Duncan (1990) yield ages greater than 2.6 Ma within their 95 per cent confidence limits; we treat this as one volcano unlike Brousse *et al.* (1983) and Diraison *et al.* (1991)
Raiatea Island	−16.83, −151.45[yy]	2.52 ± 0.02	Alkali basalt flow dated by K/Ar from the uppermost part of this shield volcano (Blais *et al.* 1997)

Table 1. (*Continued.*)

Volcano	Location, N°, E°	Age $\pm 1\sigma$, Myr old	Description and age basis
Tahaa Island	−16.62, −151.51[yy]	2.8	Main shield building ended 2.8 Ma, although minor activity continued until 2.5 Ma (White *et al.* 1989)
Bora Bora Island	−16.51, −151.75[zz]	3.21 ± 0.02	Dyke from shield that yields youngest K-Ar date (Duncan & McDougall 1976)
Taupiti Atoll	−16.25, −151.82[xx]	3.66 ± 0.013	Weighted average K-Ar date of a lava block thrown up on island during a hurricane (Diraison *et al.* 1991)
Maupiti Island	−16.44, −152.26[ab]	4.05 ± 0.03	Biotite-bearing olivine dolerite dyke dated by K-Ar that cuts shield rocks (Duncan & McDougall 1976)
Yellowstone (North America)			*Age of Major Ash-Flow Sheets*
Low-velocity zone	44.71, −110.33[ac]	Active?	Upper crustal body with a low *P*-wave speed (4 km s^{-1}) and a negative Bouguer anomaly; these properties are consistent with a 10–50% partial melt of rhyolite composition, although these characteristics are also consistent with steam and water-filled cracks (Schilly *et al.* 1982; Lehman *et al.* 1982)
Third-cycle caldera	44.50, −110.64[ad]	0.602 ± 0.002	Weighted average of single-crystal Ar-Ar dates on sanidine from member B of the Lava Creek Tuff (Gansecki *et al.* 1998)
Second-cycle caldera	44.31, −111.42[ad]	1.293 ± 0.006	Weighted average of single-crystal Ar-Ar dates on sanidine from the Mesa Falls Tuff (Gansecki *et al.* 1998)
First-cycle caldera	44.37, −110.92[ad]	2.003 ± 0.007	Weighted average of single-crystal Ar-Ar dates on sanidine from the Huckleberry Ridge Tuff (Gansecki *et al.* 1998); oldest bimodal lavas erupted about 2.2 Ma (Christiansen, 1982; referencing K-Ar dates from J. D. Obradovich, written communication, 1982)
Kilgore caldera	44.01, −111.94[ae]	4.3	Eruption of the Tuff of Kilgore (Morgan *et al.* 1984)
Blue Creek caldera	43.76, −112.67[ae]	6.0 ± 0.2	Whole rock K-Ar date on the Tuff of the Blue Creek (Morgan 1988 referencing Marvin, written communication, 1986)
Blacktail caldera	43.74, −112.17[ae]	6.5	Eruption of the Tuff of Blacktail (Morgan *et al.* 1984)

Radiometric ages have been corrected to the decay constants of Steiger & Jager (1977). Magnetostratigraphy ages from Hilgen (1991a,b).
[a] Highest peak from that part of the Ahu Volcanic Field surveyed by Stoffers *et al.* (1994).
[b] Summit from map in Fretzdorff *et al.* (1996).
[c] Position of volcano (Stoffers *et al.* 1994).
[d] Centre of seamount summit from bathymetry in Hagen *et al.* (1990).
[e] Centre of summit caldera; summit caldera geometry from Chubb (1933); island location and topography the map of Defense Mapping Agency Aerospace Center (1978).
[f] Position of island from the map of Defense Mapping Agency Aerospace Center (1978).
[g] Island summit from the map of Defense Mapping Agency Aerospace Center (1990a).
[h] Island centre from the map of Defense Mapping Agency Aerospace Center (1990a).
[i] Approximate centre of a remnant volcano from map and description in McBirney & Williams (1969).
[j] Approximate caldera centre from the map of Defense Mapping Agency Aerospace Center (1990b).
[k] Island summit from the map of Defense Mapping Agency Aerospace Center (1990b).
[l] Dredge location (Sinton *et al.* 1996).
[m] Summit of seamount from map in Malahoff (1987).
[n] Projected intersection of the rift zones at the summit caldera from a map in Holcomb (1987).
[o] Projected intersection of the rift zones at the summit caldera from a map in Lockwood *et al.* (1987).
[p] Volcano summit from the map of Defense Mapping Agency Aerospace Center (1969).
[q] Position of volcano from map in Moore & Clague (1992).
[r] Projected intersection of rift zones at the summit caldera from maps in Langenheim & Clague (1987).
[s] Approximate centre of the possible Hawaiian volcano (David Clague, pers. comm., 1989).
[t] Centre of caldera from map in Langenheim & Clague (1987).
[u] Extrapolated centre of now-eroded Niihau's summit caldera from sketch in Stearns & Macdonald (1947).
[v] Summit of island from the map of Defense Mapping Agency Aerospace Center (1969).
[w] Approximate summit of seamount (Ken Farley, pers. comm., 1992).
[x] Volcano summit from the map of Defense Mapping Agency Aerospace Center (1975).
[y] Binard *et al.* (1991).
[z] Position is based on the midpoint of four rocks shown on map of Director of Military Survey (1976a).
[aa] Centre of bay on map of Director of Military Survey (1976a); centre of bay is roughly the centre of a collapsed caldera (Chubb 1927).
[bb] Dredge location (Desonie *et al.* 1993).
[cc] Caldera centre (caldera geometry from Brousse *et al.* (1990); island location from map of Aeronautical Chart Service (1951)).
[dd] Island centre from map of Aeronautical Chart Service (1951).
[ee] Approximate centre of seamount from bathymetric map by Mammerickx (1992a).
[ff] Centre of Atuona Caldera (caldera geometry from Gonzales-Marabal (1984); island location from map of Aeronautical Chart Service (1951)).
[gg] Centre of seamount/bank from map in Liotard *et al.* (1986).
[hh] Island summit from map of Aeronautical Chart Service (1951).
[ii] Centre of main island from the map of Defense Mapping Agency Aerospace Center (1989a).
[jj] Centre of seamount summit from bathymetry from Cherkis *et al.* (1989).

[kk] Highest peak on island from map in Almeida (1961).
[ll] Binard *et al.* (1992b).
[mm] Caldera centre (caldera geometry from Carter (1967); island location from of Director of Military Survey (1976b)).
[nn] Approximate centre of atoll from the map of Director of Military Survey (1976b).
[oo] Approximate centre of lagoon from the map of Defense Mapping Agency Aerospace Center (1989b).
[pp] Centre of atoll from the map of Defense Mapping Agency Aerospace Center (1976).
[qq] Seamount summit (Johnson 1984).
[rr] Centre of Bouguer gravity anomaly from map in Machesky (1965).
[ss] Centre of PPT summit (as defined by the 1000-m contour) from map in Hawkins & Natland (1975).
[tt] Centre of Fagaloa caldera; caldera geometry from Natland & Turner (1985), island location from the map of Defense Mapping Agency Aerospace Center (1976).
[uu] Island summit from the map of Defense Mapping Agency Aerospace Center (1976).
[vv] Binard *et al.* (1992a).
[ww] Centre of plutonic complex from map in Williams (1933).
[xx] Centre of island or atoll from the map of Defense Mapping Agency Aerospace Center (1983).
[yy] Island summit from the map of Defense Mapping Agency Aerospace Center (1983).
[zz] Caldera centre from map in Stark & Howland (1941).
[ab] Island summit from the map of Defense Mapping Agency Aerospace Center (1973).
[ac] Approximate centre of the zone of 4 km s^{-1} *P*-wavespeed (Schilly *et al.* 1982).
[ad] Caldera centre from outline in Christiansen (1984).
[ae] Centre of caldera from outline in Pierce & Morgan (1992).

volcano to grow from the seafloor to the sea surface is poorly constrained by observations. Growth of the main shield occurs rapidly followed by a transition to eruptions at much lower rates and usually with different compositions and styles (McDougall & Duncan 1980; Clague & Dalrymple 1987). The duration of the whole volcanic cycle at a single hotspot volcano may be inversely related to plate speed (Emerick & Duncan 1982). It also appears likely that the length of time of main shield building may be inversely related to plate speed, at least between Hawaii (≈100 km Myr^{-1}) and Galapagos (≈20 km Myr^{-1}).

To keep the analysis simple, we assign a single instant in time to each volcano based on the age of its exposed rocks and, rarely, rocks obtained from drilling. If the transition from high to low eruptive rate has been dated for many young volcanoes in a track, as for the Hawaiian, Society and Yellowstone tracks, then we assign the age of this transition to be the volcano age. For volcanoes still in their main stage of growth, as for Loihi, Kilauea and Mehetia, we assign a non-numerical age of *active* rather than using a too-old date or guessing when the stage of high eruptive volume will end. For estimating volcanic propagation rates, we of course use only the numerical ages. The non-numerical ages are essential, however, for determining which volcanoes to include when estimating trends.

For most hotspot tracks, no stages or horizons have been correlated because the eruptive histories of the individual volcanoes are so dissimilar, the exposures are so poor, mapping is so limited, or the age estimates are so few. For these chains we generally assign volcano age as the oldest reliable age date unless the volcano is still in its main phase of growth. Many volcanoes have no age estimates. We assign a non-numerical age of *young* if an undated volcano lies on young seafloor, if it is an undated volcanic island, or if it is a seamount from which only fresh or recently hydrothermally altered rocks have been dredged. A volcano may be composed of both young and old rocks. If dated, we assign to it the age of the earlier volcanism, otherwise we assign a non-numerical age of *mixed*. We assign a non-numerical age of *undated* to a volcano having no useful estimate of age.

In principle, numerical age estimates should be increased by the length of time it takes each volcano to grow from inception to the eruption of its dated horizon. To do so would be unrealistic, especially because of the variable length of time it takes to grow a volcano. Nevertheless one can use the age progression along a chain to estimate the minimum length of time needed to build a volcanic shield. Various straight-line fits to volcano ages versus distance along the Hawaii and Society chains indicate that it takes 0.8 Myr to build volcanoes in either of these chains (Table 2, Appendix B). Thus the HS3-NUVEL1A angular velocities, which span active to 5.0 Ma, average plate motions relative to the hotspots over the past ≈5.8 Myr.

Level two: trends and rates and their uncertainties

Trends

The observed segment trend is the direction of plate motion relative to a hotspot as delineated by its surface track for a specific time interval. Strictly speaking, the segments should be small circles about the (unknown) pole of rotation. For those short segments we examine, however, the data are fit nearly as well by a great circle as by a small circle. The additional parameter needed to specify the curvature of a small circle is highly uncertain and adds no useful information (*cf.* Gordon *et al.* 1984). Consequently, we take the observed segment trend to be the tangent to the great circle that best fits the individual volcanoes of the time interval (Table 3). We solve for the best-fit great circle by minimizing the following expression

$$\sum_{j=1}^{N_{\text{volc}}} (\hat{\mathbf{m}}_j \cdot \hat{\mathbf{b}})^2 \tag{1}$$

where N_{volc} is the number of volcanoes in the segment, $\hat{\mathbf{m}}_j$ is the unit position vector of the jth volcano and $\hat{\mathbf{b}}$ is the unit vector of the best-fit pole.

We use exact error propagation, instead of a linearized approximation, to propagate the uncertainty in chain width into uncertainty in trend, i.e.

$$\sigma_{\text{trend}} = \tan^{-1}\left(\frac{\sigma_{\text{width}}}{l^{\text{obs}}/2}\right) \tag{2}$$

where l^{obs} is the observed length of the segment and σ_{width} is the across-trend standard deviation of volcanoes in a hotspot track, as is discussed further below. The trend uncertainty is independent of the number of volcanoes within the segment and trends from short segments have greater uncertainty than those with long segments.

Table 2. HS3-NUVEL1A active to 5 Ma rate observations.

Hotspot (Plate): Criteria and Comments Volcanoes used	Observed time interval (Ma)	Age error (Myr)	χ_ν^{2a}	Volcanic propagation rate (km Myr^{-1})	$l = 0$ intercept ($\pm 1\sigma$ Ma)^b
Hawaii (Pacific)					
Volcanoes with reasonably dated shield-postshield transition, age errors from radiometric dates					
Mauna Kea, Hualalai, Haleakala, Kahoolawe, West Molokai ($\sigma_{age} = \pm 1$ Myr), Waianae, Niihau	0.1 to 4.9	date error	28.7	107 ± 1	-0.78 ± 0.01 (at Loihi)
Volcanoes with reasonably dated shield-postshield transition, age error from dispersion					
Mauna Kea, Hualalai, Haleakala, Kahoolawe, West Molokai, Waianae, Niihau	0.1 to 4.9	± 0.19	$\equiv 1.00$	108 ± 5	-0.73 ± 0.13 (at Loihi)
Volcanoes with reasonably dated shield-postshield transition, plus Mauna Loa, Kilauea, and Loihi set to 0.0 Ma, age error from dispersion					
Loihi ($\equiv$0.0 Ma), Kilauea ($\equiv$0.0 Ma), Mauna Loa ($\equiv$0.0 Ma), Mauna Kea, Hualalai, Haleakala, Kahoolawe, West Molokai, Waianae, Niihau	0.0 to 4.9	± 0.27	$\equiv 1.00$	118 ± 7	-0.45 ± 0.13 (at Loihi)
Society (Pacific)					
Volcanoes with estimates for the end of shield building, age error from dispersion					
Tahiti-Iti, Tahiti Nui, Moorea, Huahine, Raiatea, Tahaa, Bora Bora, Maupiti	0.4 to 4.0	± 0.27	$\equiv 1.00$	106 ± 9	-0.74 ± 0.26 (at Volcano 16)

[a] χ_ν^2 is reduced chi-square and equals $(\chi^2_{rate})/\nu$, where ν is the number of degrees of freedom, which in this case is the number of volcanoes minus 2.
[b] l is the length along the observed segment trend measured from the young end of the segment.

Trend uncertainty

To estimate trend uncertainty (eq. 2), one needs an estimate of the width of hotspot segments, which we take to be the standard deviation of volcano location about the best-fitting great circle and which can be directly estimated for nine of the eleven chains. Values range from 3 to 55 km (Table 3). Using a two-sided F-test to test the null hypothesis that two segments have the same standard deviation, we find that 27 of 36 pairs of standard deviation are indistinguishable at the 95 per cent confidence level (Table 4). Each of the nine that differ significantly include either Galapagos (whole archipelago; four of the comparisons) or Yellowstone (six of the comparisons) or both (one comparison). The significantly smaller Yellowstone standard deviation (7^{+19}_{-3} km, 95 per cent confidence level here and below), does not incorporate the $\approx$100 km width of the calderas (Appendix A) and we consider it no further. The significantly larger Galapagos standard deviation (55^{+25}_{-13} km) reflects the existence of two subtracks, the Carnegie Ridge and the Wolf–Darwin lineament (Appendix A). That Easter has the next largest sample standard deviation (43^{+52}_{-15} km) and that it differs more from Hawaii than from Galapagos, suggests that hotspots on young lithosphere have greater widths than those on older lithosphere.

All chains except Easter and Galapagos were assigned a 1σ width of 33 km, which is the average of the 1σ width for Hawaii and Society, the two chains with the best data. This agrees well with the weighted average 1σ width of the Hawaiian, Juan Fernandez, Marquesas, Pitcairn, Samoa and Society chains, which is 32^{+8}_{-6} km (95 per cent confidence limits). We assign a larger 1σ width of 55 km to the two hotspots (Easter and Galapagos) that are on young lithosphere.

Rates

Volcanic propagation rate was estimated from the slope of the line that best fits assigned volcano age vs length along the chain, with age taken as the dependent variable and distance as the independent variable. We omit age dates from active volcanoes, because the use of dates within the active phase would bias the volcanic propagation rates upward. For example, if we had set the ages of Mauna Loa, Kilauea and Loihi, which are all active, to 0.0 Ma, then the estimated Hawaiian rate would have been 10 km Myr^{-1} greater than the rate we use (Table 2). Rates are estimated only for chains where a somewhat consistent horizon has been dated for many volcanoes, which leaves only the Hawaiian and Society tracks, both on the Pacific Plate.

Rate uncertainty

We consider two estimates of age uncertainty: analytical uncertainty and standard deviation. In practice, the rate regression with analytical uncertainties has values of χ^2_{rate} that are unacceptably large (Table 2, column 4). For example, the fit to Hawaiian volcano ages gives a value of 29 for χ^2_ν (reduced chi-square, i.e. χ^2 divided by ν, the number of degrees of freedom, where ν equals the number of data minus the number of adjustable parameters). The probability, p, of finding a value of χ^2_ν this large or larger if these uncertainties were appropriate is only 10^{-29}. Thus, dispersion of ages about a straight-line fit vs distance indicates a much larger uncertainty than that expected for a high-quality radiometric date. Thus, the estimated standard deviation leads to more realistic uncertainties in the propagation rates than do the analytical uncertainties.

Level three: estimating angular velocities

The angular velocities of plates relative to the hotspots are determined from a grid search for the minimum weighted, least-squares error,

$$\chi^2_{hotspot} \equiv \sum_{i=1}^{N} \left(\frac{d_i^{obs} - d_i^{cal}}{\sigma_i} \right)^2 \quad (3)$$

where d_i^{obs} is the ith datum (rate or trend), d_i^{cal} is the value calculated from the grid value for the ith datum, σ_i is the standard error of the ith datum and N is the number of data. A global set of angular velocities

Table 3. HS3-NUVEL1A active to 5 Ma trend observations.

Hotspot (Plate) volcanoes used	Observed time interval (Ma)	Number of volcanoes	Observed azimuth of trend	$\lvert\sigma_{\text{width}}\rvert$ ±95% (km)[a]	Observed length (km)	σ_{trend}
Easter (Nazca)						
Tupa, Umu, Ahu, Pukoa, Moai, Tereveka, Rano Kau, Poike	Active to 1.0	8	098.6°	43^{+52}_{-15}	178	±31.7°[b]
Galapagos (Nazca)						
Subaerial volcanoes from the whole archipelago						
Isla Darwin, Isla Wolf, Pinta, Marchena, Genovesa, Roca Redonda, Fernandina, Ecuador, Cerro Azul, Volcan Wolf, Volcan Darwin, Sierra Negra, Alcedo, San Salvador, Rabida, Pinzon, Santa Maria, Santa Cruz, Santa Fe, Espanola, San Christobal	Active to 3.4	21	140.3°	55^{+25}_{-13}	423	±14.6°[b]
Only subaerial volcanoes that lie on the Carnegie Ridge						
Roca Redonda, Fernandina, Ecuador, Cerro Azul, Volcan Wolf, Volcan Darwin, Sierra Negra, Alcedo, San Salvador, Rabida, Pinzon, Santa Maria, Santa Cruz, Santa Fe, Espanola, San Christobal	Active to 3.4	16	121.3°	33^{+19}_{-9}	278	±21.6°[b]
Subaerial volcanoes from the Wolf–Darwin lineament						
Isla Darwin, Isla Wolf, Pinta, Marchena, Genovesa	0.0 to 1.6	5	124.5°	15^{+40}_{-6}	270	±22.2°[b]
Hawaii (Pacific)						
Loihi, Kilauea, Mauna Loa, Mauna Kea, Hualalai, Kohala, Mahukona, Haleakala, Kahoolawe, West Maui, Lanai, East Molokai, West Molokai, Koolau, Waianae, Haupu, Olokele, Niihau	Active to 4.9	18	303.5°	33^{+17}_{-9}	600	±6.3°
Juan Fernandez (Nazca)						
Friday, Alejandro Selkirk, Robinson Crusoe	Young to 4.2	3	086.4°	3^{+30}_{-2}	264	±14.0°
Macdonald (Pacific)						
Macdonald, Rapa	Active to ≈5[c]	2	291.0°	NM[d]	429	±8.7°
Marquesas (Pacific)						
Fatu Hiva, Motu Nao, Motane, Tahuata, Hiva Oa, Fatu Huka, N. Dumont, Ua Pou, Ua Huka, Nuku Hiva, Hatu Iti	≈3 to ≈5[c]	11	310.0°	28^{+23}_{-9}	302	±12.3°
Martin Vaz (South America)						
Ilha do Norte, Trindade	Young to 3.4	2	264.9°	NM[d]	50	±52.7°
Pitcairn (Pacific)						
Adams, Bounty, Pitcairn	Active to 0.9	3	289.1°	12^{+104}_{-6}	91	±35.9°
Samoa (Pacific)						
Lata, A'ofa-Sila, Pago, PPT, Fagaloa, Savai'i	≈0.5 to ≈3 [c]	6	283.2°	42^{+78}_{-17}	334	±11.2°
Society (Pacific)						
16, Mehetia, 17, Moua Pihaa, Rocard, Teahitia, Tahiti-Iti, Tahiti Nui, Moorea, Maiao, Huahine, Raiatea, Tahaa, Bora Bora, Taupiti, Maupiti	Active to 4.0	16	292.6°	32^{+19}_{-9}	479	±7.8°
Yellowstone (North America)						
low velocity zone, third-cycle caldera, second-cycle caldera, first-cycle caldera, Kilgore	Active to 4.3	5	241.0°	7^{+19}_{-3}	150	±23.8°

[a] $\sigma_{\text{width}} \equiv s$, which is the sample standard deviation of width estimated for each hotspot. The 95 per cent confidence limit of σ_{width} is $s[(n-2)/\chi^2_{0.975}]^{\frac{1}{2}} \leq \sigma_{\text{width}} \leq s[(n-2)/\chi^2_{0.025}]^{\frac{1}{2}}$, where $\chi^2_{0.975}$ and $\chi^2_{0.025}$ are evaluated for $n-2$ degrees of freedom and n is the number of volcanoes (Spiegel 1975).

[b] Young seafloor $\sigma_{\text{width}} = \pm 55$ km. Old seafloor or continent $\sigma_{\text{width}} = \pm 33$ km.

[c] ≈ denotes guessed age based on better volcano ages along the track.

[d] NM ≡ 'not meaningful'. These statistics could not be meaningfully calculated because there are only two volcanoes.

uses all rates and trends from a given time interval. While testing our assumptions, we also invert a variety of data subsets to study the origin and measure the significance of the misfit to the hotspot data. A trend-only set of angular velocities uses all trends from a given time interval. We assess the influence of a single hotspot datum (either trend or rate) by removing that datum and then re-inverting the resulting smaller data set and using the results to predict that datum. From this analysis we can estimate one component of motion

Table 4. F-values and significance (two-sided) of differences between width sample standard deviations.

Hotspot → width → Hotspot	Galapagos Track ±55 km $v = 19$	Easter ±43 km $v = 6$	Samoa ±42 km $v = 4$	Hawaii ±33 km $v = 16$	Galapagos Carnegie ±33 km $v = 14$	Society ±32 km $v = 14$	Marquesas ±28 km $v = 9$	Pitcairn ±12 km $v = 1$	Yellow-stone ±7 km $v = 3$	Juan Fernandez ±3 km $v = 1$
Galapagos Track	1.0	—	—	—	—	—	—	—	—	—
Easter	1.6 (58%)	1.0	—	—	—	—	—	—	—	—
Samoa	1.8 (62%)	1.1 (98%)	1.0	—	—	—	—	—	—	—
Hawaii	**2.7 (5%)**	1.7 (38%)	1.5 (48%)	1.0	—	—	—	—	—	—
Galapagos Carnegie	2.8 (6%)	1.7 (38%)	1.6 (47%)	1.0 (97%)	1.0	—	—	—	—	—
Society	**2.9 (5%)**	1.8 (34%)	1.7 (43%)	1.1 (90%)	1.1 (93%)	1.0	—	—	—	—
Marquesas	**4.0 (4%)**	2.5 (21%)	2.3 (28%)	1.5 (56%)	1.4 (58%)	1.4 (64%)	1.0	—	—	—
Pitcairn	22.5 (33%)	14.0 (40%)	12.8 (41%)	8.3 (53%)	8.1 (54%)	7.8 (55%)	5.6 (63%)	1.0	—	—
Yellowstone	**63.5 (1%)**	**39.6 (1%)**	**36.2 (1%)**	**23.6 (2%)**	**23.0 (3%)**	**21.9 (3%)**	**15.9 (4%)**	2.8 (38%)	1.0	—
Juan Fernandez	227.8 (9%)	173.0 (12%)	158.1 (12%)	103.1 (15%)	100.6 (16%)	95.8 (16%)	69.4 (19%)	12.4 (35%)	4.4 (67%)	1.0

— F-values and probabilities are not listed because the probability is equal to that of the opposite pair across the diagonal.
F-values in bold have probabilities of ≤5%.

(trend-perpendicular for a trend, trend-parallel for a rate) of any one hotspot relative to other hotspots from the difference between the observed and predicted datum.

Data importance, I_i, provides an estimate of the information contribution of the ith datum to its calculated value (Minster *et al.* 1974). The sum of the data importances equals the number of independent adjustable parameters, which is 3.0 in this case. An importance of 1.0 implies that there exists a reparametrization for which that datum completely specifies the value of one parameter. An importance near zero indicates that a datum contributes little information to the estimated parameters.

Uncertainties in angular velocity relative to the hotspots are estimated by linear propagation of errors. We found that statistical parameters derived from linear propagation of errors agree well with the parameters from exact propagation, which indicates that linear propagation of errors is a useful approximation for our analysis. We neglect the errors from the NUVEL-1A set of relative plate angular velocities, for which 1-D standard errors are about one tenth the length of those of the hotspot errors. Because the relative plate motion errors are neglected, the 3×3 hotspot covariance matrix is invariant with respect to which plate is held fixed. We are aware that revised estimates of current global relative plate velocities are under construction. Because of tests we performed with earlier estimates of relative plate motion, however, we believe our conclusions about short-term motion between hotspots and appropriate averaging interval are robust, although the angular velocities of the plates relative to the hotspots will need some modification when a new set of relative plate angular velocities is incorporated.

Trend fitting function

When determining angular velocities relative to the hotspots, we replace $(d_i^{\rm obs} - d_i^{\rm cal})$ in eq. (3) with $\sin(\alpha_i/2)$ where α_i is the angular difference between the observed and calculated trend (DeMets *et al.* 1990).

Rate fitting function

In eq. (3), $d_i^{\rm obs}$ is the observed volcanic propagation rate and $d_i^{\rm cal}$ is the calculated volcanic propagation rate. It is unclear what is the most appropriate fitting function to use for calculated volcanic propagation rate. For some models for how a mantle plume interacts with the lithosphere, the appropriate function would be the projection of the calculated velocity onto the observed trend $(|\mathbf{v}_i^{\rm cal}| \cos\alpha_i)$ (Chase 1972). For other models, the appropriate function would be the deprojection of the calculated velocity from the observed trend $(|\mathbf{v}_i^{\rm cal}|/\cos\alpha_i)$, similar to apparent velocity. There is really no good evidence to choose between these two fitting functions. Thus, we choose to split the difference between them by using a third fitting function, the trend-independent formulation of Minster *et al.* (1974), which assumes $d_i^{\rm cal} = |\mathbf{v}_i^{\rm cal}|$. These three fitting functions give identical results only if the trend calculated for a hotspot with an observed rate is identical to the observed trend. The difference in results from the fitting functions increases as the angle between a calculated and an observed trend increases.

For the time interval of active to 5 Ma the difference between observed and calculated trends is 3.3° for Hawaii and 1.9° for Society. Use of the Minster *et al.* (1974) fitting function results in a Pacific-hotspot rotation rate only 0.002 deg Myr^{-1} less than that which would have resulted if the fitting function of Chase (1972) had been used instead.

Level four: evaluation and comparison of global sets of angular velocities

Trends and rates were analysed from ten overlapping time spans: active to 3.2 Ma, active to 4.0 Ma, active to 5.0 Ma, active to

Table 5. Inferred durations and their statistical implications.

Chain	Inferred duration[a] (Myr)	Δt^b (Myr)	Length		σ_{trend}		F^d	$p(F)^e$
			Observed (km)	Predicted[c] (km)	Observed	Predicted		
Easter	5.7	−0.1	178	181	±31.7°[g]	±31.2°[g]	—	—
Galapagos	12.7	+6.9	278	127	±21.6°[g]	±40.9°[g]	$F_{9,14} = 3.6$	**2%**
Hawaii[f]	6.5	+0.7	600	534	±6.3°	±7.0°	$F_{8,16} = 1.2$	34%
Juan Fernandez	8.2	+2.4	264	186	±14.0°	±19.6°	$F_{9,1} = 2.0$	51%
Macdonald	3.6	−2.2	429	688	±8.7°	±5.5°	—	—
Marquesas	2.6	−3.2	302	686	±12.3°	±5.5°	—	—
Martin Vaz	1.0	−4.8	50	282	±52.7°	±13.2°	—	—
Pitcairn	0.8	−5.0	91	694	±35.9°	±5.4°	—	—
Samoa	2.8	−3.0	334	692	±11.2°	±5.5°	—	—
Society[f]	3.8	−2.0	479	733	±7.8°	±5.1°	—	—
Yellowstone	5.5	−0.3	150	158	±23.8°	±22.7°	—	—

[a] Inferred duration, $t^{\text{pred}} = l^{\text{obs}}/|\mathbf{v}^{\text{pred}}|$.
[b] $\Delta t = t^{\text{pred}} - t^{\text{model}} = t^{\text{pred}} - 5.8\text{Myr}$.
[c] Predicted length is the maximum predicted length and $= t^{\text{model}}/|\mathbf{v}^{\text{pred}}| = 5.8\text{Myr}/|\mathbf{v}^{\text{pred}}|$.
[d] $F = (\frac{\sigma^{\text{pred}}_{\text{trend}}}{\sigma^{\text{obs}}_{\text{trend}}})^2$.
[e] Probabilities are for the one-tailed F-test. Probabilities = 5% are printed in **bold**.
[f] Both rate and trend removed.
[g] Young seafloor $\sigma_{\text{width}} = \pm 55$ km.

6.0 Ma, 0.0 to 4.0 Ma, 0.0 to 5.0 Ma, 0.0 to 6.0 Ma, 1.0 to 5.0 Ma, 1.0 to 6.0 Ma and 2.0 to 6.0 Ma. Results for the HS3-NUVEL1A set of angular velocities are discussed separately below.

Influence on trend uncertainty of the consistency between volcano age and plate speed

The uncertainties assigned to trends depend on the observed segment length (Table 3), which in turn depends on observed volcano age and location. If the observed segment lengths are greater than the true length formed during a time interval, then the results would be negatively affected in two ways. First, the trend would be assigned an uncertainty that was too small and thus would be given too much weight in the analysis. Second, the trend would be biased toward directions of motion outside the time interval. Most volcano ages are of insufficient accuracy and density to be used to predict segment length accurately. As an alternative the inferred duration (Table 5) is estimated using the observed segment length and plate speeds predicted from an interim data set which has trend uncertainties based solely on segment length (Table 3).

Let $t_i^{\text{pred}} \equiv l_i^{\text{obs}}/|\mathbf{v}_i^{\text{pred}}|$ be the duration inferred from the observed segment length of the ith hotspot, where $|\mathbf{v}_i^{\text{pred}}|$ is the speed predicted from an estimated set of plate angular velocities relative to the hotspots determined from all hotspot data except that of the ith hotspot. Δt_i, the difference between t_i^{pred} and the assumed duration of the model, ranges from −5.03 to +6.90 Myr for the time interval of active to 5.0 Ma (Table 5). A negative Δt may be due to a discontinuous hotspot track or to the track having been only sparsely surveyed (e.g. Martin Vaz, Pitcairn and Samoa), but a positive Δt suggests along-trend motion of the hotspot, poor age dates, long-lasting volcanism, inaccuracies in the assumed relative plate motions or some combination of these. Galapagos, Juan Fernandez and Hawaii have positive Δt's.

The maximum predicted segment length can be estimated by multiplying predicted speed by the duration (5.8 Myr). Applying eq. (2) to this predicted length gives a minimum uncertainty for the trend. We find that the only minimum trend uncertainties that are significantly larger than those originally estimated are for the Galapagos segments that include *active* volcanism (e.g. Table 5). Most of the large positive Δt's for these Galapagos segments are likely to be caused by the main stage of Galapagos growth lasting longer than the 0.8 Myr duration estimated for Hawaii. Along the observed Galapagos trend, active volcanoes span 110 km compared with 60 km for Hawaii (Appendix A). Measured along the predicted trend (084.8°), the active length is 85 km. When divided by the predicted rate, this indicates a 3.9 Myr duration for the main stage of Galapagos growth. To avoid overweighting the Galapagos data, we increased the assigned trend uncertainty for the four data sets that include active volcanism, including the active to 5 Ma data set, to be the minimum trend uncertainty. As expected, the volume of the error ellipsoids increased and the Galapagos data importance decreased, but changes in angular velocities were minor.

Mutual consistency of trends and rates

When we invert the trend-only data subset of HS3, the trends (and assigned uncertainties) are found to be mutually consistent ($\chi^2 = 5.1$ with 8 degrees of freedom, $p = 0.75$) attesting to the mutual consistency of our objectively estimated errors and the assumption that the hotspots are fixed. When we invert the HS3 global data set (of trends and rates), they are found to be mutually consistent ($\chi^2 = 8.0$ with 10 degrees of freedom, $p = 0.63$). Moreover, a one-sided F-test of the significance of the decrease in chi-square when the rates are removed from the global data set indicates that the decrease in misfit (from 8.0 to 5.1) is insignificant for the active to 5 Ma interval used for HS3-NUVEL1A. It is also insignificant for the nine other time intervals. Thus, within the dispersion of the data and our error budget, the rates and trends are mutually consistent. This does not require that the difference between the global and trend-only angular velocities is small for a given time interval. Indeed, the length of the vector difference in angular velocity ranges from 0.05 deg Myr^{-1} (active to 5 Ma) to 0.91 deg Myr^{-1} (1 to 6 Ma).

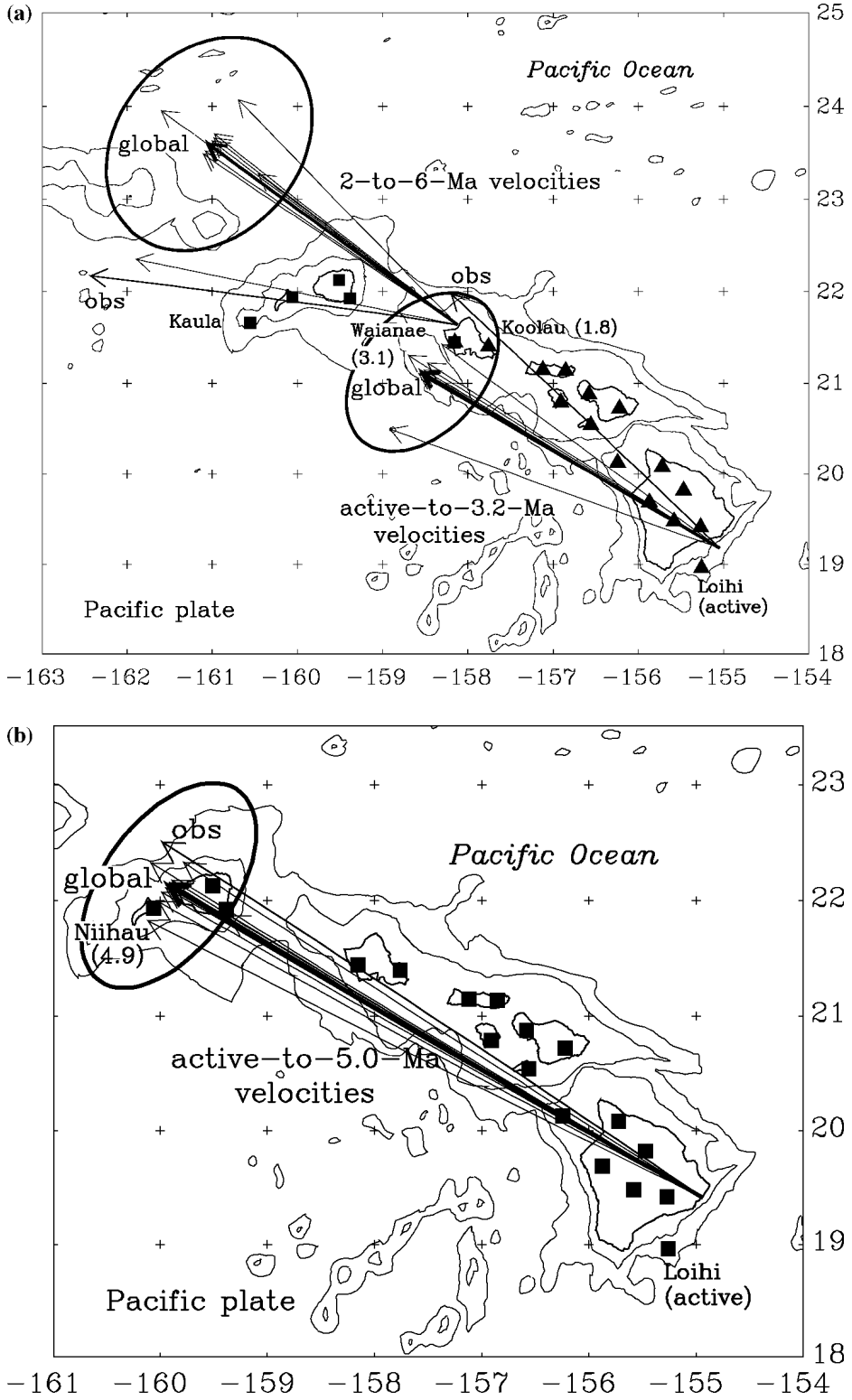

Figure 1. Bathymetric map of the Hawaiian islands. Island outlines are thick lines and 2000 m contours are thin lines (Mammerickx 1989). Mercator projection (a) Solid triangles, Hawaiian volcanoes younger than 3.2 Ma; solid squares, Hawaiian volcanoes with ages between 2 to 6 Ma. Arrows are scaled to show the displacements over 4.0 Myr. Medium arrows show the observed Hawaiian motion for the time intervals of active to 3.2 Ma and 2.0 to 6.0 Ma. Thick arrows show motion calculated from the global models for the time intervals of active to 3.2 Ma and of 2.0 to 6.0 Ma and their 2-D 95 per cent confidence ellipses. Thin arrows show the motion predicted when the Hawaiian rate or Hawaiian trend is removed and the motion calculated when a non-Hawaiian datum is removed. (b) Same as (a), but with the arrows scaled to show the displacement over 5.8 Myr (corresponding to the duration of the HS3-NUVEL1A time interval of active to 5.0 Ma). Solid squares, Hawaiian volcanoes younger than 5.0 Ma.

Table 6. Excluded trend observations.

Hotspot (plate): comments Volcanoes used	Observed time interval (Ma)	Predicted duration (Myr)	Observed length (km)	Observed trend ($\pm 1\sigma$)
Bowie (Pacific): Edifices contain mixture of young and old volcanism, current location uncertain				
Bowie, Hodgkins, Dickins	≈0 to 4.1	3.2	161	$332.0 \pm 22.3^\circ$
Cobb (Juan de Fuca): On-ridge				
Axial, Son of Brown Bear, Thompson	Active to 3.2	5.2	108	$084.1 \pm 45.6^{\circ a}$
Cobb (Pacific): On-ridge				
Axial, Brown Bear, Pipe, Cobb, Corn, Gluttony, Anger, Lust, Sloth	Active to 5.2	4.1	224	$326.9 \pm 26.1^{\circ a}$
Comores (Africa (Somali)): Active volcano lies between two older volcanoes; Observed length far greater than that predicted by a model that includes the Comores trend				
Karthala, La Grille, Moheli	Active to 5.0	7.4	98	$155.4 \pm 34.0^\circ$
Eastern Caroline (Pacific): Excessively scattered K-Ar dates				
Kosrae, Pohnpei	1.4 to 5.2	4.7	553	$288.5 \pm 6.8^\circ$
Islas Revillagigedo (Pacific): Likely not a hotspot, two volcanoes lie a top the Mathematician Ridge, which is an extinct spreading centre				
San Benidicto, Socorro, Roca Partida, Clarion	0.3 to 2.4	5.1	426	$259.2 \pm 14.5^{\circ a}$
Lord Howe (Australia): One volcano is too old, one is likely too old, the presumed youngest is unsampled				
Flinders, Balls Pyramid, Lord Howe	? to 6.9	4.5	353	$350.9 \pm 10.6^\circ$
Louisville (Pacific): Only one sampled volcano with age ≤5.0 Ma				
138.1W, 139.2W	? to = 1.1	0.9	95	$305.9 \pm 34.8^\circ$
Louisville (Pacific): On-ridge?, possibly not a hotspot track				
Hollister Ridge	Active ? to ?	2.3 [b]	230[b]	$306 \pm 26^{\circ a}$
Réunion (Africa (Somali)): The two youngest volcanoes are separated by only 30 km and lie on the same island. The third, older volcano is too old. The observed length is far greater than that predicted by a model that includes the Réunion trend				
Fournaise, de Neige, Mauritius	Active to 7.6	17.6	233	$064.9 \pm 15.8^\circ$
Tasmantid (Australia): An earthquake does not a hotspot volcano make, known seamount too old				
$m_b = 6.0$ 1983 earthquake, Gascoyne	Active? to 6.4	5.3	420	$008.4 \pm 8.9^\circ$

[a] Young seafloor width standard error is ±55. Old seafloor width standard error is ±33 km.
[b] Length is that part of the Hollister Ridge lying on seafloor formed since 5.8 Ma (based on the NUVEL-1A Antarctic–Pacific half spreading rate of 39.0 km Myr^{-1}). Trend measured by eye from a map constructed from the gravity grid of Sandwell & Smith (1995).

Solution stability and robustness

To evaluate solution stability for a given time interval, we examine the difference in the predicted and calculated trends from all sets of angular velocities determined by removing one datum and re-inverting the remaining data. We found that removal of one datum can cause large changes in predicted and calculated trends if an interval is only 4 Myr long (Fig. 1a). For example, for the 2 to 6 Ma interval, removal of one datum causes the predicted and calculated trends of Hawaii to vary by as much as 34° (Fig. 1a). In contrast, for all data sets spanning 6 Myr, removal of one datum causes the predicted and calculated trends of Hawaii to vary by no more than 10° (e.g. Fig. 1b). These results suggest, but by no means prove, that a 6-Myr-long averaging interval gives a more stable solution than does a 4-Myr-long interval. In any event, they verify the stability of the results obtained for the HS3 data set for which the variation in predicted and calculated Hawaiian trend is 6° (Fig. 1b).

Potential effect of including data that were rejected

Trends and rates. The trends of many hotspot tracks, including some used by prior workers, were rejected here for several reasons:

(1) the track formed on a spreading ridge,
(2) the plate speed was too slow to make a meaningful trend,
(3) the available dates are of poor quality, or
(4) there are fewer than two sampled volcanoes with ages of 5 Ma or younger.

To assess the effect of the rejection of these hotspot tracks on the angular velocities of HS3-NUVEL1A, we estimate observed trends for eleven rejected tracks (Table 6), adding them singly to the HS3 data set and then re-inverting the data (Table 7). We also did the same for three rates excluded from the HS3 data set (Tables 8 and 9). All rejected data, except the Comores trend, Réunion trend, Tasmantid trend and Galapagos rate, have misfits (observed minus predicted) smaller than their combined 95 per cent confidence limits (Tables 7 and 9). These same four data cause the largest changes in angular velocity, but no change is significant at the 95 per cent confidence level. The addition of any single datum, except the Comores and Réunion trends, decrease the volume of the resulting confidence ellipsoid by less than 15 per cent.

The Réunion trend has a data importance of one and decreases the error volume by more than 90 per cent without increasing χ^2_{hotspot} significantly. This result sounds promising, but must be rejected. The resulting African-hotspot pole of rotation is shifted just north of the Réunion hotspot; consequently, rotation about the pole could not have created the observed length of the corresponding track in 40 Myr, much less in 5.8 Myr! The Réunion trend and rate, the latter of which was inferred from only two volcano ages, are incompatible with each other when included in the HS3 data set. The Comores track has the same problems, but no meaningful statistics could be

Table 7. Influence of some unacceptable trends.

Hotspot	HS3-NUVEL1A predictions		Observed trend ±1σ	Trend misfit (α) ±95%	Δv_t^a ±95% (km Myr^{-1})	Model including unacceptable trend			
	Rate ±1σ (km Myr^{-1})	Trend ±1σ				Calculated trend ±1σ	I[b]	$\frac{V_0-V}{V_0}$ [c]	$\Delta\chi^{2d}$
Bowie	50.7 ± 4.5	323.8 ± 9.3°	332.0 ± 22.3°	8.2 ± 47.4°	7 ± 42	325.1 ± 8.6°	0.15	9%	0.1
Cobb (JdF)	20.5 ± 7.5	036.0 ± 14.9°	084.1 ± 45.6°[e]	48.1 ± 94.0°	15 ± 24	039.7 ± 13.1°	0.08	7%	1.0
Cobb (PA)	54.7 ± 4.9	312.9 ± 8.2°	326.9 ± 26.1°[e]	14.0 ± 53.6°	13 ± 50	314.3 ± 7.9°	0.09	6%	0.3
Comores	13.3 ± 7.1	297.3 ± 19.5°	155.4 ± 34.0°	**−141.9 ± 76.8°**	−8 ± 15	161.2° ± NM[f]	NM[f]	NM[f]	3.8
Eastern Caroline Islas	117.7 ± 5.7	296.8 ± 4.0°	288.5 ± 6.8°	−8.3 ± 15.5°	−17 ± 32	294.3 ± 3.6°	0.27	9%	1.0
Revillagigedo	84.1 ± 6.1	284.9 ± 3.9°	259.2 ± 14.5°[e]	−25.7 ± 29.4°	−36 ± 39	283.2 ± 3.7°	0.06	5%	2.9
Lord Howe	77.7 ± 8.0	345.9 ± 5.1°	350.9 ± 10.6°	5.0 ± 23.0°	7 ± 31	346.8 ± 4.6°	0.18	10%	0.2
Louisville (off-ridge)	103.4 ± 7.0	294.3 ± 3.2°	305.9 ± 34.8°	11.6 ± 68.5°	21 ± 121	294.4 ± 3.2°	0.01	0%	0.1
Louisville (on-ridge)	99.8 ± 7.1	295.4 ± 3.3°	306 ± 26°[e]	11 ± 51°	18 ± 87	295.5 ± 3.3°	0.02	1%	0.2
Réunion	13.3 ± 7.2	314.2 ± 19.2°	064.9 ± 15.8°	**110.7 ± 48.8°**	12 ± 13	063.1 ± 15.7°	1.00	95%	3.6
Tasmantid	79.6 ± 8.0	346.2 ± 5.0°	008.4 ± 8.9°	**22.2 ± 20.0°**	**30 ± 26**	351.2 ± 4.2	0.22	14%	4.7
Non-African trends (9)	Various	Various	Various	Various	Various	Various	0.75	36%	11.8

[a] Δv_t is the component of motion of the unacceptable hotspot relative to that predicted from HS3-NUVEL1A in the direction perpendicular to the observed trend, where $\Delta v_{t_i} = |\mathbf{v}_i^{\text{pred}}| \sin(\alpha_i^{\text{pred}})$, $|\mathbf{v}_i^{\text{pred}}|$ is the speed predicted from the model, and α_i^{pred} is the observed trend minus the predicted trend. The 1-D errors are calculated using multivariate error analysis.

[b] I is the data importance the unacceptable datum has in a data set consisting of the HS3-NUVEL1A data and the unacceptable datum.

[c] $\frac{(V_0-V)}{V_0}$ is the percentage volume decrease relative to the HS3-NUVEL1A error ellipsoid, where V_0 is the volume of the HS3-NUVEL1A standard error ellipsoid and V is the volume of the standard error ellipsoid when an unacceptable trend is added to the HS3-NUVEL1A data set.

[d] $\Delta\chi^2$ is the increase in χ^2_{hotspot} relative to that of HS3-NUVEL1A ($\chi^2_{\text{hotspot}} = 8.0$) when an unacceptable trend is added to the HS3-NUVEL1A data set.

[e] Young seafloor $\sigma_{\text{width}} = \pm 55$ km.

[f] NM ≡ 'not meaningful.' These statistics could not be meaningfully calculated.

Trend misfits and Δv_t's printed in bold differ significantly from zero with ≥95 per cent confidence.

calculated for any data set including the Comores trend. Although the inability to satisfactorily fit these tracks may be partly due to treating Africa as a single plate instead of separate Nubian and Somalian plates (*cf.* Chu & Gordon 1999), the main difficulties are surely due to the unreliability of short tracks and possibly to long-lasting volcanism on slow plates.

Even if we added all rejected trend data listed in Table 6, except those from Africa, to the HS3 data set, the volume of the confidence ellipsoid would only decrease by 36 per cent.

On-ridge hotspots. Morgan (1978) and Schouten *et al.* (1987) proposed that some on-ridge hotspots are caused by the channelling of a near-ridge source to the closest point on a nearby spreading ridge. Here we use the model of Schouten *et al.* (1987), which excludes the ridge-perpendicular component of plate velocity relative to the hotspots, to predict trends for the Wolf–Darwin lineament of the Galapagos and for both Cobb tracks. These predicted trends are closer to the observed trends (Table 10) than are those predicted from HS3-NUVEL1A. None of these observations differ significantly from the HS3-NUVEL1A predictions (Table 10) however, and thus the Schouten *et al.* (1987) model can be neither excluded nor confirmed.

HS3-NUVEL1A

Angular velocities

HS3-NUVEL1A describes the motion of 15 assumed-rigid plates relative to a global set of hotspots over the past several million years (Tables 11 and 12, Fig. 2). The data used to estimate the relative plate motions are averaged over different time intervals. Earthquake focal mechanisms reflect motion averaged over years or decades to tens of thousands of years, transform faults average motion over hundreds of thousands to millions of years and spreading rates average motion over 3.2 Myr (DeMets *et al.* 1990, 1994). The volcanoes used to

Table 8. Excluded rate observations.

Hotspot (plate): comments Volcanoes used	Observed time interval (Ma)	σ_{age} (Myr)	Observed rate ±1σ (km Myr^{-1})
Cobb (Pacific): On-ridge			
Axial (≡0.0), Cobb, Gluttony, Lust, Sloth	active to 5.2	±1.30	51 ± 19
Galapagos (Nazca): Long-lasting volcanism, no known consistent horizon to date			
Ecuador, San Salvador, Raibida, Pinzon, Santa Maria, Santa Cruz, Santa Fe, Espanola, San Christobal	0.1 to 3.4	±0.45	84 ± 14
Yellowstone (North America): Only 4 volcanoes			
third-cycle caldera, second-cycle caldera, first-cycle caldera, Kilgore	0.6 to 4.3	±0.96	36 ± 14

Table 9. Influence of some unacceptable rates.

Hotspot	HS3-NUVEL1A Predicted rate $\pm1\sigma$ km Myr^{-1}	Observed rate $\pm1\sigma$ km Myr^{-1}	Rate misfit $\pm95\%$ km Myr^{-1}	Δv_r^a $\pm95\%$ km Myr^{-1}	Model including unacceptable rate: Calculated rate $\pm1\sigma$ (km Myr^{-1})	I	$\frac{V_0-V}{V_0}$	$\Delta\chi^2$
Cobb (PA)	54.7 ± 4.9	51 ± 19	-4 ± 38	-2 ± 40	54.5 ± 4.9	0.06	3%	0.0
Galapagos	21.3 ± 5.9 [b]	84 ± 14	$\mathbf{63\pm30}$	$\mathbf{66\pm33}$	30.8 ± 5.6	0.16	10%	17.0
Yellowstone	26.8 ± 7.8 [b]	36 ± 14	9 ± 32	10 ± 31	29.1 ± 7.8	0.01	−1%	0.3
rates (3)	Various	Various	Various	Various	Various	0.23	2%	18.2
rates (3) and Non-African trends (9)	Various	Various	Various	Various	Various	0.98	41%	28.3

Same conventions as in Table 7.

[a] Δv_r is the component of motion of the unacceptable hotspot relative to that predicted from HS3-NUVEL1A in the direction parallel to the observed trend, where $\Delta v_{r_i} = r_i^{\text{obs}} - |\mathbf{v}_i^{\text{pred}}|\cos(\alpha_i^{\text{pred}})$, which is equivalent to the rate fitting function of Chase (1972), and r_i^{obs} is the observed volcanic propagation rate. The 1-D errors are calculated using multivariate error analysis.

[b] Observed trend was included in the model for this prediction.

estimate trends and rates for HS3-NUVEL1A all have observed ages of 5 Ma or younger. Summing the 5 Myr length of the 0 to 5 Ma time interval with the minimum time (≈0.8 Myr) that we estimate it takes a shield volcano to grow indicates that the time interval averaged for HS3-NUVEL1A is ≈5.8 Myr long. Our 'global' hotspot data span only a hemisphere and consist of eleven segment trends and two volcanic propagation rates. The segment trends lie on the Pacific, Nazcan, North American and South American plates.

For the angular velocities of both Minster & Jordan (1978) and Gripp & Gordon (1990), the motion of the Antarctic, Caribbean and Eurasian plates relative to the hotspots differed insignificantly from zero. In contrast, the angular velocities of all plates relative to the hotspots differ significantly from zero ($p \leq 0.008$) in HS3-NUVEL1A. The difference is due both to smaller uncertainties in HS3-NUVEL1A and to its having greater rotation rates relative to the hotspots. Some plates in HS3-NUVEL1A nevertheless move slowly relative to the hotspots (Table 12, Fig. 2). The slowest moving plates are the Juan de Fuca, Antarctic, African and Eurasian plates with root-mean-square (rms) velocities of 10, 15, 16 and 20 km Myr^{-1}, respectively. The fastest moving plates are the Pacific, Philippine, Australian, Cocos, South American and Indian plates with rms velocities of 105, 86, 74, 50, 45 and 45 km Myr^{-1}, respectively. The remaining plates, the North American, Nazca, Scotia, Caribbean and Arabian plates move at 27, 30, 30, 30 and 30 km Myr^{-1}, respectively. The Caribbean angular velocity and rms velocity are likely to be unreliable because geodetic observations indicate that the velocity of the Caribbean Plate relative to North America differs significantly from that in NUVEL-1A (Dixon *et al.* 1998).

Plates with large continental area tend to move slower than oceanic plates, but there is much overlap in the rms velocities with, for example, the Juan de Fuca, Scotia, Caribbean and Nazca plates all moving more slowly than the South American, Indian and Australian plates (Fig. 3a). Plates with a substantial portion (28–44 per cent) of their boundaries attached to subducting slabs tend to move faster than plates with little (≤9 per cent) or none of their boundaries attached to subducting slabs (Forsyth & Uyeda 1975), but again with overlap in rms velocities (Fig. 3b). Among the six plates attached to substantial subducting slabs (Juan de Fuca, Nazca, Cocos, Australia, Philippine and Pacific), the rms velocity tends to increase with increasing age of the lithosphere being subducted (Carlson *et al.* 1983) (Fig. 3c). Some of the slowest moving plates move in surprising directions (Figs 2 and 4). The Antarctic Plate moves slowly but significantly away from the Peru–Chile trench. The African Plate and, to a lesser extent, the Juan de Fuca Plate move obliquely relative to their short trenches. These directions of motion may be real, but small systematic errors, especially in observed rates and in NUVEL-1A (*cf.* Gordon *et al.* 1999), might better explain these results. In HS3-NUVEL1A the Pacific Plate moves 8–9 km Myr^{-1} faster to the west-northwest than in HS2-NUVEL1 (Fig. 4).

As a check on the robustness of our angular velocities, we investigate their sensitivity to the omission of a single datum. Removing any one datum always results in an angular velocity that lies inside

Table 10. Velocity predictions using the Schouten *et al.* (1987) model for on-ridge hotspots.

Hotspot	HS3-NUVEL1A: Predicted rate $\pm\sigma$ (km Myr^{-1})	HS3-NUVEL1A: Predicted trend $\pm1\sigma$	Observed trend $\pm1\sigma$	Schouten *et al.* (1987)[b]: Predicted trend	Schouten *et al.* (1987)[b]: Predicted rate (km Myr^{-1})	Observed rate $\pm1\sigma$ (km Myr^{-1})
Cobb (JdF)	21.3 ± 7.5	$034.1\pm14.6^\circ$	$084.1\pm45.6^\circ$ [a]	074°	35	—
Cobb (PA)	55.0 ± 5.0	$311.5\pm8.1^\circ$	$326.9\pm26.1^\circ$ [a]	326°	35	51 ± 19
Galapagos (CO)	57.7 ± 6.1	$026.1\pm5.3^\circ$	—	043°	33	—
Galapagos, Wolf–Darwin (NZ)	20.0 ± 5.9	$092.5\pm15.8^\circ$	$124.5\pm22.2^\circ$ [a]	149°	33	—
Louisville, Hollister (PA)	99.6 ± 7.1	$294.8\pm3.3^\circ$	$306\pm26^\circ$ [a]	294°	39	—

[a] Young seafloor $\sigma_{\text{width}} = \pm55$ km.

[b] Schouten *et al.* (1987) velocities are predicted using NUVEL-1A for the relative plate velocity at the spreading ridge, using HS3-NUVEL1A for plate velocity relative to the hotspots predicted at the spreading ridge, and assuming the spreading ridge is perpendicular to spreading direction.

Table 11. HS3-NUVEL1A active to 5 Ma observed, calculated, and predicted values.

Hotspot	Location[a]		Observed Trend	HS3-NUVEL1 calculated values		Observed trend −	Predicted Values	
	°N	°E	±1σ	trend ±1σ	Rate ±1σ (km Myr^{-1})	calculated trend	Trend ±1σ	Rate ±1σ (km Myr^{-1})
Easter	−27.11	−110.06	098.6 ± 31.7°[b]	107.0 ± 9.9°	32.7 ± 5.3	−8.4°	108.0 ± 10.5°	32.5 ± 5.3
Galapagos	−0.54	−90.83	121.3 ± 40.9°[b]	089.9 ± 14.9°	21.3 ± 5.9	31.4°	084.8 ± 15.9°	21.9 ± 6.0
Hawaii	20.65	−156.91	303.5 ± 6.3°	300.2 ± 4.4°	103.3 ± 4.5	3.3°	296.5 ± 6.1°[c]	103.6 ± 4.6[c]
Juan Fernandez	−33.73	−80.45	086.4 ± 14.0°	081.0 ± 9.6°	33.8 ± 5.8	5.4°	075.4 ± 12.3°	36.0 ± 7.0
Macdonald	−28.31	−142.31	291.0 ± 8.7°	292.6 ± 3.1°	116.5 ± 6.0	−1.6°	292.9 ± 3.3°	116.4 ± 6.0
Marquesas	−9.59	−139.37	310.0 ± 12.3°	291.6 ± 3.2°	116.5 ± 5.2	18.4°	290.2 ± 3.3°	116.9 ± 5.2
Martin Vaz	−20.49	−29.09	264.9 ± 52.7°	251.2 ± 9.9°	47.2 ± 5.2	13.7°	250.6 ± 10.0°	47.3 ± 5.2
Pitcairn	−25.21	−129.59	289.1 ± 35.9°	287.9 ± 2.9°	117.9 ± 5.6	1.2°	287.9 ± 2.9°	117.9 ± 5.6
Samoa	−14.19	−170.74	283.2 ± 11.2°	298.5 ± 3.8°	116.8 ± 5.9	−15.3°	300.6 ± 4.0°	117.4 ± 5.8
Society	−17.33	−149.95	292.6 ± 7.8°	294.5 ± 3.3°	117.9 ± 5.6	−1.9°	295.0 ± 3.7°[d]	117.9 ± 5.6[d]
Yellowstone	44.38	−111.05	241.0 ± 23.8°	249.5 ± 10.7°	26.8 ± 7.8	−8.5°	251.8 ± 12.0°	26.9 ± 7.9

[a] Location = centre of moment of volcano locations. It is a by-product of the solution for best-fit pole to the volcano locations.
[b] Young seafloor $\sigma_{\text{width}} = \pm 55$ km.
[c] Hawaiian rate included in prediction.
[d] Society rate included in prediction.

Hotspot	Observed rate ±1σ (km Myr^{-1})	HS3-NUVEL1A Calculated rate ±1σ (km Myr^{-1})	Observed rate − calculated rate (km Myr^{-1})	Predicted values (rate removed)		Predicted values (rate and trend removed)	
				Rate ±1σ (km Myr^{-1})	Trend ±1σ	Rate ±1σ (km Myr^{-1})	Trend ±1σ
Hawaii	108 ± 5	103.3 ± 4.5	5	92.2 ± 8.5[e]	300.7 ± 4.4°[e]	92.5 ± 8.9	298.0 ± 6.2°
Society	106 ± 9	117.9 ± 5.6	−12	125.1 ± 6.2[f]	294.6 ±3.2°[f]	125.1 ± 6.2	295.0 ± 3.6°

[e] Hawaiian trend included in prediction.
[f] Society trend included in prediction.

Table 12. Angular velocities of HS3-NUVEL1A.

Plate	Angular Velocity			Approx. Standard Error Ellipse			σ_ω	$p(\chi^2(\omega_{HS3} - \mathbf{0}))^b$	Rms Speed	$p(\chi^2(\omega_{HS3} - \omega_{HS2}))^c$
	°N	°E	°Myr^{-1}	$\sigma_{\max}$	$\sigma_{\min}$	$\zeta^a_{\max}$	° Myr^{-1}		km Myr^{-1}	
Africa	−43.386	21.136	0.1987	28.05°	15.02°	052°	0.0585	$\mathbf{8 \times 10^{-3}}$	15.9	**3%**
Antarctica	−47.339	74.514	0.2024	26.61°	17.64°	006°	0.0569	$\mathbf{1 \times 10^{-3}}$	15.0	**5%**
Arabia	2.951	23.175	0.5083	10.63°	7.37°	058°	0.0611	$\mathbf{2 \times 10^{-20}}$	30.3	**2%**
Australia	−0.091	44.482	0.7467	6.73°	4.35°	043°	0.0704	$\mathbf{4 \times 10^{-28}}$	73.8	**2%**
Caribbean	−73.212	25.925	0.2827	20.79°	11.81°	045°	0.0543	$\mathbf{1 \times 10^{-6}}$	30.1	**4%**
Cocos	13.171	−116.997	1.1621	4.32°	2.69°	149°	0.0714	$\mathbf{<1 \times 10^{-43}}$	50.3	$\mathbf{5 \times 10^{-3}}$
Eurasia	−61.901	73.474	0.2047	27.38°	17.52°	003°	0.0524	$\mathbf{4 \times 10^{-4}}$	20.0	**5%**
India	3.069	26.467	0.5211	10.22°	7.08°	056°	0.0628	$\mathbf{3 \times 10^{-20}}$	45.0	**2%**
Juan da Fuca	−39.211	61.633	1.0122	5.58°	3.33°	021°	0.0618	$\mathbf{<1 \times 10^{-43}}$	10.3	**15%**
Nazca	35.879	−90.913	0.3231	16.51°	12.26°	004°	0.0583	$\mathbf{1 \times 10^{-9}}$	29.6	$\mathbf{9 \times 10^{-3}}$
North America	−74.705	13.400	0.3835	15.59°	8.70°	056°	0.0548	$\mathbf{1 \times 10^{-11}}$	26.9	6%
Pacific	−61.467	90.326	1.0613	5.71°	3.69°	166°	0.0498	$\mathbf{<1 \times 10^{-43}}$	105.4	32%
Philippine	−53.880	−16.668	1.1543	5.26°	2.64°	081°	0.0581	$\mathbf{<1 \times 10^{-43}}$	85.5	8%
Scotia	−76.912	52.228	0.4451	13.56°	7.99°	019°	0.0523	$\mathbf{6 \times 10^{-18}}$	29.9	—
South America	−70.583	80.401	0.4358	13.82°	8.59°	174°	0.0503	$\mathbf{4 \times 10^{-19}}$	45.3	8%
NNR-NUVEL1A	−55.908	69.930	0.4359	13.48°	8.28°	008°	0.0545	$\mathbf{8 \times 10^{-17}}$	—	—

[a] $\zeta_{\max}$ is the azimuth of the major axis of the error-ellipse.
[b] $p(\chi^2(\omega_{HS3} - \mathbf{0})$ is the probability of obtaining data as different or more different as those used herein if the angular velocity of the plate is zero.
[c] $p(\chi^2(\omega_{HS3} - \omega_{HS2})$ is the probability of obtaining data as different or more different as those used in HS3-NUVEL1A if the angular velocity of the plate is that of HS2-NUVEL1.
Probabilities of ≤5% are printed in bold.
The HS3-NUVEL1A covariance matrix in Cartesian coordinates and in units of 10^{-10} radians^2 Myr^{-2} is

$$\begin{bmatrix} \sigma_x^2 & \sigma_{yx}^2 & \sigma_{zx}^2 \\ \sigma_{xy}^2 & \sigma_y^2 & \sigma_{zy}^2 \\ \sigma_{xz}^2 & \sigma_{yz}^2 & \sigma_z^2 \end{bmatrix} = \begin{bmatrix} 7662 & 3518 & -1782 \\ 3518 & 15615 & 3094 \\ -1782 & 3094 & 8553 \end{bmatrix}.$$

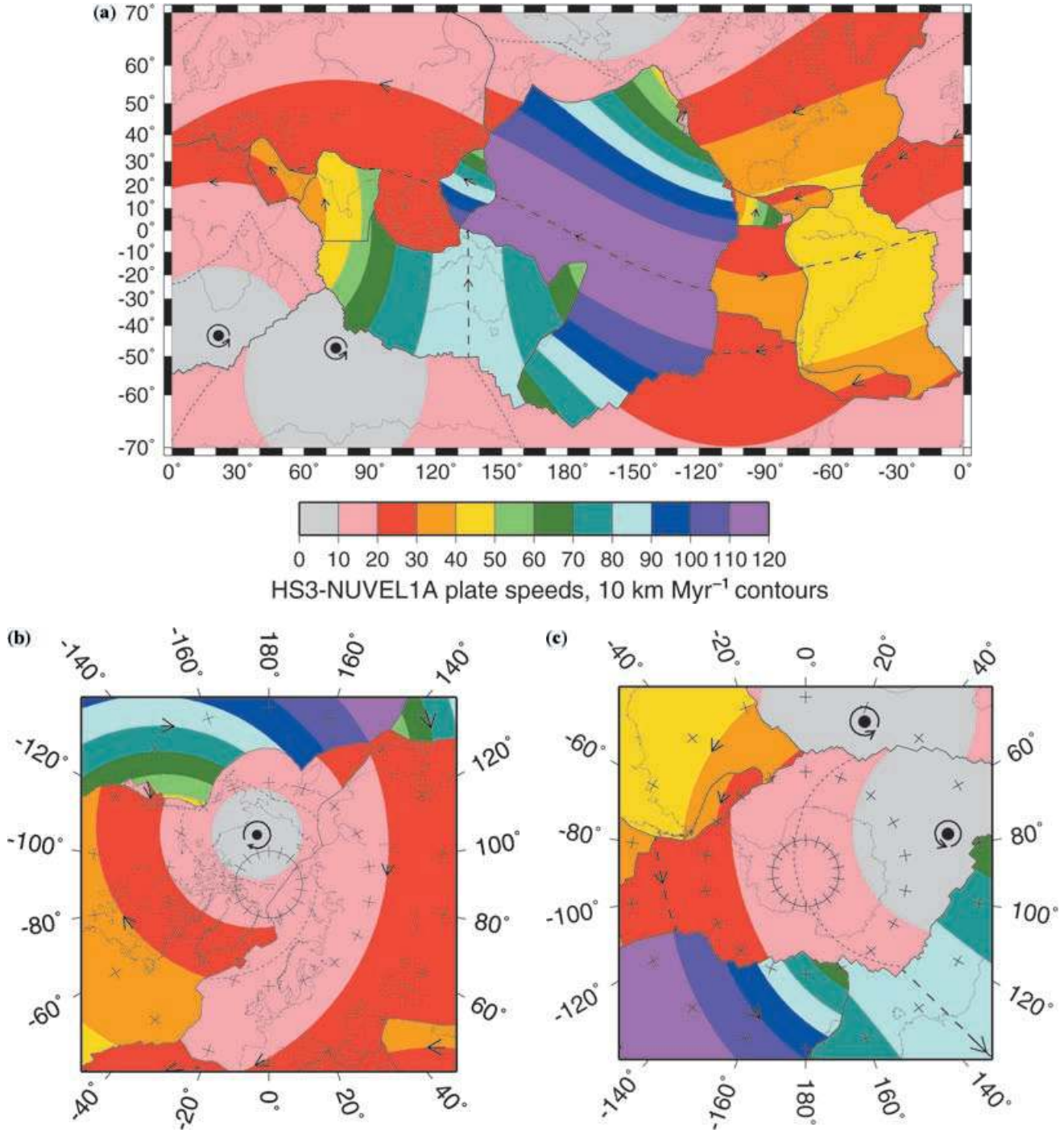

Figure 2. Contour map of plate speed relative to the hotspots for the HS3-NUVEL1A angular velocities. Thick dashed lines mark equators to poles of the angular velocities.Thin dashed lines delimit where plate speed differs from zero at the 95 per cent confidence level. Filled circles mark pole (or antipole) locations if pole (or antipole) lies on its own plate. Medium solid lines are the approximate plate boundaries. (a) Mercator projection. (b) Stereographic projection about north pole. (c) Stereographic projection about south pole.

the 95 per cent confidence ellipsoid of HS3-NUVEL1A. The omission of the Hawaiian rate has the most significant effect ($p = 0.10$ whereas $p \geq 0.34$ for all other cases). Thus the set of angular velocities appears to be robust.

If the rates are omitted, a set of angular velocities can be estimated from the trend-only data set, which has an uncertainty of the component in angular velocity parallel to the Pacific-hotspot pole that is ± 0.62 deg Myr^{-1} (95 per cent confidence), which is six times greater than that for HS3-NUVEL1A.

Net-rotation of the lithosphere

NNR-NUVEL1A is a set of angular velocities, consistent with the NUVEL-1A relative plate velocities, of the plates in a reference

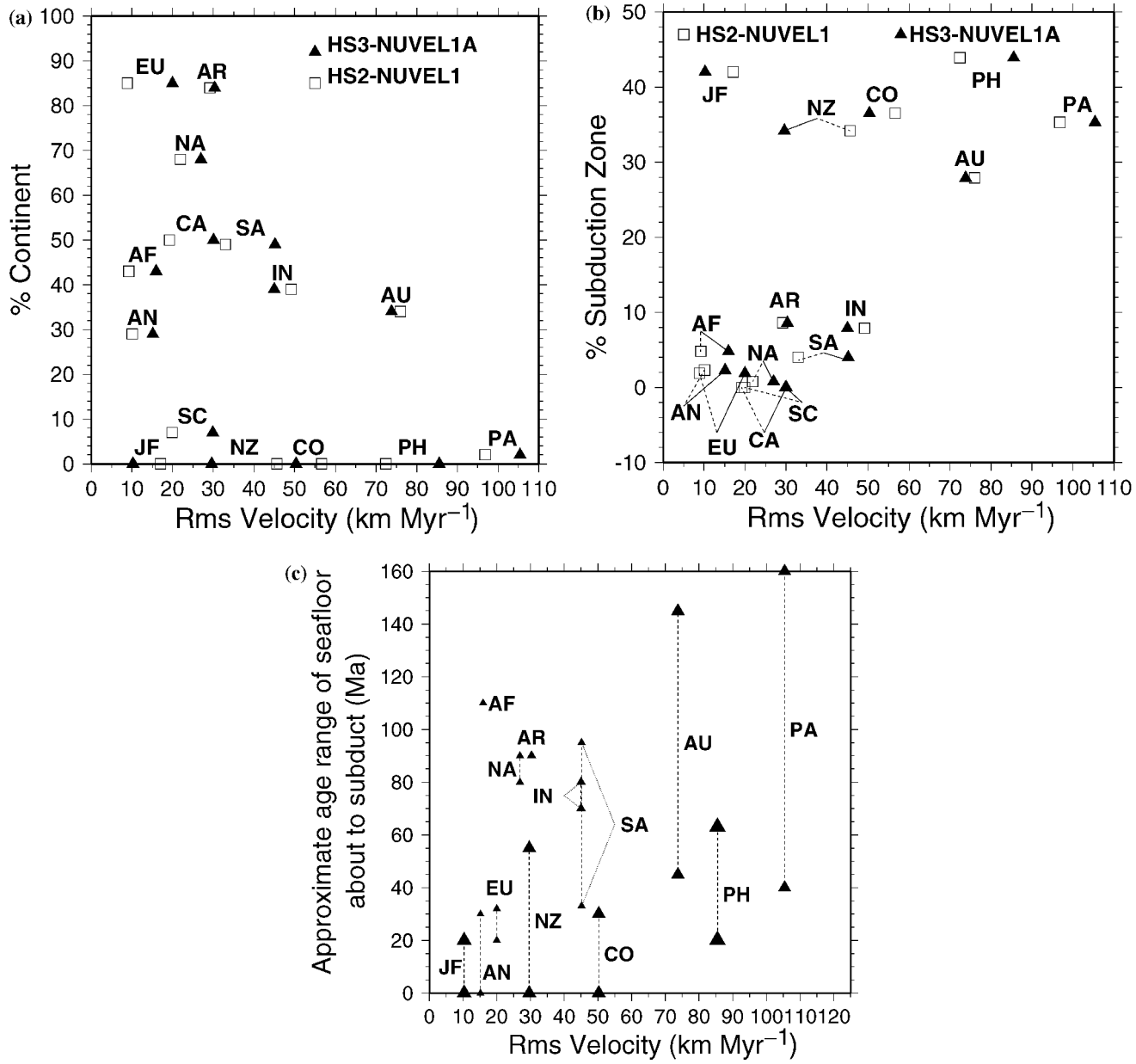

Figure 3. Plate parameter plotted against rms velocity. Filled triangles show velocities from HS3-NUVEL1A; open squares show velocities from HS2-NUVEL1. (a) The percentage of the plate area that is continental, as defined by the 2-km-deep contour, is plotted against rms velocity. (b) The approximate percentage of plate boundary that is attached to a subducting slab (based on the subduction zones marked in Fig. 4) is plotted against rms velocity. (c) The approximate range of the age of the seafloor about to be subducted (read off of map of Mueller *et al.* (1996), except that of Africa, which is from Jarrard (1986), and that of Eurasia, which was read off of the map of Cande *et al.* (1989)) is plotted against rms velocity. Symbol size increases with increasing percentage of boundary attached to a slab.

frame in which there is no net rotation of the lithosphere (Argus & Gordon 1991; DeMets *et al.* 1994). The uncertainty of the angular velocity of a plate relative to the no-net-rotation reference frame (Gripp 1994) is small relative to the uncertainty of the angular velocity of the same plate relative to the hotspots. It is thus neglected below. The angular velocity of any plate relative to the NNR-NUVEL1A no-net-rotation reference frame differs significantly from the corresponding angular velocity relative to the hotspots specified in HS3-NUVEL1A ($p = 8 \times 10^{-17}$) (Table 12). Thus, the lithosphere has a net rotation relative to the hotspots of 0.44 ± 0.11 deg Myr^{-1} (95 per cent confidence level here and below) about a pole of 56°S, 70°E, faster than the net rotation (0.33 ± 0.17 deg Myr^{-1}) for HS2-NUVEL1 (Argus & Gordon 1991). The newly determined net rotation can be compared with predictions from models for plate driving forces. For example, Cocksworth (1995) used the NUVEL-1 relative plate motions as observables to invert for the relative contribution of plate driving forces. He predicted that the net rotation of the lithosphere relative to the deep mantle should be 0.252 deg Myr^{-1} about 59°S, 48°E (after a small correction to bring the prediction to consistency with NUVEL-1A). This prediction lies outside the 3-D 95 per cent confidence region ($p = 4 \times 10^{-4}$), but the predicted pole does lie inside the 2-D 95 per cent confidence ellipsoid for the pole location. The statistical significance of the net rotation depends critically on

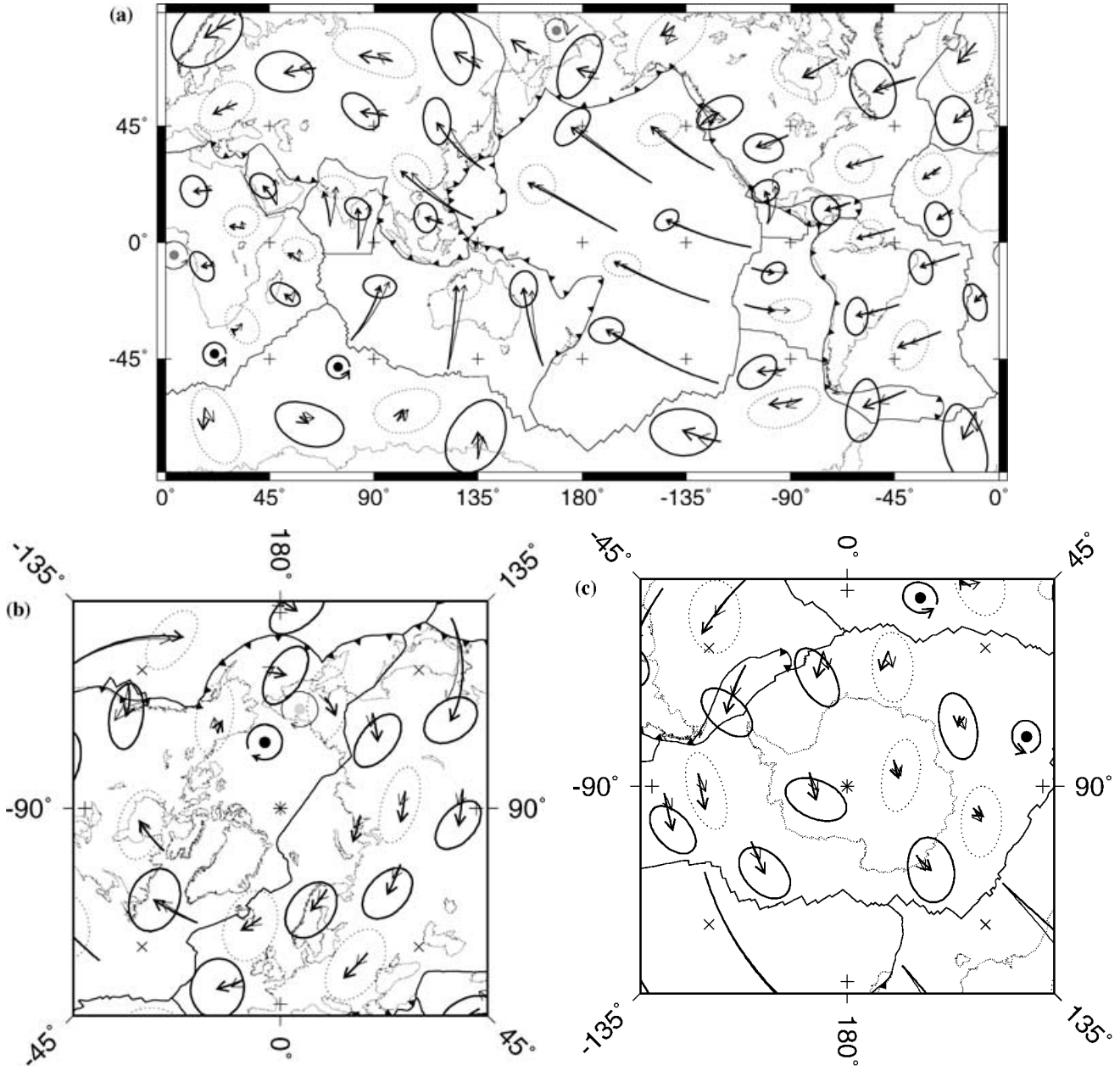

Figure 4. Plate velocities relative to the hotspots. Each arrow shows the displacement path of a point on a plate if the plate were to maintain its current angular velocity relative to the hotspots for 40 Myr. Ellipses show the 2-D 95 per cent confidence ellipse of velocity multiplied by 40 Myr. Thick arrows with thick confidence ellipses are determined from the HS3-NUVEL1A angular velocities. Thin arrows with dotted confidence ellipses are determined from the HS2-NUVEL1 angular velocities. Filled circles show the pole (or antipole) locations if the pole (or antipole) lies on its own plate; stippled circles show those for HS2-NUVEL1 and black circles show those for HS3-NUVEL1A. Medium solid lines are the approximate plate boundaries. Barbed lines show the approximate location of subduction zones with barbs on the overthrust plate. (a) Mercator projection. (b) Lambert's azimuthal equal area projection about north pole. (c) Lambert's azimuthal equal area projection about south pole.

the inclusion of volcanic propagation rates. Its magnitude would be 0.41 ± 0.61 deg Myr^{-1} if the rates were excluded.

COMPARISON WITH PRIOR RESULTS

Uncertainties in, and information content of, trends and rates

For the HS3 data set, trend standard errors on the Pacific Plate range from $\pm 6.3^\circ$ for 600-km-long Hawaii to $\pm 35.9^\circ$ for 90-km-long Pitcairn (Table 3). In contrast, prior data sets have Pacific Plate standard errors ranging from $\pm 10^\circ$ to $\pm 20^\circ$ (Table 13). For the HS3 data set, trend standard errors on the Nazca Plate range from $\pm 14.0^\circ$ for Juan Fernandez to $\pm 40.9^\circ$ for Galapagos. This compares with $\pm 10^\circ$ to $\pm 20^\circ$ in prior data sets. Relative to previously assigned uncertainties, our length-dependent trend uncertainties lead to the following:

(1) a greater variation in assigned standard errors

Table 13. Trend uncertainties and data importance for a selection of models of current plate motion relative to the hotspots.

Plate	Hotspot	HS3-NUVEL1A		Ricard *et al.* (1991)		Pollitz (1986)		Minster & Jordan (1978)		Minster *et al.* (1974)	
		σ_{trend}	I[b]	σ_{trend}	I[b]	σ_{trend}	I[b]	σ_{trend}	I[b]	σ_{trend}	I[b]
AF	Ascension	—	—	±10°	0.60	—	—	—	—	±20°	0.07
AF	Bouvet	—	—	—	—	—	—	—	—	±10°	0.31
AF	Comores	±34.0°	*NM*[c]	—	—	—	—	—	—	—	—
AF	Réunion	±15.8°	*1.00*	±10°	0.77	—	—	—	—	±10°	0.54
AF	St. Peter and Paul's rocks	—	—	—	—	—	—	—	—	±30°	0.04
AF	Tristan da Cuhna	—	—	±20°	0.17	—	—	—	—	±20°	0.06
AN	Kerguelen	—	—	—	—	—	—	—	—	±20°	0.29
AN	Prince Edward	—	—	—	—	—	—	—	—	±20°	0.84
AU	Lord Howe	±10.6°	*0.18*	—	—	—	—	—	—	—	—
AU	Tasmantid	±8.9°	*0.22*	—	—	—	—	—	—	—	—
CO	Galapagos	—	—	±10°	0.11	—	—	±10°	0.17	±10°	0.02
EU	Iceland	—	—	—	—	—	—	—	—	±30°	0.08
JF	Cobb	±45.6°[d]	*0.08*	—	—	—	—	—	—		
NA	Iceland	—	—	±30°	0.18	—	—	—	—	±20°	0.14°
NA	Raton	—	—	—	—	—	—	—	—	±30°	0.02
NA	**Yellowstone**	±23.8°	**0.20**	±20°	0.35	—	—	±20°	0.46	±20°	0.04
NZ	**Easter**	±31.7°[d]	**0.10**	—	—	—	—	—	—	±20°	0.00
NZ	**Galapagos**	±40.9°[d]	**0.13**	±10°	0.20	±14.0°	0.36	±10°	0.48	±10°	0.02
NZ	**Juan Fernandez**	±14.0°	**0.47**	—	—	±15.0°	0.24	—	—	—	—
PA	Bowie	±22.3°	*0.15*	—	—	—	—	—	—	—	—
PA	Cobb	±26.1°	*0.09*	±15	0.03	—	—	±15°	0.39	±20°	0.01°
PA	Easter	—	—	—	—	—	—	—	—	±20°	0.00
PA	Eastern Caroline	±6.8°	*0.27*	—	—	±10.0°	0.18	—	—	—	—
PA	**Hawaii**	±6.3°	**0.49**	±10°	0.02	±10.0°	0.15	±10°	0.29	±10°	0.01
PA	Islas Revillagigedo	±14.5°[d]	*0.06*	—	—	—	—	—	—	—	—
PA	Louisville (off-ridge)	±34.8°	*0.01*	—	—	—	—	—	—	—	—
PA	Louisville (on-ridge)	±26°[d]	*0.02*	—	—	—	—	—	—	—	—
PA	**Macdonald**	±8.7°	**0.13**	±15°	0.02	±10.0°	0.06	±15°	0.07	±10°	0.02
PA	**Marquesas**	±12.3°	**0.07**	±15°	0.01	—	—	±15°	0.08	—	—
PA	**Pitcairn**	±35.9°	**0.01**	±15°	0.02	±10.0°	0.06	±15°	0.06	—	—
PA	**Samoa**	±11.2°	**0.12**	—	—	—	—	—	—	—	—
PA	**Society**	±7.8°	**0.18**	±15°	0.01	±10.0°	0.06	±15°	0.08	—	—
SA	**Martin Vaz**	±52.7°	**0.04**	—	—	—	—	—	—	±10°	0.45
SA	Tristan da Cuhna	—	—	±30°	0.15	—	—	—	—	±30°	0.04
AF	Sum of AF trends	—	—	Various	1.54	—	—	—	—	Various	1.02
AN	Sum of AN trends	—	—	—	—	—	—	—	—	Various	1.13
CO	Sum of CO trends	—	—	Various	0.11	—	—	Various	0.17	Various	0.02
EU	Sum of EUtrends	—	—	—	—	—	—	—	—	Various	0.08
NA	Sum of NA trends	Various	**0.20**	Various	0.53	—	—	Various	0.46	Various	0.20
NZ	Sum of NZ trends	Various	**0.70**	Various	0.20	Various	0.60	Various	0.48	Various	0.02
PA	Sum of PA trends	Various	**1.00**	Various	0.11	Various	0.51	Various	0.97	Various	0.04
SA	Sum of SA trends	Various	**0.04**	Various	0.15	—	—	—	—	Various	0.49
	Sum of non-PA trends	Various	**0.94**	Various	2.53	Various	0.60	Various	1.11	Various	2.96

[a] Bold hotspots were used in HS3-NUVEL1A.
[b] I is data importance. A data importance in bold is the data importance the trend has in HS3-NUVEL1A. A data importance in italics is the data importance the trend would have had in HS3-NUVEL1A if it had not been excluded from that data set. Data importances were not published in Pollitz (1986) and Ricard *et al.* (1991), but were calculated herein.
[c] NM = 'not meaningful.' Importance could not be meaningfully calculated.
[d] Young seafloor width standard error is ±55 km.

(2) smaller uncertainties for the trends on the Pacific Plate, especially for the Hawaiian trend, and

(3) larger uncertainties for the trends on other (less fast moving) plates (Table 13).

Our results indicate that the uncertainties assigned to trends for the slow-moving plates in prior work were too small and in some prior data sets unrealistically small (*cf.* Ricard *et al.* 1991) (Table 13). The rates in HS3 have a total data importance of 1.1 (Table 14).

The greater weighting given herein to Pacific Plate trends seems appropriate. For a hotspot segment to have a discernible trend, its length should be at least twice its width. The $\pm 1\sigma$ width of a typical hotspot track is 66 km (equal to twice the standard deviation). Thus a discernible trend requires a length of ≈130 km or more. For the fastest moving plate, the Pacific Plate, which moves ≈100 km Myr^{-1}, it takes 1.3 Myr to build a track this long. For a plate with the median plate speed (30 km Myr^{-1}), it takes 4.3 Myr. For a slow moving plate (10–20 km Myr^{-1}), it takes 6.5 to 13 Myr. Thus, useful hotspot tracks for the HS3-NUVEL1A set of angular velocities with its ≈5.8 Myr duration come dominantly from the fastest-moving plate (the Pacific Plate), with less useful tracks from plates moving at about the median speed (South American, Nazcan

Table 14. Rate uncertainties and data importance for a selection of models of current plate motion relative to the hotspots.

Plate	Hotspot	HS3-NUVEL1A		Ricard *et al.* (1991)		Pollitz (1986)		(Minster & Jordan 1978)		Minster *et al.* (1974)	
		σ_{rate} (km Myr^{-1})	I^b	σ_{rate} (km Myr^{-1})	I^b	σ_{rate} (km Myr^{-1})	I^b	σ_{rate} (km Myr^{-1})	I^b	σ_{rate} (km Myr^{-1})	I^b
NA	Yellowstone	±14	*0.01*	—	—	—	—	—	—	—	—
NZ	Galapagos	±14	*0.16*	—	—	—	—	—	—	—	—
PA	Bowie	—	—	—	—	±4.0	0.75	—	—	—	—
PA	Cobb	±19	*0.06*	—	—	—	—	—	—	—	—
PA	Hawaii	±5	**0.74**	±20	0.09	±2.5	0.81	±20	0.14	—	—
PA	Macdonald	—	—	±20	0.05	±15.6	0.08	±20	0.24	—	—
PA	Marquesas	—	—	±20	0.09	±17.5	0.04	±20	0.20	—	—
PA	Pitcairn	—	—	±20	0.04	—	—	±30	0.10	—	—
PA	Society	±9	**0.34**	±20	0.08	±9.7	0.20	± 20	0.22	—	—
PA	Sum of PA rates	Various	**1.08**	Various	0.35	Various	1.88	Various	0.90	—	—

Same conventions as Table 13.

and North American plates) and no useful tracks from slow-moving plates.

Differences between HS3-NUVEL1A and HS2-NUVEL1

The volume of the 3-D error ellipsoid of HS3-NUVEL1A is about half that of HS2-NUVEL1. Nine of fourteen of the HS2-NUVEL1 angular velocities lie outside the 95 per cent confidence region of the corresponding HS3-NUVEL1A angular velocity (Table 12). However, all fourteen of the HS3-NUVEL1A angular velocities (with counterparts in HS2-NUVEL1) lie inside the 95 per cent confidence region of the corresponding HS2-NUVEL1 angular velocity. The vector difference between the angular velocity of a plate relative to the hotspots in HS3-NUVEL1A and its counterpart in HS2-NUVEL1 varies from plate to plate. The largest difference (a vector with a length of 0.17 deg Myr^{-1}) is for the Cocos Plate, which is statistically significant ($p = 5 \times 10^{-3}$) and the smallest difference (0.08 deg Myr^{-1}) is for the Pacific Plate, which is statistically insignificant ($p = 0.32$) (Fig. 4, Table 12).

These changes can be thought of as having two components. The first component is the change in assumed relative angular velocities. The change in vector length of an angular velocity relative to the Pacific Plate in NUVEL-1 and the corresponding angular velocity in NUVEL-1A varies from a high of 0.09 deg Myr^{-1} for the Cocos Plate to a low of 0.02 deg Myr^{-1} for the Juan de Fuca Plate. The second component is the change of the Pacific Plate angular velocity between HS2-NUVEL1 and HS3-NUVEL1A, which may be caused by several factors including the following:

(1) Volcanic propagation rates were fit by the Chase (1972) rate fitting function in determining HS2-NUVEL1, but by the Minster *et al.* (1974) fitting function in determining HS3-NUVEL1A.

(2) The set of relative plate angular velocities was changed from the NUVEL-1 angular velocities in HS2-NUVEL1 to the (4.38 per cent) smaller NUVEL-1A angular velocities in HS3-NUVEL1A.

(3) The data set of volcano trends and propagation rates, along with their assigned uncertainties, was revised.

Numerical experiments indicate that the third factor, the revisions to the volcanic trends, propagation rates and their associated uncertainties has an effect many times greater than the other two factors. The size of the effect of the third factor is indicated by two numerical experiments. First, we combine the HS3 data set with the NUVEL-1 angular velocities using the Chase rate fitting function and compare it with HS2-NUVEL1 (which was determined using the Chase rate fitting function). The resulting Pacific-hotspot rate of rotation is 0.08 deg Myr^{-1} higher, and the calculated rate at Hawaii is 9 km Myr^{-1} higher, than in HS2-NUVEL1. Second, we combine the HS2 data set with the NUVEL-1A angular velocities using the Minster *et al.* (1974) fitting function to compare it with HS3-NUVEL1A (which was determined using the Minster *et al.* (1974) rate fitting function). The resulting Pacific-hotspot rate of rotation is 0.11 deg Myr^{-1} lower, and the calculated rate at Hawaii is 12 km Myr^{-1} lower, than in HS3-NUVEL1A. These changes are as large or larger than those between HS2-NUVEL1 and HS3-NUVEL1A.

Many changes to the data contribute to the speed up of the estimated Pacific Plate angular velocity. A key change, however, is the change between HS2 and HS3 data sets of the observed Hawaiian rate and its uncertainty. In HS2, the observed Hawaiian rate is 100 ± 20 km Myr^{-1} ($\pm 1\sigma$), whereas in HS3, it is 108 ± 5 km Myr^{-1} ($\pm 1\sigma$). Making this single change to the HS2-NUVEL1 data set would produce an increase in the estimated Pacific Plate rate of rotation of 0.09 deg Myr^{-1} and increase the calculated rate at Hawaii by 10 km Myr^{-1}, which is more than sufficient to account for the entire change in Pacific Plate rotation rate between HS2-NUVEL1 and HS3-NUVEL1A.

Pacific Plate angular velocity

The Pacific Plate hotspot angular velocities estimated by Minster & Jordan (1978), Pollitz (1986) and Gripp & Gordon (1990) (both for NUVEL-1 and rescaled to NUVEL-1A) all lie within the 95 per cent confidence ellipsoid of HS3-NUVEL1A (Table 15, Fig. 5). Perhaps surprisingly, the recent estimate by Wessel & Kroenke (1997) lies far outside the 95 per cent confidence ellipsoid of HS3-NUVEL1A ($p < 10^{-41}$). Their pole of rotation lies 55° from that of HS3-NUVEL1A and their rotation rate is 0.14 deg Myr^{-1} faster (Fig. 5). The length of the vector difference between their angular velocity and the Pacific Plate angular velocity of HS3-NUVEL1A exceeds the length of the latter (Table 15). Wessel & Kroenke's (1997) pole is so different from that of HS3-NUVEL1A because their estimate is heavily weighted towards fitting the active to 3 Ma trend of Hawaii at the cost of poorly fitting nearly all other hotspot trends that we use. Fig. 6 shows that their angular velocity predicts directions of motion that have a median misfit to the trends of other chains of ≈50°, which is huge by any standard.

Table 15. Other estimates of the angular velocity of the Pacific plate relative to the hotspots.

Model	Instant or Finite[a]	Pacific relative to hotspots = $\boldsymbol{\omega}$			$\lvert\boldsymbol{\omega}_{HS3} - \boldsymbol{\omega}\rvert$		$\lvert\boldsymbol{\omega}_{HS3T} - \boldsymbol{\omega}\rvert$ $p(\chi^2(\Delta\omega))^c$
		°N	°E	deg Myr^{-1}	deg Myr^{-1}	$p(\chi^2(\Delta\omega))^c$	
active to 5 Ma HS3-NUVEL1A	Instant	−61.467	90.326	1.0613	–	–	96%
active to 5 Ma trend-only, HS3T-NUVEL1A	Instant	−60.517	87.556	1.0273	0.0453	74%	–
NNR-NUVEL1A (Argus & Gordon 1991)	Instant	−63.037	107.360	0.6411	0.4359	**8×10^{-17}**	29%
0–1 Ma Epp (1978)	Finite	−36	104	0.84	0.51	**4×10^{-16}**	**2×10^{-9}**
0–3 Ma Wessel & Kroenke (1997)	Finite	−25.00	153.00	1.2	1.1	**$<10^{-43}$**	**$<10^{-43}$**
0–3 Ma Petronotis & Gordon (1999)	Finite	−61.000	85.000	1.000	0.077	25%	97%
0-(3.2–5) Ma Pollitz (1986)	Instant	−61	85	0.99	0.09	18%	97%
0–4 Ma Harada & Hamano (2000)	Finite	−40.90	75.20	0.9006	0.4142	**3×10^{-15}**	**3×10^{-5}**
0–5 Ma Petronotis & Gordon (1999)	Finite	61.700	97.200	0.960	0.117	23%	58%
0–10 Ma AM1-2 (Minster & Jordan 1978)	Instant	−61.66	97.19	0.967	0.111	28%	57%
0–10 Ma HS2-NUVEL1 (Gripp & Gordon 1990)	Instant	−60.2	90.0	0.98	0.08	32%	98%
0–10 Ma HS2-NUVEL1 trend-only	Instant	−61.0	92.7	0.88	0.18	**2×10^{-3}**	91%
0–10 Ma HS2-NUVEL1A	Instant	−59.918	89.687	0.9465	0.1181	7%	98%
0-(up to 10's of Ma) AM1 Minster *et al.* (1974)	Instant	−67.3	120.6	0.83	0.33	**3×10^{-6}**	**7×10^{-3}**
0-(up to 10's of Ma) Ricard *et al.* (1991)	Instant	−62	102	0.79	0.29	**7×10^{-7}**	41%
1–15 Ma Epp (1978)	Finite	−65	140	0.86	0.42	**4×10^{-9}**	**7×10^{-7}**
3.0–15.1 Ma Wessel & Kroenke (1997)	Finite	−71.00	92.50	1.09	0.18	10%	**4%**
5–20 Ma Petronotis & Gordon (1999)	Finite	−69.754	109.527	0.950	0.228	**1%**	**2%**
0–18 Ma Fleitout & Moriceau (1992)	Finite	−72.15	101.87	0.802	0.32	**7×10^{-8}**	12%
0–20 Ma Petronotis & Gordon (1999)	Finite	−68.000	105.000	0.950	0.193	**4%**	9%
0–20 Ma Harada & Hamano (2000)	Finite	−64.00	83.50	0.8220	0.2481	**2×10^{-7}**	71%
0–25 Ma Lonsdale (1988)	Finite	−75	120	0.88	0.34	**7×10^{-6}**	**2×10^{-3}**
19.9–43.1 Ma Wessel & Kroenke (1997)	Finite	−57.17	117.52	0.53 [b]	0.56	**2×10^{-27}**	**5%**
20–43 Ma Petronotis & Gordon (1999)	Finite	−55.431	132.455	0.526 [b]	0.609	**4×10^{-29}**	**2×10^{-3}**
23–42 Ma Epp (1978)	Finite	−59	126	0.4 [b]	0.7	**2×10^{-43}**	6%
24–43 Ma Fleitout & Moriceau (1992)	Finite	−54	122	0.643 [b]	0.494	**4×10^{-18}**	**1×10^{-3}**
0–42 Ma Duncan & Clague (1985)	Finite	−68.0	105.0	0.72 [b]	0.37	**2×10^{-11}**	29%
0–43 Ma Watts *et al.* (1988)	Finite	−65	120	0.70 [b]	0.41	**1×10^{-12}**	**3%**
0–43 Ma Fleitout & Moriceau (1992)	Finite	−66.09	119.37	0.724 [b]	0.395	**3×10^{-11}**	**3%**
0–43 Ma Petronotis & Gordon (1999)	Finite	−64.200	121.600	0.698 [b]	0.422	**6×10^{-13}**	**2%**
0–42 Ma Harada & Hamano (2000)	Finite	−65.80	110.20	0.6630 [b]	0.4232	**3×10^{-15}**	22%

[a] Instant/Finite refers to whether the model is an instantaneous velocity or finite displacement solution. Finite rotations were approximated as angular velocities by dividing the rotation angle by the given duration of the time interval, except for models including the Hawaiian-Emperor bend, which was rescaled to 47 Ma (see below).

[b] Rotation rate rescaled to a 47 Ma Hawaii-Emperor bend (Sharp & Clague 1999).

[c] $p(\chi^2_\nu(\Delta\omega))$ is the probability of obtaining the data as different or more different as the data used herein if the predictions of the specified angular velocity are true.

Probabilities of $\leq$5% are printed in bold.

The covariance matrix of the active to 5 Ma trend-only (HS3T-NUVEL1A) set of angular velocities in Cartesian coordinates and in units of 10^{-10} radians^2 Myr^{-2} is

$$\begin{bmatrix} \sigma_x^2 & \sigma_{yx}^2 & \sigma_{zx}^2 \\ \sigma_{xy}^2 & \sigma_y^2 & \sigma_{zy}^2 \\ \sigma_{xz}^2 & \sigma_{yz}^2 & \sigma_z^2 \end{bmatrix} = \begin{bmatrix} 10221 & 13820 & -18498 \\ 13820 & 98021 & -132363 \\ -18498 & -132363 & 225893 \end{bmatrix}.$$

MOTION BETWEEN HOTSPOTS

Our angular velocities are estimated assuming that the hotspots are fixed with respect to one another. This assumption is, at best, an approximation, but one that allows us to formulate and to quantitatively test a variety of hypotheses.

Active to 5.0 Ma (HS3 time interval)

The difference between each observed trend (or rate) and the same trend (or rate) predicted from a set of angular velocities, determined after the removal of that one trend (or rate), provides a way to examine how well each datum agrees with the rest of the data. No datum is misfit outside the combined 95 per cent confidence limit of the predicted and observed trend (or rate) (Table 16, column 4). The misfits, when expressed as a component of velocity relative to the other hotspots, range from a low of 3 ± 145 km Myr^{-1} (95 per cent confidence limit here and below) for Pitcairn to a high of 40 ± 48 km Myr^{-1} for Marquesas (Table 16, column 9). The least uncertain component of motion between hotspots corresponds to the Hawaiian rate, 16 ± 19 km Myr^{-1} parallel to its observed trend. The most uncertain component of motion between hotspots corresponds to the Pitcairn trend, 3 ± 145 km Myr^{-1} perpendicular to its observed trend. Typical uncertainties are $\pm$20 to $\pm$40 km Myr^{-1}, which reflect the resolution of our data and resulting model. Thus our finding of insignificant motion between hotspots is not inconsistent with the 10–20 km Myr^{-1} motion found by Molnar & Stock (1987) between the Hawaiian hotspot and the hotspots in the Atlantic and Indian oceans over the past 50–65 Myr.

Four 4-Myr-long time intervals

We also repeated these same tests for four data sets with 4 Myr durations: active to 3.2 Ma, 0.0 to 4.0 Ma, 1.0 to 5.0 Ma and 2.0 to 6.0 Ma. For the resulting four global models, χ^2_{hotspot} indicates consistency with the assumption of fixed hotspots ($0.09 \leq p \leq 0.76$; Table 17).

For each of the four data sets, the difference between each observed trend (or rate) and the same trend (or rate) predicted from a set of angular velocities, determined after the removal of that one trend (or rate), was examined. Out of the 43 possible tests, two indicated significant motion: the Hawaiian trend for 2.0 to 6.0 Ma and the Marquesas trend for 2.0 to 6.0 Ma (Table 17). Because we used the 95 per cent confidence level, for each individual test there is a 5% chance of wrongly concluding that the null hypothesis (i.e. that there is no significant motion between hotspots) is false when it is in fact true. Given that we employed this test 43 times, the expected number of false positives is two, which is consistent with the two positives that we find. Thus, these results give no evidence for motion between hotspots.

CHANGE IN PACIFIC PLATE MOTION RELATIVE TO THE HOTSPOTS

Hawaii versus the rest of the globe

Interpretation of recent changes in plate motion are very strongly influenced by the alignment of young volcanoes in the Hawaiian chain (Epp 1978; Cox & Engebretson 1985; Engebretson *et al.* 1985; Pollitz 1986; Wessel & Kroenke 1997). Here we use sets of hotspot rates and trends to test the consistency between the Hawaiian track and tracks from the rest of the globe. Specifically we examine the trend of the Hawaiian track over four overlapping 4-Myr-long intervals, 2.0 to 6.0 Ma, 1.0 to 5.0 Ma, 0.0 to 4.0 Ma and active to 3.2 Ma, for which the observed Hawaiian trend respectively is $278^\circ \pm 15^\circ$, $293^\circ \pm 9^\circ$, $302^\circ \pm 8^\circ$ and $314^\circ \pm 9^\circ$ ($\pm 1\sigma$). Thus, between the 2.0 to 6.0 Ma and the active to 3.2 Ma time intervals, the observed Hawaiian trend rotates $36^\circ \pm 17^\circ$ ($\pm 1\sigma$) clockwise (CW) (Table 17). We compare this with the trend of Hawaii predicted from the rest of the global data for the same four time intervals, for which the predicted Hawaiian trend respectively is $315^\circ \pm 10^\circ$, $312^\circ \pm 9^\circ$, $294^\circ \pm 8^\circ$ and $290^\circ \pm 8^\circ$ ($\pm 1\sigma$). Thus, while the observed trend rotates $36^\circ \pm 17^\circ$ clockwise, the predicted trend rotates $25^\circ \pm 13^\circ$ anticlockwise. The difference between observed and predicted trends progresses over the same four time intervals as follows: $-38^\circ \pm 35^\circ$ CW, $-19^\circ \pm 24^\circ$ CW, $+8^\circ \pm 22^\circ$ CW and $+24^\circ \pm 24^\circ$ CW (95 per cent confidence limits). Thus, during the past few millions years, the Hawaiian trend is clockwise of that predicted from the rest of the global hotspot tracks, but insignificantly so. For the prior few millions years, the Hawaiian trend is anticlockwise of that predicted and the difference is insignificant or barely significant, depending on the precise time interval considered. These results suggest that the change in trend over the past $\approx$6 Myr is local to the Hawaiian track and probably within its uncertainty given the observed width of hotspot tracks. These results are not inconsistent, however, with interpretations that postulate a change in Pacific hotspot motion at or before 5 Ma (Cox & Engebretson 1985; Engebretson *et al.* 1985; Pollitz 1986; Cande *et al.* 1995), but contradict interpretations that place the change at about 3 Ma (Harbert & Cox 1989; Wessel & Kroenke 1997). The essential conclusion is that great caution should be exercised in interpreting changes in plate motion based on the short-term changes in trend along a single hotspot track.

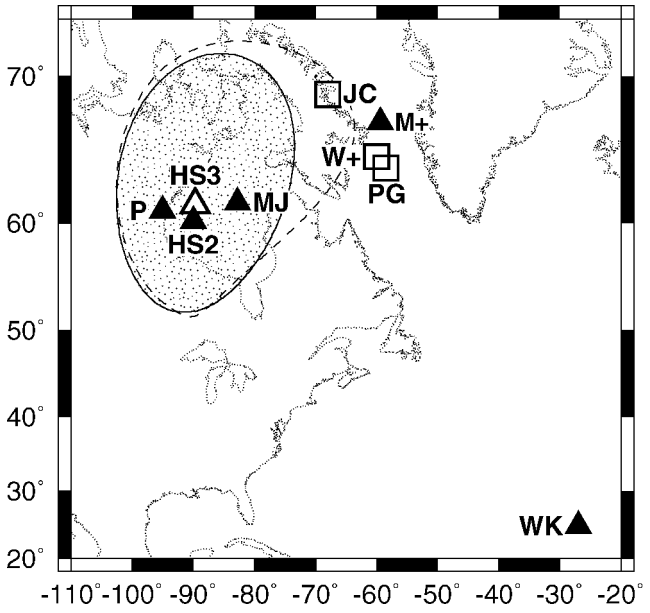

Figure 5. Pole locations for the motion of the hotspots relative to the Pacific Plate for angular velocities and finite rotations selected from Table 15. Open triangle is the angular velocity from HS3-NUVEL1A; the shaded ellipsoid is its 2-D 95 per cent confidence ellipsoid from linear propagation of errors and the dashed line is its 2-D 95 per cent confidence limit from exact error propagation. Solid triangles show estimated poles of current plate motion relative to the hotspots (P, Pollitz (1986); HS2, Gripp & Gordon (1990); MJ, Minster & Jordan (1978); M+, Minster *et al.* (1974); WK, Wessel & Kroenke (1997)). Open squares mark poles of finite rotations with time intervals of 0 to 47 Ma selected from Table 15 (PG, Petronotis & Gordon (1999); W+, Watts *et al.* (1988); JC, Jarrard & Clague (1977)).

The Marquesas chain, which lies on the same plate, makes an interesting contrast with Hawaii. Its length is only 360 km, which is shorter than the length used to estimate three of the four Hawaiian trends. During the 2.0 to 6.0 Ma time interval, the 360-km-long observed Marquesas trend is $44^\circ \pm 26^\circ$ CW of the predicted trend. This clockwise misfit of the Marquesas hotspot track relative to other hotspots is coeval with the anticlockwise misfit of the Hawaiian track relative to the other hotspots.

Late Miocene change in Pacific hotspot motion

The most recent clearly resolvable change in Pacific–Antarctic motion occurred at 6–8 Ma (Cande *et al.* 1995; Atwater & Stock 1998). Was this change accompanied by a resolvable change in the velocity of the Pacific Plate relative to the hotspots?

Because appropriate error estimates are unavailable for finite rotations of the Pacific Plate relative to the hotspots, the most one can determine is whether a past pole and rate of rotation lie inside the HS3-NUVEL1A 95 per cent confidence ellipsoid (Table 15). All finite rotations describing Pacific hotspot motion along the entire Hawaiian Ridge lie outside the 95 per cent confidence ellipsoid of HS3-NUVEL1A when approximated as an angular velocity that has stayed fixed in orientation for tens of millions of years ($p \leq 2 \times 10^{-11}$) (Table 15; Fig. 5). The differences in rotation rate are large, with the HS3-NUVEL1A rate of 1.06 deg Myr^{-1} being, for example, approximately 50 per cent faster than the average rotation rate since 47 Ma of the Pacific hotspot rotations of Watts *et al.* (1988) or of Petronotis & Gordon (1999). On the other hand, the poles of

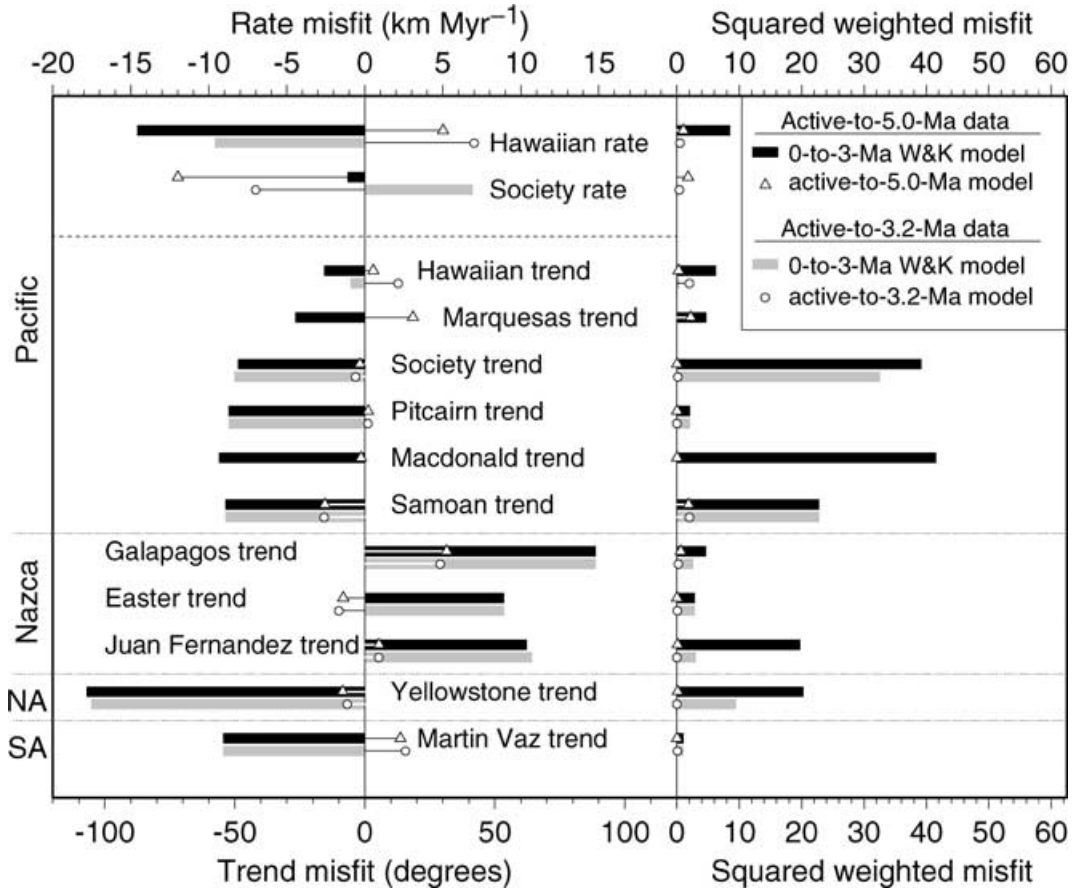

Figure 6. Misfit to plate motion data. Left column: misfits to rates or trends. Right column: squared weighted misfit (square of the ratio of the misfit to its assigned 1σ error). Data from active to 5 Ma are compared with (1) values predicted by the Pacific-hotspot angular velocity of Wessel & Kroenke (1997) (solid black bar) combined with the relative plate velocities of NUVEL-1A and (2) values calculated from the angular velocities of HS3-NUVEL1A (open triangle and thin lines). Data from active to 3 Ma are compared with (1) values predicted from the Pacific hotspot angular velocity of Wessel & Kroenke (1997) (stippled bar) combined with the relative plate velocities of NUVEL-1A and (2) values calculated angular velocities fit herein to these data (open circles and thin lines). Wessel & Kroenke's angular velocity poorly fits the active to 5 Ma data, with huge (3 to 6 σ) misfits to half a dozen observations. In contrast, HS3-NUVEL1A fits all the active to 5 Ma data within their uncertainties. Wessel & Kroenke's angular velocity also poorly fits the active to 3.2 Ma data, with huge (3 to 6 σ) misfits to three observations. Not only are the non-Hawaiian Pacific trends poorly fit, with the Society, Pitcairn and Samoa trends each being misfit by 50°, but so are non-Pacific trends, with the Yellowstone trend being misfit by more than 100° and Martin Vaz being misfit by 50°. In contrast, the angular velocity estimated herein fits all the active to 3.2 Ma data within their uncertainties.

rotation for 0–47 Ma lie near the edge of the 95 per cent confidence region for the current pole of rotation (Fig. 5). These 0–47 Ma poles lie outside the confidence region, but if and when their uncertainties are estimated, we think it is unlikely that the 0–47 Ma poles will prove to differ significantly from the current pole of rotation. Thus, no statistically significant change in direction is resolvable from only the hotspot tracks, although there is other evidence to support a change in direction of motion at 6–8 Ma (Engebretson *et al.* 1985; Cox & Engebretson 1985; Cande *et al.* 1995; Atwater & Stock 1998). The volcanic propagation rates strongly indicate, however, that the Pacific Plate has sped up relative to the hotspots sometime in the past 47 Myr.

SHORT-TERM CHANGES IN TREND

To explain the short-term (≈4 Myr) changes in trend along hotspot tracks, if real, that are not due to changes in plate motion relative to global hotspots, we suggest three end members for the behaviour of the lithosphere and sublithospheric source. First, if the tracks perfectly trace the zone of melting in the shallow sublithospheric source, then over 4 Myr some melting zones may move relative to each other. At Yellowstone, the surface and mantle tracks appear to be parallel at least at the 8 Ma part of the track. For at least 470 km across the 8 Ma track of Yellowstone, the average fast direction of *S* waves (244°, Schutt *et al.* 1998) differs insignificantly from that calculated from HS3-NUVEL1A (249° ± 21° 95 per cent confidence here and below). It also differs insignificantly from the trend predicted with Yellowstone removed from the HS3 data set (252° ± 24°) and from the observed trend (241° ± 47°). More complex patterns of *S*-wave splitting have been observed from isolated measurements in French Polynesia (Russo & Okal 1998) and Hawaii (Russo *et al.* 1998). Second, if the magma in the lithosphere is laterally redirected, then short-term motion between hotspots might be created from an otherwise fixed zone of melting. Flexural stresses, preexisting lithospheric structures, existing volcanoes or lithospheric intrusions might laterally redirect hotspot magma. Hieronymus & Bercovici (1999) have shown that flexural stresses may cause paired volcanic loci to form from a simple source. Based on the distribution of diverse seismic events beneath Kilauea volcano, its magma conduit appears to be subvertical for the first 20 km below the

Table 16. Consistency of HS3-NUVEL1A data when one datum or hotspot is removed[a].

Removed datum or data	Observed length (km)	Calculated duration[b] (Myr)	Misfit[c] ±95%	I[d]	$\Delta\chi^2$[e]	$p(\Delta\chi^2)$[f]	Δv_t[g] or Δv_r[h] ±95% (km Myr^{-1})
Easter	178	5.4	$-9.4 \pm 65.5°$	0.10	0.08	78%	Δv_t -5 ± 36
Galapagos	278[i]	6.0[i]	$36.5 \pm 86.0°$	0.13	0.67	41%	Δv_t 13 ± 28
Hawaiian trend	600	5.8	$7.0 \pm 17.2°$	0.49	0.59	44%	Δv_t 13 ± 31
Hawaiian rate	600	5.8	16 ± 19 km Myr^{-1}	0.74	2.94	9%	Δv_r 16 ± 19
Hawaiian segment	600	5.8	$5.5 \pm 17.3°$	0.49	3.32	19%	Δv_t 9 ± 28
			15 ± 20 km Myr^{-1}	0.74			Δv_r 16 ± 20
Juan Fernandez	264	7.8	$11.0 \pm 36.6°$	0.47	0.30	58%	Δv_t 7 ± 24
Macdonald	429	3.7	$-1.9 \pm 18.3°$	0.13	0.04	84%	Δv_t -4 ± 37
Marquesas	302	2.6	$19.8 \pm 25.0°$	0.07	2.38	12%	Δv_t 40 ± 48
Martin Vaz	50	1.1	$14.3 \pm 105.1°$	0.04	0.07	79%	Δv_t 12 ± 84
Pitcairn	91	0.8	$1.2 \pm 70.6°$	0.01	0.00	96%	Δv_t 3 ± 145
Samoa	334	2.9	$-17.4 \pm 23.3°$	0.12	2.11	15%	Δv_t -35 ± 46
Society trend	479	4.1	$-2.4 \pm 16.9°$	0.18	0.08	78%	Δv_t -5 ± 35
Society rate	479	4.1	-19 ± 21 km Myr^{-1}	0.34	2.88	9%	Δv_r -19 ± 21
Society segment	479	4.1	$-2.4 \pm 16.8°$	0.18	2.96	23%	Δv_t -5 ± 37
			-19 ± 21 km Myr^{-1}	0.34			Δv_r -19 ± 22
Yellowstone	150	5.6	$-10.8 \pm 52.3°$	0.20	0.16	68%	Δv_t -5 ± 24

[a]For HS3-NUVEL1A, $\chi^2_{\text{hotspot}} = 8.0$, $\chi^2_\nu = 0.80$, $\nu = 10$, $p(\chi^2_\nu) = 63$ per cent.
[b]Calculated duration $= l^{\text{obs}}/|\mathbf{v}^{\text{cal}}|$.
[c]Misfit is the observed datum minus the predicted datum.
[d]I is the data importance when estimating the HS3-NUVEL1A set of angular velocities.
[e]$\Delta\chi^2$ is the chi-square of HS3-NUVEL1A minus the chi-square after removing the datum or hotspot in question.
[f]$p(\Delta\chi^2)$ is the probability of obtaining a datum as different or more different as the datum removed if the hotspots are fixed. Differences would be significant only if $p < 5$ per cent.
[g]Δv_t is the component of motion of the removed hotspot perpendicular to its observed trend relative to that predicted from an angular velocity determined after removing that trend/hotspot.
[h]Δv_r is the component of motion of the removed hotspot parallel to its observed trend relative to that predicted from an angular velocity determined after removing that rate/hotspot.
[i]is the observed length of Galapagos, but the duration is calculated using the rescaled length.

volcano, but becomes more subhorizontal at greater depth (Ryan *et al.* 1981; Klein *et al.* 1987). These interpretations, however, should be considered tentative until confirmed both by events recorded during the earliest years of the seismic network and by detailed source and hypocentre characterization of recorded events. Third, if the zone of melting is as broad or broader than the surface width estimated from the dispersion of volcano locations, but the volcanoes form above only part of the melting zone, then the trends measured from the volcanoes might be irregular even if the geometry of the melting zone is time invariant and magma only

Table 17. Select statistical parameters for models with ≈4 Myr durations.

Time Span (Ma)	Observed length (km)	Calculated duration (Myr)	Observed trend ±1σ	Predicted trend ±1σ	Trend misfit ±95%	Calculated trend ±1σ	I	$\Delta\chi^2$	$p(\Delta\chi^2)$	Δv_t ±95 per cent km Myr^{-1}
Hawaiian trend removed										
active-to-3.2	409	4.0	$313.5 \pm 9.2°$	$289.9 \pm 7.7°$	**$23.6 \pm 23.5°$**	$300.6 \pm 6.1°$	0.44	3.6	6%	**43 ± 42**
0.0-to-4.0	492	4.8	$301.9 \pm 7.6°$	$293.5 \pm 8.4°$	$8.4 \pm 22.2°$	$298.6 \pm 5.7°$	0.56	0.5	49%	15 ± 40
1.0-to-5.0	419	4.1	$292.7 \pm 8.9°$	$311.8 \pm 8.8°$	$-19.1 \pm 24.5°$	$301.2 \pm 6.5°$	0.53	2.1	15%	-34 ± 42
2.0-to- 6.0	249	2.4	$277.9 \pm 14.8°$	$315.4 \pm 10.1°$	**$-37.5 \pm 35.2°$**	$305.8 \pm 8.8°$	0.35	5.4	**2%**	**-58 ± 50**
Marquesas trend removed										
active-to-3.2	—	—	—	$291.6 \pm 4.4°$	—	—	—	—	—	—
0.0-to-4.0	116	1.0	$332.1 \pm 29.7°$	$289.2 \pm 4.3°$	$42.9 \pm 58.8°$	$290.3 \pm 4.3°$	0.02	1.9	16%	79 ± 88
1.0-to-5.0	302	2.6	$310.0 \pm 12.3°$	$287.7 \pm 4.9°$	$22.3 \pm 25.9°$	$291.2 \pm 4.8°$	0.15	2.7	10%	46 ± 51
2.0-to- 6.0	359	3.1	$320.8 \pm 10.4°$	$277.3 \pm 8.1°$	**$43.5 \pm 25.9°$**	$296.7 \pm 6.6°$	0.40	9.7	**0.2%**	**77 ± 40**

Same conventions as in Table 16.
Active to 3.2 Ma: $\chi^2_{\text{hotspot}} = 5.6$, $\chi^2_\nu = 0.70$, $\nu = 8$, $p(\chi^2 = 5.6) = 70\%$;
0.0 to 4.0 Ma: $\chi^2_{\text{hotspot}} = 7.9$, $\chi^2_\nu = 0.88$, $\nu = 9$, $p(\chi^2 = 7.9) = 54\%$;
1.0 to 5.0 Ma: $\chi^2_{\text{hotspot}} = 4.2$, $\chi^2_\nu = 0.61$, $\nu = 7$, $p(\chi^2 = 4.2) = 75$ %;
2.0 to 6.0 Ma: $\chi^2_{\text{hotspot}} = 12.3$, $\chi^2_\nu = 1.8$, $\nu = 7$, $p(\chi^2 = 12.3) = 9\%$.
Calculated duration is $l^{\text{obs}}/|\mathbf{v}^{\text{cal}}|$, where $\mathbf{v}^{\text{cal}}$ is calculated from HS3-NUVEL1A.
Values printed in bold either (1) have differences in trend or Δv_t that differ significantly from zero at the ≥95 per cent confidence limit or (2) have probabilities of ≥5 per cent.

moves vertically. At the 8 Ma section of the Yellowstone track, the basalt-covered calderas of the Snake River Plain are underlain in the mantle by a zone of low *P*-wave speed that is 125 km wide and 200 km deep (Saltzer & Humphreys 1997). This width is close to the 130 km width we estimate for hotspot tracks on older lithosphere. Beyond the plain, the rocks have high *P*-wave speed, which Saltzer & Humphreys (1997) suggest is buoyant residuum. It remains unclear, however, how an 8-Myr-old mantle width relates to the zone of melting beneath an active hotspot.

CONCLUSIONS

(1) Over the past ≈5.8 Myr, the average width of hotspot tracks on older lithosphere is ≈130 km ($=4\sigma$), as indicated by the dispersion of volcanoes about the great circles that best fit the Hawaiian, Juan Fernandez, Marquesas, Pitcairn, Samoan and Society tracks. The width of hotspots on young lithosphere may be much wider, ≈220 km, as suggested by the dispersion about the Galapagos track.

(2) These widths are many times greater than the typical 1–5 km transition width of magnetic anomalies due to seafloor spreading (Macdonald 1986) or the 0.5–2 km width of transform fault zones (i.e. the width of the zone of current deformation) (Fox & Gallo 1984, 1986; Searle 1986). Thus current plate motion relative to hotspots can be estimated only with much lower accuracy than can current relative plate motion.

(3) The uncertainties for hotspot trends and rates, which are objectively estimated herein, are mutually consistent with the assumption that hotspots are fixed. Motion between hotspots is statistically insignificant over the past ≈5.8 Myr, with the 95 per cent confidence limit on such motion typically being ±20 to ±40 km Myr^{-1} and the largest confidence limit being ±145 km Myr^{-1}.

(4) The change, if any, in Pacific Plate motion relative to global hotspots at 2 to 3 Ma cannot be resolved from available data. The change in Pacific Plate direction of motion relative to hotspots at 6 to 8 Ma inferred from its change in motion relative to the Antarctic Plate also cannot be statistically significantly resolved from only hotspot tracks.

(5) Hotspot data sets with durations of 6–7 Myr produce stable results, but data sets with durations of 4 Myr or less produce unstable results.

(6) Except for the AM1 angular velocity (Minster *et al.* 1974) and 0–3.0 Ma angular velocity of Wessel & Kroenke (1997), prior estimates of current motion of the Pacific Plate relative to the hotspots differ insignificantly from our new Pacific Plate angular velocity relative to the hotspots. Current Pacific Plate motion relative to the hotspots is about 50 per cent faster than its average over the past 47 Ma (the age of the Hawaiian–Emperor bend; Sharp & Clague 1999), but no statistically significant change in direction of motion is resolvable.

(7) Nine of the fourteen HS2-NUVEL1 angular velocities lie outside the 95 per cent confidence region of the corresponding HS3-NUVEL1A angular velocity, while all fourteen of the HS3-NUVEL1A angular velocities lie inside the 95 per cent confidence region of the corresponding HS2-NUVEL1 angular velocity.

(8) There is a significant net rotation of the lithosphere relative to the hotspots of $0.44^\circ \pm 0.11$ deg Myr^{-1} (95 per cent confidence level) about a pole of 56°S, 70°E.

(9) Continental plates tend to move more slowly than oceanic plates but there is much overlap in rms velocities with, for example, the Juan de Fuca, Scotia and Nazca plates all moving slower than the South American, Indian and Australian plates.

(10) Plates with a substantial fraction (28–44 per cent) of their boundary attached to subducting slabs tend to move faster than plates with little or no slab, but with overlap in rms velocities (Forsyth & Uyeda 1975). Among the plates with substantial attached slab, the speed tends to increase with increasing age of the lithosphere being subducted (Carlson *et al.* 1983).

ACKNOWLEDGMENTS

AEG especially wishes to thank the many researchers who shared their detailed knowledge of hotspot volcanoes. She also thanks the US Geological Survey Postdoctoral Research program for giving her the opportunity to spend a year at the Hawaii Volcano Observatory, thus allowing her to develop a skeptical view of Hawaii. Gary Acton, Don Argus, Dennis Geist and Bruce Buffet gave helpful reviews. Ben Horner-Johnson assisted with figure preparation. Many of the figures were created with the plotting software of Wessel & Smith (1991). This work was supported by National Science Foundation grants EAR-9814673 and EAR-9903763 to Rice University.

REFERENCES

Aeronautical Chart Service, 1951. *Marquesas Islands (map),*U.S. Air Force, Washington.

Almeida, F.F.M. de, 1961. Geologia e petrologia da ilha da Trindade, Divisao de Geologica e Mineralogia, Monograph, Vol. XVIII, p. 197. Depapartmento Nacional Producao Mineral, Rio de Janeiro.

Anders, M.H., Geissman, J.W., Piety, L.A. & Sullivan, J.T., 1989. Parabolic distribution of circumeastern Snake River Plain seismicity and latest Quaternary faulting: migratory pattern and association with the Yellowstone hotspot, *J. geophys. Res.,* **94,** 1589–1621.

Argus, D.F. & Gordon, R.G., 1991. No-net-rotation model of current plate velocities incorporating plate motion model NUVEL-1, *Geophys. Res. Lett.,* **18,** 2038–2042.

Armstrong, R.L., Leeman, W.P. & Malde, H.E., 1975. K-Ar dating, Quaternary and Neogene volcanic rocks of the Snake River Plain, Idaho, *Am. J. Sci.,* **275,** 225–251.

Atwater, T. & Stock, J., 1998. Pacific–North America plate tectonics of the Neogene southwestern United States: An update, *International Geology Review,* **40,** 375–402.

Bailey, K., 1976. Potassium–argon ages from the Galapagos Islands, *Science,* **192,** 465–467.

Baker, P.E., 1973. Islands of the South Atlantic, in *The Oceans, Basins and Margins,* Vol. 1, pp. 493–553, eds Nairn, A. & Stelhi, F., Plenum Press, New York.

Baker, P.E., Buckley, F. & Holland, J.G., 1974. Petrology and geochemistry of Easter Island, *Contrib. Mineral. Petrol.,* **44,** 85–100.

Baker, P.E., Gledhill, A., Harvey, P.K. & Hawkesworth, C.J., 1987. Geochemical evolution of the Juan Fernandez islands, SE Pacific, *J. geol. Soc. Lond.,* **144,** 933–944.

Baudry, N., Von Stackelberg, U. & Recy, J., 1988. Alignements volcaniques dans les Iles Australs: Analyse et interpretation de donnees SEASAT et Seabeam, *C. R. Acad. Sci. Paris,* **306,** 643–648.

Binard, N., Hekinian, R., Cheminee, J.L., Searle, R.C. & Stoffers, P., 1991. Morphological and structural studies of the Society and Austral hotspot regions in the South Pacific, *Tectonophysics,* **186,** 293–312.

Binard, N., Hekinian, R., Cheminee, J.L. & Stoffers, P., 1992a. Styles of eruptive activity on intraplate volcanoes in the Society and Austral hotspot regions: Bathymetry, petrology and submersible observations, *J. geophys. Res.,* **97,** 13 999–14 015.

Binard, N., Hekinian, R. & Stoffers, P., 1992b. Morphostructural study and type of volcanism of submarine volcanoes over the Pitcairn hotspot in the South Pacific, *Tectonophysics,* **206,** 245–264.

Binard, N., Maury, R.C., Guille, G., Talandier, J., Gillot, P.-Y. & Cotten, J., 1993. Mehetia Island, South Pacific: geology and petrology of the

emerged part of the Society hotspot, *J. Volc. Geotherm. Res.,* **55,** 239–260.

Binard, N., Stoffers, P., Hekinian, R. & Searle, R.C., 1996. Intraplate en echelon volcanic ridges in the south Pacific west of the Easter microplate, *Tectonophysics,* **263,** 23–37.

Blais, S., Guille, G., Maury, R.C., Guillou, H., Miau, D. & Cotten, J., 1997. Geologie et petrologie de l'ile de Raiatea (Societe, Polynesie francaise), *C. R. Acad. Sci. Paris,* **324,** 435–442.

Bonatti, E., Harrison, C.G.A., Fisher, D.E., Honnorez, J., Schilling, J.-G., Stipp, J.J. & Zentilli, M., 1977. Easter volcanic chain (southeast Pacific): a mantle hot line, *J. geophys. Res.,* **82,** 2457–2478.

Bonhommet, N., Beeson, M.H. & Dalrymple, G.B., 1977. A contribution to the geochronology and petrology of the island of Lanai, Hawaii, *Geol. Soc. Am. Bull.,* **88,** 1282–1286.

Bow, C.S., 1979. Geology and petrogenesis of lavas from Floreana and Santa Cruz islands, Galapagos archipelago, *PhD thesis,* University of Oregon, Eugene.

Brocher, T.M. & Holmes, R., 1985. The marine geology of sedimentary basins south of Viti Levu, Fiji, in *Investigations of the Northern Melanesian Borderland, Circum-Pacific Council for Energy and Mineral Resources Earth Science Series,* Vol. 3, pp. 123–138, ed. Brocher, T.M., Circum-Pacific Council for Energy and Mineral Resources, Houston.

Brousse, R., 1984. Le volcan sous-marin actif Moua Pihaa a l'extremite Sud-Est de l'archipel de la Societe (Polynesie Francaise), *C. R. Acad. Sci. Paris,* **299,** 995–998.

Brousse, R., Macherey, C., Berger, E. & Boutault, G., 1983. L'ile de Huahine: trois volcans successifs (Archipel de la Societe, Polynesie), *C. R. Acad. Sci. Paris,* **296,** 1559–1562.

Brousse, R., Barsczus, H.G., Bellon, H., Cantagrel, J.-M., Guillou, H. & Leotot, C., 1990. Les marquises (Polynesie francaise): volcanologie, geochronologie, discussion d'un modele de point chaud, *Bull. Soc. Geol. France,* **8,** 933–949.

Burke, K. & Dewey, J.F., 1973. Plume-generated triple junctions: Key indicators in applying plate tectonics to old rocks, *J. Geol.,* **81,** 406–433.

Cande, S.C., LaBrecque, J.L., Larson, R.L., Pitman, W.C., III, Golovchenko, X. & Haxby, W.E., 1989. *Magnetic Lineations of the World's Ocean Basins, AAPG (map),* AAPG, Tulsa.

Cande, S.C., Raymond, C.A., Stock, J. & Haxby, W.F., 1995. Geophysics of the Pitman fracture zone and Pacific–Antarctic plate motions during the Cenozoic, *Science,* **270,** 947–953.

Carlson, R.L., Hilde, T.W.C. & Uyeda, S., 1983. The driving mechanism of plate tectonics: Relation to age of the lithosphere at trenches, *Geophys. Res. Lett.,* **10,** 297–300.

Caroff, M., Maury, R.C., Vidal, P., Guille, G., Dupuy, C., Cotten, J., Guillou, H. & Gillot, P.-Y., 1995. Rapid temporal changes in ocean island basalt composition: evidence from an 800 m deep drill hole in the Eiao shield (Marquesas), *J. Petrol.,* **36,** 1333–1365.

Carter, R.M., 1967. The geology of Pitcairn Island, South Pacific ocean, *B. P. Bishop Mus. Bull.,* **231,** 38.

Chase, C.G., 1972. The n-plate problem of plate tectonics, *Geophys. J. R. astr. Soc.,* **29,** 117–122.

Chase, C.G., 1978. Plate kinematics: The Americas, East Africa, and the rest of the world, *Earth planet. Sci. Lett.,* **37,** 355–368.

Cheminee, J.L., Hekinian, R., Talandier, J., Albarede, F., Devey, C.W., Francheteau, J. & Lancelot, Y., 1989. Geology of an active hotspot: Teahitia-Mehetia region in the South Central Pacific, *Mar. Geophys. Res.,* **11,** 27–50.

Chen, C.-Y., Frey, F.A., Garcia, M.O., Dalrymple, G.B. & Hart, S.R., 1991. The tholeiitic to alkalic basalt transition at Haleakala Volcano, Maui, Hawaii, *Contrib. Mineral. Petrol.,* **106,** 183–200.

Cherkis, N.Z., Fleming, H.S. & Brozena, J.M., 1989. Bathymetry of the South Atlantic Ocean-3°S to 40°S, *Geol. Soc. Am. Map Chart Ser.,* MCH-069.

Christiansen, R.L., 1982. Late Cenozoic volcanism of the Island Park area, eastern Idaho, pp. 345–368, eds Bonnichsen, B. & Breckenridge, R.M.

Christiansen, R.L., 1984. Yellowstone magmatic evolution: its bearing on understanding large-volume explosive volcanism, in *Explosive volcanism; inception, evolution, and hazards,* pp. 84–95, National Academy of Sciences, Washington.

Christiansen, R.L. & Blank, H.R., Jr., 1972. Volcanic stratigraphy of the Quaternary rhyolite plateau in Yellowstone National Park, *U. S. Geol. Surv. Prof. Pap.,* **18,** 729-B.

Chu, D. & Gordon, R.G., 1999. Evidence for motion between Nubia and Somalia along the Southwest Indian Ridge, *Nature,* **398,** 64–67.

Chubb, L.J., 1927. The geology of the Austral or Tubuai islands (southern Pacific), Quarterly, *J. geol. Soc. Lond.,* **83,** 291–316.

Chubb, L.J., 1930. Geology of the Marquesas Islands, *B. P. Bishop Mus. Bull.,* **68,** 71.

Chubb, L.J., 1933. Geology of Galapagos, Cocos, and Easter islands, *B. P. Bishop Mus. Bull.,* **110,** 67.

Clague, D.A., 1987. Petrology of West Molokai Volcano (abstract), *Geol. Soc. Am. Abstr. Prog.,* **19,** 366.

Clague, D.A., 1996. The growth and subsidence of the Hawaiian-Emperor volcanic chain, in *The Origin and Evolution of Pacific Island Biotas, New Guinea to Eastern Polynesia: patterns and processes,* pp. 35–50, eds Keast, A. & Miller, S.E., SPB Academic Publishing, Amsterdam.

Clague, D.A. & Dalrymple, G.B., 1987. The Hawaiian-Emperor volcanic chain Part I, *U. S. Geol. Survey Prof. Paper,* **1350,** 5–54.

Clague, D.A. & Dalrymple, G.B., 1988. Age and petrology of alkalic post-shield and rejuvenated-stage lava from Kauai, Hawaii, *Contrib. Mineral. Petrol.,* **99,** 202–218.

Clague, D.A. & Moore, J.G., 1991a. Geology and petrology of Mahukona volcano, Hawaii, *Bull. of Volcanology,* **53,** 159–172.

Clague, D.A. & Moore, J.G., 1991b. Comment on Mahukona: The missing Hawaiian volcano by Garcia, M.O., Kurz, M.D. & Muenow, D.W., 1990, *Geology,* **19,** 1049–1050.

Clague, D.A., Holcomb, R.T., Sinton, J.M., Detrick, R.S. & Torresan, M.E., 1990. Pliocene and Pleistocene alkalic flood basalts on the seafloor north of the Hawaiian islands, *Earth planet. Sci. Lett.,* **98,** 175–191.

Clark, J.G., 1975. Age, chemistry, and tectonic significance of Easter and Sala y Gomez islands, *M.S. Thesis,* Oregon State University, Eugene.

Cocksworth, G.R., 1995. Modelling plate driving forces for the present and the Cenozoic, *PhD thesis,* University of Cambridge, Cambridge.

Cordani, U.G., 1968. Idade do vulcanismo no Oceano Atlantico Sul, *PhD thesis,* University of Sao Paulo, Sao Paulo.

Cordani, U.G., 1970. Idade do vulcanismo no Oceano Atlantico Sul, *Bol. Inst. Geociencias e Astronomia,* Univ. de Sao Paulo, **1,** 9–75.

Cox, A., 1971. Paleomagnetism of San Cristobal Island, Galapagos, *Earth planet. Sci. Lett.,* **11,** 152–160.

Cox, A. & Dalrymple, G.B., 1966. Palaeomagnetism and potassium–argon ages of some volcanic rocks from the Galapagos Islands, *Nature,* **209,** 776–777.

Cox, A. & Engebretson, D., 1985. Change in motion of Pacific plate at 5 Myr BP, *Nature,* **313,** 472–474.

Cullen, A. & McBirney, A.R., 1987. The volcanic geology and petrology of Isla Pinta, Galapagos archipelago, *Geol. Soc. Am. Bull.,* **98,** 294–301.

Dalrymple, G.B., Jarrard, R.D. & Clague, D.A., 1975. K–Ar ages of some volcanic rocks from the Cook and Austral Islands, *Geol. Soc. Am. Bull.,* **86,** 1463–1467.

Defense Mapping Agency Aerospace Center, 1969. Hawaiian Islands, Operational Navigational Chart (map), scale 1:1,000,000 J-19, St. Louis, Missouri.

Defense Mapping Agency Aerospace Center, 1973. France, New Zealand, Operational Navigational Chart (map), scale 1:1,000,000 P-19, St. Louis, Missouri.

Defense Mapping Agency Aerospace Center, 1975. Archipelago Juan Fernandez, Operational Navigational Chart (map), scale 1:1,000,000 R-22, St. Louis, Missouri.

Defense Mapping Agency Aerospace Center, 1976. American Samoa, Western Samoa, Operational Navigational Chart (map), scale 1:1,000,000 N-18, St. Louis, Missouri.

Defense Mapping Agency Aerospace Center, 1978. Isla de Pascua, Sala y Gomez, Operational Navigational Chart (map), scale 1:1,000,000 Q-23, St. Louis, Missouri.

Defense Mapping Agency Aerospace Center, 1983. *Society Islands, Operational Navigational Chart (map), scale 1:1,000,000 P-20,*2nd edn, St. Louis, Missouri.

Defense Mapping Agency Aerospace Center, 1989a. Trindade, Martin Vaz, Operational Navigational Chart (map), scale 1:1,000,000 P-29, St. Louis, Missouri.

Defense Mapping Agency Aerospace Center, 1989b. Iles Tuamotu, Oneo Island, and south Pacific, Operational Navigational Chart (map), scale 1:1,000,000 P-21, revised, St. Louis, Missouri.

Defense Mapping Agency Aerospace Center, 1990a. *Galapagos, Operational Navigational Chart (map), scale 1:1,000,000 L-25,*2nd edn, St. Louis, Missouri.

Defense Mapping Agency Aerospace Center, 1990b. *Galapagos, Operational Navigational Chart (map), scale 1:1,000,000 M-24,*3rd edn, St. Louis, Missouri.

DeMets, C., Gordon, R.G., Argus, D.F. & Stein, S., 1990. Current plate motions, *Geophys. J. Int.,* **101,** 425–478.

DeMets, C., Gordon, R.G., Argus, D.F. & Stein, S., 1994. Effect of recent revisions to the geomagnetic reversal time scale on estimates of current plate motion, *Geophys. Res. Lett.,* **21,** 2191–2194.

Desonie, D.L., Duncan, R.A. & Natland, J.H., 1993. Temporal and geochemical variability of volcanic products of the Marquesas hotspot, *J. geophys. Res.,* **98,** 17 649–17 665.

Devey, C.W., Albarede, F., Cheminee, J.-L., Michard, A., Muhe, R. & Stoffers, P., 1990. Active submarine volcanism on the Society hotspot swell (west Pacific): A geochemical study, *J. geophys. Res.,* **95,** 5049–5066.

Diament, D. & Baudry, N., 1987. Structural trends in the Southern Cook and Austral archipelagoes (South Central Pacific) based on an analysis of SEASAT data: geodynamic implications, *Earth planet. Sci. Lett.,* **85,** 427–438.

Diraison, C., Bellon, H., Leotot, C., Brousse, R. & Barsczus, H.G., 1991. L'alignement de la Societe (Polynesie francaise): volcanologie, geochronologie, propositino d'un modele de point chaud, *Bull. Soc. Geol. France,* **9,** 479–496.

Director of Military Survey, 1976a. Ile Rapa, Ilots de Bass (France), Operational Navigational Chart (map), scale 1:1,000,000 Q-20, Ministry of Defense, United Kingdom.

Director of Military Survey, 1976b. Pitcairn Island Group, Operational Navigational Chart (map), scale 1:1,000,000 Q-21, Ministry of Defense, United Kingdom.

Dixon, T.H., Farina, F., DeMets, C., Jansma, P.E., Mann, P. & Calais, E., 1998. Relative motion between the Caribbean and North American plates and related boundary zone deformation from a decade of GPS observations, *J. geophys. Res.,* **103,** 15 157–15 182.

Doell, R. & Dalrymple, G.B., 1973. Potassium–Argon ages and paleomagnetism of the Waianae and Koolau volcanic series, Oahu, Hawaii, *Geol. Soc. Am. Bull.,* **84,** 1217–1241.

Duncan, R.A., 1985. Radiometric ages from volcanic rocks along the New Hebrides-Samoa Lineament, in *Investigations of the Northern Melanesian Borderland, Circum-Pacific Council for Energy and Mineral Resources Earth Science Series,* Vol. 3, pp. 67–76, ed. Brocher, T. M., Circum-Pacific Council for Energy and Mineral Resources, Houston, Texas.

Duncan, R.A. & Clague, D.A., 1985. Pacific plate motion recorded by linear volcanic chains, in *The Ocean Basins and Margins, Vol. 7A: The Pacific Ocean,* pp. 89–121, eds Nairn, A.E., Stehli, F.G. & Uyeda, S., Plenum Press, New York.

Duncan, R.A. & McDougall, I., 1974. Migration of volcanism with time in the Marquesas Islands, French Polynesia, *Earth planet. Sci. Lett.,* **21,** 414–420.

Duncan, R.A. & McDougall, I., 1976. Linear volcanism in French Polynesia, *J. Volc. Geotherm. Res.,* **1,** 197–227.

Duncan, R.A., McDougall, I., Carter, R.M. & Coombs, D.S., 1974. Pitcairn Island- another Pacific hotspot?, *Nature,* **251,** 679–682.

Duncan, R.A., McCullough, M.T., Barsczus, H.G. & Nelson, D.R., 1986. Plume vs lithospheric sources for melts at Ua Pou, Marquesas Islands, *Nature,* **322,** 534–538.

Eiler, J.M., Farley, K.A., Valley, J.W., Hofmann, A.W. & Stolper, E.M., 1996. Oxygen isotope constraints on the sources of Hawaiian volcanism, *Earth planet. Sci. Lett.,* **144,** 453–468.

Emerick, C.M. & Duncan, R.A., 1982. Age progressive volcanism in the Comores Archipelago, western Indian Ocean and implications for Somali plate tectonics, *Earth planet. Sci. Lett.,* **60,** 415–438.

Engebretson, D.C., Cox, A. & Gordon, R.G., 1985. Relative motions between oceanic and continental plates in the Pacific basin, *Geol. Soc. Amer.,* Special Paper, **206,** p. 59.

Epp, D., 1978. Age and tectonic relationships among volcanic chains on the Pacific plate, *PhD thesis,* University of Hawaii, Manoa.

Farley, K.A., Natland, J., Macdougall, J.D. & Craig, H., 1990. He, Sr and Nd isotopes in Samoan basalts: Evidence for enriched and undepleted mantle components (abstract), *Trans. Am. Geophys. Union,* **67,** 1669.

Feighner, M.A. & Richards, M.A., 1994. Lithospheric structure and compensation mechanisms of the Galapagos Archipelago, *J. geophys. Res.,* **99,** 6711–6729.

Fisher, R.L. & Norris, R.M., 1960. Bathymetry and Geology of Sala y Gomez, southeast Pacific, *Geol. Soc. Am. Bull.,* **71,** 497–502.

Fleitout, L. & Moriceau, C., 1992. Short-wavelength geoid, bathymetry and convective pattern beneath the Pacific Ocean, *Geophys. J. Int.,* **110,** 6–28.

Fodor, R.V., Frey, F.A., Bauer, G.R. & Clague, D.A., 1992. Ages, rare-earth element enrichment, and petrogenesis of tholeiitic and alkalic basalts from Kahoolawe Island, Hawaii, *Contrib. Mineral. Petrol.,* **110,** 442–462.

Forsyth, D.W. & Uyeda, S., 1975. On the relative importance of the driving forces of plate motion, *Geophys. J. R. astr. Soc.,* **43,** 163–200.

Fox, P.J. & Gallo, D.G., 1984. A tectonic model for ridge-transform-ridge plate boundaries: Implications for the structure of oceanic lithosphere, *Tectonophysics,* **104,** 205–242.

Fox, P.J. & Gallo, D.G., 1986. The geology of North Atlantic transform plate boundaries and their aseismic extensions, in *The Western North Atlantic Region, Decade of North American Geology M,* pp. 157–172, eds Vogt, P.R. & Tucholke, B.E., Geological Society of America, Boulder.

Fretzdorff, S., Haase, K.M. & Garbe-Schoenberg, C.-D., 1996. Petrogenesis of lavas from the Umu Volcanic Field in the young hotspot region west of Easter Island, southeastern Pacific, *Lithos,* **38,** 23–40.

Frey, F.A., Clague, D., Mahoney, J.J. & Sinton, J.M., 2000. Volcanism at the edge of the Hawaiian plume; petrogenesis of submarine alkalic lavas from the North Arch volcanic field, *J. Petrol.,* **41,** 667–691.

Gansecki, C.A., Mahood, G.A. & McWilliams, M., 1998. New ages for the climactic eruptions at Yellowstone: Single-crystal 40 Ar/39 Ar dating identifies contamination, *Geology,* **26,** 343–346.

Garcia, M.O., Frey, F.A. & Grooms, D.G., 1986. Petrology of volcanic rocks from Kaula Island, Hawaii: Implications for the origin of Hawaiian phonolites, *Contrib. Mineral. Petrol.,* **94,** 461–471.

Garcia, M.O., Foss, D.J., West, H.B. & Mahoney, J.J., 1995. Geochemical and isotopic evolution of Loihi Volcano, Hawaii, *J. Petrol.,* **36,** 1647–1674.

GEBCO, 1982. General bathymetric chart of the oceans (map), *Can. Hydrogr. Serv.,* Ottawa.

Geist, D.J., 1992. An appraisal of melting processes and the Galapagos hotspot: Major- and trace-element evidence, *J. Volc. Geotherm. Res.,* **52,** 65–82.

Geist, D.J., McBirney, A.R. & Duncan, R.A., 1985. Geology of Santa Fe Island: the oldest Galapagos volcano, *J. Volc. Geotherm. Res.,* **26,** 203–212.

Geist, D.J., McBirney, A.R. & Duncan, R.A., 1986. Geology and petrogenesis of lavas from San Cristobal Island, Galapagos archipelago, *Geol. Soc. Am. Bull.,* **97,** 555–566.

Geist, D.J., White, W.M. & McBirney, A.R., 1988. Plume-asthenosphere mixing beneath the Galapagos archipelago, *Nature,* **333,** 657–660.

Geist, D., Howard, K.A., Jellinek, A.M. & Rayder, S., 1994. Volcanic history of Volcan Alcedo, Galapagos Archipelago: a case study of rhyolitic oceanic volcanism, *Bull. of Volcanology,* **56,** 243–260.

Gonzales-Marabal, A.M., 1984. L'ile de Hiva Oa (Marquises, Pacific central). Petrologie et evolution volcanologique, *Thèse, Univ. Paris Sud., Orsay.*

Gordon, R.G., Cox, A. & O'Hare, S., 1984. Paleomagnetic Euler poles and the apparent polar wander and absolute motion of North America since the Carboniferous, *Tectonics,* **3,** 499–537.

Gordon, R.G., Argus, D.F. & Heflin, M.B., 1999. Revised estimate of the angular velocity of India relative to Eurasia (abstract), *Trans. Am. Geophys. Union,* **80,** 273.

Gripp, A.E., 1994. Current plate motions; reference frames and uncertainties, *PhD thesis,* Northwestern University, Evanston, Illinois.

Gripp, A.E. & Gordon, R.G., 1990. Current plate velocities relative to the hotspots incorporating the NUVEL-1 global plate motion model, *Geophys. Res. Lett.,* **17,** 1109–1112.

Guillou, H., Brousse, R., Gillot, P.-Y. & Guille, G., 1993. Geological reconstruction of Fangataufa atoll, south Pacific, *Mar. Geol.,* **110,** 377–391.

Guillou, H., Gillot, P.-Y. & Guille, G., 1994. Age (K-Ar) et position de iles Gambier dans l'alignement du point chaud de Pitcairn (Pacific sud), *C. R. Acad. Sci. Paris,* **318,** 635–641.

Guillou, H., Sinton, J., Laj, C., Kissel, C. & Szeremeta, N., 2000. New K-Ar ages of shield lavas from Waianae Volcano, Oahu, Hawaiian Archipelago, *J. Volc. Geotherm. Res.,* **96,** 229–242.

Haase, K.M. & Devey, C.W., 1996. Geochemistry of lavas from the Ahu and Tupa volcanic fields, Easter Hotspot, southeast Pacific: Implications for intraplate magma genesis near a spreading axis, *Earth planet. Sci. Lett.,* **137,** 129–143.

Haase, K.M., Devey, C.W. & Goldstein, S.L., 1996. Two-way exchange between the Easter mantle plume and the Easter microplate spreading axis, *Nature,* **382,** 344–346.

Haase, K.M., Stoffers, P. & Garbe-Schoenberg, C.D., 1997. The petrogenic evolution of lavas from Easter Island and neighbouring seamounts, near-ridge hotspot volcanoes in the SE Pacific, *J. Petrol.,* **38,** 785–813.

Hagen, R.A., Baker, N.A., Naar, D.F. & Hey, R.N., 1990. A SeaMARC II survey of recent submarine volcanism near Easter Island, *Mar. Geophys. Res.,* **12,** 297–315.

Hall, M.L., 1983. Origin of Espanola Island and the age of terrestrial life on the Galapagos Islands, *Science,* **221,** 545–547.

Hannan, B.B. & Schilling, J.-G., 1989. Easter Microplate evolution: Ph isotopic evidence, *J. geophys. Res.,* **94,** 7432–7448.

Harada, Y. & Hamano, Y., 2000. Recent progress on the plate motion relative to hotspots, in *The History and Dynamics of Global Plate Motions, Geophysical Monograph,* Vol. 121, pp. 327–338, eds Richards, M., Gordon, R.G. & van der Hilst, R.D., American Geophysical Union.

Harbert, W. & Cox, A., 1989. Late Neogene motion of the Pacific plate, *J. geophys. Res.,* **94,** 3052–3064.

Harpp, K.S. & White, W.M., 1990. Geochemistry of Galapagos seamounts (abstract), *Trans. Am. Geophys. Union,* **71,** 1695.

Hart, S.R. *et al.*, 1999. Fa'afafine Volcano: the active samoan hotspot (abstract), *Trans. Am. Geophys. Union,* **80,** 1102.

Hawkins, J.W. & Natland, J.H., 1975. Nephelinites and Basanites of the Samoan Linear Volcanic chain: their possible tectonic significance, *Earth planet. Sci. Lett.,* **24,** 427–439.

Hekinian, R., Bideau, D., Stoffers, P., Cheminee, J. L., Muhe, R., Puteanus, D. & Binard, N., 1991. Submarine intraplate volcanism in the South Pacific: Geological setting and petrology of the Society and Austral regions, *J. geophys. Res.,* **96,** 2109–2138.

Hekinian, R., Stoffers, P., Akermand, D., Binard, N., Francheteau, J., Devey, C. & Garbe-Schoenberg, D., 1995. Magmatic evolution of the Easter microplate-Crough Seamount region (south east Pacific), *Mar. Geophys. Res.,* **17,** 375–397.

Herz, N., 1977. Timing of spreading in the South Atlantic: Information from Brazilian alkalic rocks, *Geol. Soc. Am. Bull.,* **88,** 101–112.

Hey, R., 1977. Tectonic evolution of the Cocos-Nazca spreading center, *Geol. Soc. Am. Bull.,* **88,** 1404–1420.

Hieronymus, C.F. & Bercovici, D., 1999. Discrete alternating hotspot islands formed by interaction of magma transport and lithospheric flexure, *Nature,* **397,** 604–607.

Hilgen, F.J., 1991a. Astronomical calibration of Gauss to Matuyama sapropels in the Mediterranean and implications for the geomagnetic polarity time scale, *Earth planet. Sci. Lett.,* **104,** 226–244.

Hilgen, F.J., 1991b. Extension of the astronomically calibrated (polarity) time scale to the Miocene/Pliocene boundary, *Earth planet. Sci. Lett.,* **107,** 349–368.

Hoffert, M., Cheminee, J.-L., Larque, P. & Person, A., 1987. Depot hydrothermal associe au volcanisme sous-marin intraplaque oceanique. Prelevement effectue avec Cyana, sur le volcan sous-marin actif de Teahitia (Polynesie francaise), *C. R. Acad. Sc. Paris,* **304,** 829–832.

Holcomb, R.T., 1987. Eruptive history and long-term behavior of Kilauea Volcano, *U. S. Geol. Survey Prof. Paper,* **1350,** 261–350.

Holden, J.C. & Dietz, R.S., 1972. Galapagos gore, NazCoPac triple junction and the Carnegie/Cocos ridges, *Nature,* **235,** 266–269.

Ihinger, P.D., 1995. Mantle flow beneath the Pacific plate: evidence from seamount segments in the Hawaiian-Emperor chain, *Am. J. Sci.,* **295,** 1035–1057.

Jackson, E.D., Silver, E.A. & Dalrymple, G.B., 1972. Hawaiian-Emperor chain and its relation to Cenozoic circumpacific tectonics, *Geol. Soc. Am. Bull.,* **83,** 601–618.

Jarrard, R.D., 1986. Relations among subduction parameters, *Rev. Geophys.,* **24,** 217–284.

Jarrard, R.D. & Clague, D.A., 1977. Implications of Pacific island and seamount ages for the origin of volcanic chains, *Rev. Geophys. Space Phys.,* **15,** 57–76.

Johnson, G.L. & Lowrie, A., 1972. Cocos and Carnegie ridges result of the Galapagos hotspot?, *Earth planet. Sci. Lett.,* **14,** 279–280.

Johnson, R.H., 1984. Exploration of the submarine volcanoes in the South Pacific, *National Geographic Soc. Rep.,* **16,** 405–419.

Johnson, R.H. & Malahoff, A., 1971. Relation of Macdonald volcano to migration of volcanism along the Austral chain, *J. geophys. Res.,* **76,** 3282–3290.

Kaneoka, I. & Katsui, Y., 1985. K-Ar ages of volcanic rocks from Easter Island, *Bull. Volcanol. Soc. Japan,* **30,** 33–36.

Katao, H., Morinaga, H., Hyodo, M., Inokuchi, H., Matsuda, J. & Yaskawa, K., 1988. Geomagnetic paleosecular variation and K-Ar ages in Hiva-Oa Island Marquesas, French Polynesia, *J. Geomag. Geoelectr.,* **40,** 703–714.

Keating, B., 1985. Paleomagnetic studies of the Samoan Islands: results from the islands of Tutuila and Savaii, in *Investigations of the Northern Melanesian Borderland, Circum-Pacific Council for Energy and Mineral Resources Earth Science Series,* Vol. 3, pp. 187–199, ed. Brocher, T.M., Circum-Pacific Council for Energy and Mineral Resources, Houston, Texas.

Klein, F.W., Koyanagi, R.Y., Nakata, J.S. & Tanigawa, W.R., 1987. The seismicity of Kilauea's magma system, *U. S. Geol. Survey Prof. Paper,* **1350,** 1010–1186.

Krummenacher, D. & Noetzlin, J., 1966. Ages isotopiques K/A de roches prelevees dans les possessions francaises du Pacifique, *Bull. Soc. Geol. France,* **8,** 173–175.

Langenheim, V.A.M. & Clague, D.A., 1987. The Hawaiian-Emperor volcanic chain Part II, *U. S. Geol. Survey. Prof. Paper,* **1350,** 55–84.

Lassiter, J.C., DePaolo, D.J. & Tatsumoto, M., 1996. Isotopic evolution of Mauna Kea Volcano; results from the initial phase of the Hawaiian Scientific Drilling Project, *J. geophys. Res.,* **101,** 11769–11780.

Leeman, W.P., 1982. Development of the Snake River Plain-Yellowstone Plateau province, Idaho and Wyoming: An overview and petrologic model, in *Cenozoic Geology of Idaho, Idaho Bur. of Mines and Geol. Bull.,* Vol. 26, pp. 155–177, eds Bonnichsen, B. & Breckenridge, R.M.

Lehman, J.A., Smith, R.B. & Schilly, M.M., 1982. Upper crustal structure of the Yellowstone caldera from seismic delay time analyses and gravity correlations, *J. geophys. Res.,* **87,** 2713–2730.

Liotard, J.-M. & Barsczus, H.G., 1983a. Contribution a la connaissance petrographique et geochemique de l'ile de Fatu Huka, Archipel des Marquises, Polynesie Francaise (Ocean Pacifique Centre-Sud), *C. R. Acad. Sci. Paris,* **297,** 509–512.

Liotard, J.-M. & Barsczus, H.G., 1983b. Contribution a la connaissance petrographique et geochemique de l'ile de Hatutu, Archipel des Marquises, Polynesie Francaise (Ocean Pacifique Centre-Sud), *C. R. Acad. Sci. Paris,* **297,** 725–728.

Liotard, J.M., Barsczus, H.G., Dupuy, C. & Dostal, J., 1986. Geochemistry and origin of basaltic lavas from Marquesas Archipelago, French Polynesia, *Contrib. Mineral. Petrol.,* **92,** 260–268.

Lipman, P.W., Clague, D.A., Moore, J.G. & Holcomb, R.T., 1989. South arch volcanic field- newly identified young lava flows on the sea floor south of the Hawaiian Ridge, *Geology,* **17,** 611–614.

Lockwood, J.P., Dvorak, J.J., English, T.T., Koyanagi, R.Y., Okamura, A.T., Summers, M.L. & Tanigawa, W.R., 1987. Mauna Loa 1974–1984: a decade of intrusive and extrusive activity, *U. S. Geol. Survey Prof. Paper,* **1350,** 537–570.

Lonsdale, P., 1988. Geography and history of the Louisville hotspot chain in the southwest Pacific, *J. geophys. Res.,* **93,** 3078–3104.

Ludwig, K.R., Szabo, B.J., Moore, J.G. & Simmons, K.R., 1991. Crustal subsidence rate off Hawaii determined from $^{234}U/^{238}U$ ages of drowned coral reefs, *Geology,* **19,** 171–174.

Macdonald, G.A. & Abbott, A.T., 1970. *Volcanoes in the Sea,*University of Hawaii Press, Honolulu.

Macdonald, K.C., 1986. The crest of the Mid-Atlantic Ridge: Models for crustal generation processes and tectonics, in *The Geology of North America, Volume M, The Western North Atlantic Region,* pp. 51–68, eds Vogt, P.R. & Tucholke, B.E., The Geological Society of America, Boulder.

Machesky, L.F., 1965. Gravity Relations in American Samoa and the Society Islands, *Pacific Science,* **19,** 367–373.

Malahoff, A., 1987. Geology of the summit of Loihi Seamount, *U. S. Geol. Survey Prof. Paper,* **1350,** 133–144.

Mammerickx, J., 1989. Large-scale undersea features of the northeast Pacific, in *The Eastern Pacific Ocean and Hawaii, The Geology of North America N,* pp. 5–13, eds Winterer, E.L., Hussong, D.M. & Decker, R.W., Geological Society of America, Boulder.

Mammerickx, J., 1992. Bathymetry of the southcentral Pacific, *Trans. Am. Geophys. Union,* **73,** 586.

Mammerickx, J., 1992. The Foundation seamounts: tectonic setting of a newly discovered seamount chain in the South Pacific, *Earth planet. Sci. Lett.,* **113,** 293–306.

Mammerickx, J. & Smith, S.M., 1980. Bathymetry of the Northeast Pacific, Map and Chart Series (Geological Society of America). MC-43, Geological Society of America, Boulder.

McBirney, A.R., 1990. Differentiated rocks of the Galapagos hotspot (abstract), *Trans. Am. Geophys. Union,* **71,** 1695–1696.

McBirney, A.R. & Williams, H., 1969. *Geology and Petrology of the Galapagos Islands, Geological Society of America Memoir 118,* Geological Society of America, Boulder.

McDougall, I., 1964. Potassium-Argon ages from lavas of the Hawaiian Islands, *Geol. Soc. Am. Bull.,* **75,** 107–128.

McDougall, I., 1985. Age and evolution of the volcanoes of Tutuila, American Samoa, *Pac. Sci.,* **39,** 311–320.

McDougall, I. & Duncan, R.A., 1980. Linear volcanic chains—recording plate motions?, *Tectonophysics,* **63,** 275–295.

McDougall, I. & Swanson, D.A., 1972. Potassium-argon ages of Lavas from the Hawi and Pololu volcanic series, Kohala Volcano, Hawaii, *Geol. Soc. Am. Bull.,* **83,** 3731–3738.

McNutt, M.K., Caress, D.W., Reynolds, J., Jordahl, K.A. & Duncan, R.A., 1997. Failure of plume theory to explain midplate volcanism in the southern Austral islands, *Nature,* **389,** 479–482.

Menard, H.W., 1964. *Marine Geology of the Pacific,* McGraw-Hill, New York.

Minster, J.B. & Jordan, T.H., 1978. Present-day plate motions, *J. geophys. Res.,* **83,** 5331–5354.

Minster, J.B., Jordan, T.H., Molnar, P. & Haines, E., 1974. Numerical modeling of instantaneous plate tectonics, *Geophys. J. R. astr. Soc.,* **36,** 541–576.

Molnar, P. & Stock, J., 1987. Relative motions of hotspots in the Pacific, Atlantic and Indian Oceans since late Cretaceous time, *Nature,* **327,** 587–591.

Moore, J.G., 1987. Subsidence of the Hawaiian Ridge, *U. S. Geol. Survey Prof. Paper,* **1350,** 85–100.

Moore, J.G. & Clague, D.A., 1988. Offshore geology of Mahukona, Kohala, Mauna Kea, Hualalai, and Mauna Loa volcanoes to the northeast of Hawaii (abstract), *Trans. Am. Geophys. Union,* **69,** 1445.

Moore, J.G. & Clague, D.A., 1992. Volcano growth and evolution of the island of Hawaii, *Geol. Soc. Am. Bull.,* **104,** 1471–1484.

Moore, J.G., Clague, D.A. & Normark, W.R., 1982. Diverse basalt types from Loihi seamount, Hawaii, *Geology,* **10,** 88–92.

Morgan, L.A., 1988. Explosive rhyolitic volcanism on the eastern Snake River Plain, *PhD thesis,* University of Hawaii, Manoa.

Morgan, L.A., Doherty, D.J. & Leeman, W.P., 1984. Ignimbrites of the eastern Snake River Plain: Evidence for major caldera-forming eruptions, *J. geophys. Res.,* **89,** 8665–8678.

Morgan, W.J., 1972. Deep mantle convection plumes and plate motions, *Am. Assoc. Petrol. Geol. Bull.,* **56,** 203–213.

Morgan, W.J., 1978. Rodriguez, Darwin, Amsterdam..., A second type of hotspot island, *J. geophys. Res.,* **83,** 5355–5360.

Mueller, R.D., Roest, W.R., Royer, J.-Y., Gahagan, L.M. & Sclater, J.G., 1996. A digital age map of the ocean floor (map), SIO Reference Series 93–30, Scripps Institution of Oceanography.

Natland, J.H., 1980. The progression of volcanism in the Samoan linear volcanic chain, *Am. J. Sci.,* **280-A,** 709–735.

Natland, J.H. & Turner, D.L., 1985. Age progression and petrological development of Samoan shield volcanoes: evidence from K-Ar ages, lava compositions, and mineral studies, in, *Investigations of the Northern Melanesian Borderland, Circum-Pacific Council for Energy and Mineral Resources Earth Science Series,* Vol. 3, pp. 139–171, ed. Brocher, T.M., Circum-Pacific Council for Energy and Mineral Resources, Houston.

Naumann, T. & Geist, D., 2000. Physical volcanology and structural development of Cerro Azul Volcano, Isabela Island, Galapagos: implications for the development of Galapagos-type shield volcanoes, *Bull. Volcanology,* **61,** 497–514.

Norris, R.A. & Johnson, R.H., 1969. Submarine volcanic eruptions recently located in the Pacific by Sofar hydrophones, *J. geophys. Res.,* **74,** 650–664.

O'Connor, J.M., Stoffers, P. & McWilliams, M.O., 1995. Time-space mapping of Easter Chain volcanism, *Earth planet. Sci. Lett.,* **136,** 197–212.

O'Connor, J.M., Stoffers, P. & Wijbrans, J.R., 1998. Migration rate of volcanism along the Foundation Chain, SE Pacific, *Earth planet. Sci. Lett.,* **164,** 41–59.

Okal, E.A. & Cazenave, A., 1985. A model for the plate tectonic evolution of the east-central Pacific based on SEASAT investigations, *Earth planet. Sci. Lett.,* **72,** 99–116.

Pan, Y. & Batiza, R., 1998. Major element chemistry of volcanic glasses from the Easter Seamount Chain: Constraints on melting conditions in the plume channel, *J. geophys. Res.,* **103,** 5287–5304.

Petronotis, K.E. & Gordon, R.G., 1999. A Maastrichtian palaeomagnetic pole for the Pacific plate determined from a skewness analysis of marine magnetic anomaly 32, *Geophys. J. Int.,* **139,** 227–247.

Pierce, K.L. & Morgan, L.A., 1992. The track of the Yellowstone hotspot: Volcanism, faulting and uplift, in *Regional Geology of Eastern Idaho and Western Wyoming,* Vol. 179, pp. 1–53, eds Link, P.K., Kuntz, M.A. & Platt, L.B., Geological Society of America, Boulder.

Pilger, R.H., Jr. & Handschumacher, D.W., 1981. The fixed-hotspot hypothesis and origin of the Easter-Sala y Gomez-Nazca trace, *Geol. Soc. Am. Bull.,* **92,** 437–446.

Pollitz, F.F., 1986. Pliocene change in Pacific-plate motion, *Nature,* **320,** 738–741.

Poreda, R.J. & Farley, K.A., 1992. Rare gases in Samoan xenoliths, *Earth planet. Sci. Lett.,* **113,** 129–144.

Price, R.C., Maillet, P., McDougall, I. & Dupont, J., 1991. The geochemistry of basalts from the Wallis Islands, Northern Melanesian Borderland: Evidence for a lithospheric origin for Samoan-type basaltic magmas?, *J. Volc. Geotherm. Res.,* **45,** 267–288.

Reynolds, R.W., Geist, D. & Kurz, M.D., 1995. Physical volcanology and structural development of Sierra Negra, Isabella Island, Galapagos archipelago, *Geol. Soc. Am. Bull.,* **107,** 1398–1410.

Ricard, Y., Doglioni, C. & Sabadini, R., 1991. Differential rotation between the lithosphere and the mantle: a consequence of lateral viscosity variations, *J. geophys. Res.,* **95,** 8407–8415.

Richards, A.F., 1962. *Catalogue of the active volcanoes of the Archipielago de colon, Isla San Felix and Islas Juan Fernandez, Catalogue of the active volcanoes of the world,* XIV, International Association of Volcanology, Rome.

Rodgers, D.W., Hackett, W.R. & Ore, H.T., 1990. Extension of the Yellowstone plateau, eastern Snake River Plain, and Owyhee plateau, *Geology,* **18,** 1138–1141.

Roperch, P. & Duncan, R.A., 1990. Records of geomagnetic reversals from volcanic islands of French Polynesia 1. Paleomagnetic study of a polarity transition in a lava sequence from the island of Huahine, *J. geophys. Res.,* **95,** 2713–2726.

Russo, R.M. & Okal, E.A., 1998. Shear wave splitting and upper mantle deformation in French Polynesia: Evidence for small-scale heterogeneity related to the Society hotspot, *J. geophys. Res.,* **103,** 15 089–15 107.

Russo, R.M., Wolfe, C.J., Okal, E.A., Silver, P.G. & Solomon, S.C., 1998. Shear-wave splitting beneath the Hawaiian Islands (abstract), *Trans. Am. Geophys. Union,* **79,** 208.

Ryan, M.P., Koyanagi, R.Y. & Fiske, R.S., 1981. Modeling the three-dimensional structure of macroscopic magma transport systems; application to Kilauea Volcano, Hawaii, *J. geophys. Res.,* **86,** 7111–7129.

Saltzer, R.L. & Humphreys, E.D., 1997. Upper mantle P wave velocity structure of the eastern Snake River Plain and its relationship to geodynamic models of the region, *J. geophys. Res.,* **102,** 11 829–11 841.

Sandwell, D.T. & Smith, W.H.F., 1995. Marine Gravity from Satellite Altimetry (poster), The Geological Data Center, Scripps Inst. of Oceanography, La Jolla, CA 92093, (digital file, Version 7.2) anonymous ftp to baltica.ucsd.edu.

Schilling, J.-G., Anderson, R.N. & Vogt, P., 1976. Rare earth, Fe and Ti variations along the Galapagos spreading centre, and their relationship to the Galapagos mantle plume, *Nature,* **261,** 108–113.

Schilly, M.M., Smith, R.B., Braile, L.W. & Ansorge, J., 1982. The 1978 Yellowstone-eastern Snake River Plain seismic profiling experiment: Data and upper crustal structure of the Yellowstone region, *J. geophys. Res.,* **87,** 2692–2704.

Schouten, H., Dick, J.B. & Klitgord, K.D., 1987. Migration of mid-ocean ridge volcanic segments, *Nature,* **326,** 835–839.

Schutt, D., Humphreys, E.D. & Dueker, K., 1998. Anisotropy of the Yellowstone hot spot wake, eastern Snake River Plain, Idaho, *Pure appl. Geophys.,* **151,** 443–462.

Searle, R.C., 1986. GLORIA investigations of oceanic fracture zones: Comparative study of the transform fault zone, *J. geol. Soc. Lond.,* **143,** 743–756.

Sharp, W.D. & Clague, D.A., 1999. A new older age of 47 Ma for the Hawaiian-Emperor bend (abstract), *Trans. Am. Geophys. Union,* **80,** 1196.

Sinton, C.W., Christie, D.M. & Duncan, R.A., 1996. Geochronology of Galapagos seamounts, *J. geophys. Res.,* **101,** 13 689–13 700.

Smith, R.B. & Braile, L.W., 1994. The Yellowstone hotspot, *J. Volc. Geotherm. Res.,* **61,** 121–187.

Spengler, S.R. & Garcia, M.O., 1988. Geochemistry of Hawi lavas, Kohala Volcano, Hawaii, *Contrib. Mineral. Petrol.,* **99,** 90–104.

Spiegel, M.R., 1975. *Schaum's Outline of Theory and Problems of Probability and Statistics,* McGraw-Hill, New York.

Standish, J., Geist, D., Harpp, K. & Kurz, M.D., 1998. The emergence of a Galapagos shield volcano, Roca Redonda, *Contrib. Mineral. Petrol.,* **133,** 136–148.

Stark, J.T. & Howland, A.L., 1941. Geology of Bora Bora, Society Islands, *B. P. Bishop Mus. Bull.,* **169,** 43.

Stearns, H.T., 1940. Four-phase volcanism in Hawaii (abstract), *Geol. Soc. Am. Bull.,* **51,** 1947–1948.

Stearns, H.T., 1946. Geology of the Hawaiian Islands, Hawaii Division of Hydrography, *Bulletin,* **8,** 106.

Stearns, H.T. & Macdonald, G.A., 1947. Geology and ground-water resources of the Island of Niihau, Hawaii, Hawaiian Division of Hydrogeography, *Bulletin,* **12,** 51.

Steiger, R.H. & Jager, E., 1977. Subcommission on geochronolgy: convention on the use of decay constants in geo- and cosmochronology, *Earth planet. Sci. Lett.,* **36,** 359–362.

Stice, G.D. & McCoy, F.W. Jr., 1968. The geology of the Manu'a Islands, Samoa, *Pac. Sci.,* **22,** 427–457.

Stoffers, P. *et al.*, 1989. Geology of Macdonald Seamount region, Austral Islands: recent hotspot volcanism in the South Pacific, *Mar. Geophys. Res.,* **11,** 101–112.

Stoffers, P. *et al.*, 1990. Active Pitcairn hotspot found, *Mar. Geol.,* **95,** 51–55.

Stoffers, P., Hekinian, R., Haase, K.M. & the Scientific Party, 1994. Geology of young submarine volcanoes west of Easter Island, Southeast Pacific, *Mar. Geology,* **118,** 177–185.

Stuessy, T.F., Foland, K.A., Sutter, J.F., Sanders, R.W. & Silva, M.O., 1984. Botanical and geological significance of potassium–argon dates from the Juan Fernandez Islands, *Science,* **225,** 49–51.

Suppe, J., Powell, C. & Berry, R., 1975. Regional topography, seismicity, Quaternary volcanism, and the present-day tectonics of the western United States, *Am. J. Sci.,* **275-A,** 397–436.

Swanson, F.J., Baitis, H.W., Lexa, J. & Dymond, J., 1974. Geology of Santiago, Rabida, and Pinzon islands, Galapagos, *Geol. Soc. Am. Bull.,* **85,** 1803–1810.

Talandier, J. & Kuster, G.T., 1976. Seismicity and submarine volcanic activity in French Polynesia, *J. geophys. Res.,* **81,** 936–948.

Talandier, J. & Okal, E.A., 1984. The volcanoseismic swarms of 1981–1983 in the Tahiti-Mehetia area, French Polynesia, *J. geophys. Res.,* **89,** 11 216–11 234.

Talandier, J. & Okal, E.A., 1987. Crustal structure in the Society and Tuamotu islands, French Polynesia, *Geophys. J. R. astr. Soc.,* **88,** 499–528.

Turner, D.L. & Jarrard, R.D., 1982. K–Ar dating of the Cook–Austral island chain: a test of the hotspot hypothesis, *J. Volc. Geotherm. Res.,* **12,** 187–220.

Verma, S.P., Schilling, J.-G. & Waggoner, D.G., 1983. Neodymium isotopic evidence for Galapagos hotspot-spreading centre system evolution, *Nature,* **306,** 654–657.

Vicenzi, E.P., McBirney, A.R., White, W.M. & Hamilton, M., 1990. The geology and geochemistry of Isla Marchena, Galapagos Archipeligo: an ocean island adjacent to a mid-ocean ridge, *J. Volc. Geotherm. Res.,* **40,** 291–315.

Watts, A.B., Weissel, J.K., Duncan, R.A. & Larson, R.L., 1988. The origin of the Louisville Ridge and its relationship to the Eltanin fracture zone system, *J. geophys. Res.,* **93,** 3051–3077.

Wessel, P. & Kroenke, L., 1997. Relocating Pacific hotspots and refining absolute plate motions using a new geometric technique, *Nature,* **387,** 365–369.

Wessel, P. & Smith, W.H.F., 1991. Free software helps map and display data, *Trans. Am. Geophys. Union,* **72,** 441–445.

White, W.M., Harpp, K., Levy, L., Cheatham, M., Duncan, R.A. & Fisk, M.R., 1989. Hawaiian style volcanic evolution on Tahaa, Societies Islands (abstract), *Trans. Am. Geophys. Union,* **70,** 1385.

White, W.M., McBirney, A.R. & Duncan, R.A., 1993. Petrology and geochemistry of the Galapagos Islands: portrait of a pathological mantle plume, *J. geophys. Res.,* **98,** 19 533–19 563.

Williams, H., 1933. Geology of Tahiti, Moorea and Maiao, *B. P. Bishop Mus. Bull.,* **105,** 89.

Wolfe, E.W., Wise, W.S. & Dalrymple, G.B., 1997. The geology and petrology of Mauna Kea Volcano, Hawaii: a study of postshield volcanism, *U. S. Geol. Survey Prof. Paper* 1557.

Woodhead, J.D. & Devey, C.W., 1993. Geochemistry of the Pitcairn seamounts, I: source character and temporal trends, *Earth planet. Sci. Lett.,* **116,** 81–99.

Wright, T.L., Shaw, H.R., Tilling, R.L. & Fiske, R.S., 1979. Origin of Hawaiian tholeiitic basalt: a quantitative model (abstract), *Hawaiian Symposium on Intraplate Volcanism and Submarine Volcanism,* p. 104.

APPENDIX A: DETAILS OF INDIVIDUAL TRACKS

We begin with Hawaii because the nomenclature of its eruptive sequence (preshield, shield, postshield and posterosional phases) has been applied to the other oceanic islands. After Hawaii we move south and the east around the globe. Details of volcano age and location are listed in Table 1.

Hawaii

The Hawaiian Islands are located on the Pacific Plate in the central Pacific Ocean (Fig. A1). The Hawaiian–Emperor seamount chain

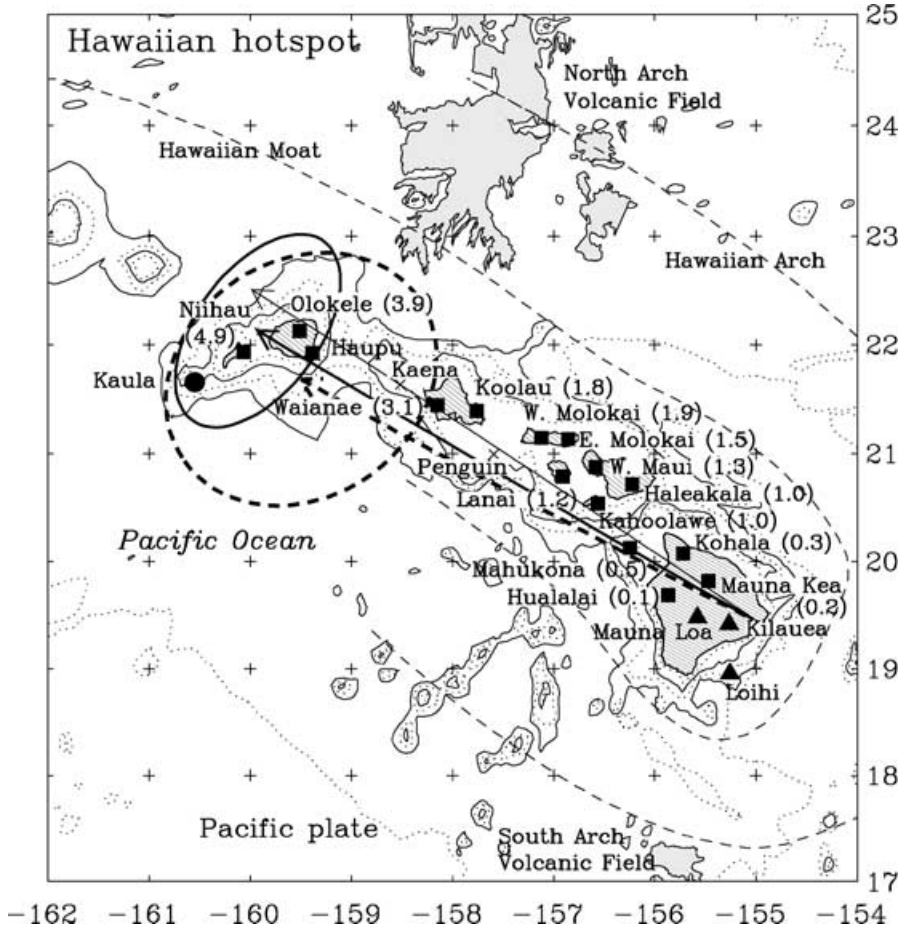

Figure A1. Bathymetric map of the Hawaiian islands. Solid triangles, Hawaiian volcanoes that have not yet ended their shield building stage; solid squares, Hawaiian volcanoes that ended their shield building as recently as 5 Ma; solid circles, Hawaiian volcanoes that likely ended their shield building before 5 Ma; ×'s, possible, but unsampled Hawaiian volcanoes. Arrows and 2-D 95 per cent confidence ellipses are scaled to show the displacement and corresponding uncertainty over 5.8 Myr. Thin arrow shows the observed Hawaiian trend and volcanic propagation rate. Thick arrow shows motion calculated from HS3-NUVEL1A. Dashed arrow shows motion predicted by removing the Hawaii rate and trend. Geometry of on-arch volcanism from Clague *et al.* (1990) and Lipman *et al.* (1989). Geometry of flexural moat and arch (both dashed) from Menard (1964). Bathymetry is from Mammerickx (1989). Islands are shaded, even 1000 m contours are solid, and odd 1000 m contours are dotted. Mercator projection.

consists of conical seamounts, guyots, atolls, and volcanic islands, which young to the southeast along the chain's 6100 km length (Clague & Dalrymple 1987; Clague 1996). Four distinct eruptive stages are typical of Hawaiian volcanism, although some stages are unknown, and possibly missing, from some volcanoes (Clague & Dalrymple 1987). Hawaiian volcanoes begin their submarine growth in the alkalic preshield stage (1–4 per cent of volcano volume). Analyses of rocks dredged from Loihi Seamount, which is the youngest shield volcano in the Hawaiian chain and the only example of preshield volcanism, suggest that preshield lavas are dominantly alkalic basalts and basanites. The next stage is the tholeiitic shield stage (95–98 per cent volcano volume), during which tholeiitic lavas erupt from the summit caldera and rift zones. The shield stage is followed immediately by the eruption, especially near the summit, of a thin veneer of alkalic lavas. These lavas of the alkalic postshield (or capping) stage include alkalic basalts and their differentiates out to trachytes. The low volume (1 per cent volcano volume) postshield stage lasts less than 1 Myr, after which erosion and reef growth begin to dominate the shaping of the edifice. Up to several million years later, erosion is slowed briefly by the eruption of a small volume (<1 per cent volcano volume) of lavas from isolated vents. These lavas of the alkalic posterosional (or rejuvenated) stage include alkalic basalts and strongly alkalic basalts such as basanites, nephelinites and melitites. Subaerial Hawaiian volcanism typically lasts 4 Myr. We assign volcano age to be the age of the shield–postshield transition (see Clague & Dalrymple (1987) for a discussion of other assignments of volcano age). Scattered minor volumes of alkalic and strongly alkalic volcanism occur on the flexural arch around Hawaii (Lipman *et al.* 1989; Clague *et al.* 1990). The radiogenic isotopic ratios of the north arch lavas are similar to those of some posterosional rocks and lie between those of the Hawaiian shield stage and modern south Pacific mid-ocean-ridge basalt (MORB) (Frey *et al.* 2000). Along the Hawaiian Ridge, the volcanoes appear to be aligned along curves (called loci) which trend up to tens of degrees clockwise of the gross trend of Hawaiian Ridge (Jackson *et al.* 1972). As originally defined, the youngest Hawaiian islands have two loci running through them: the Kea locus (Kilauea, Mauna Kea, Kohala, Haleakala, West Maui and East Molokai volcanoes) and the Loa locus (Mauna Loa, Hualalai, Kahoolawe, Lanai, West Molokai, Koolau, Waianae and Olokele volcanoes). The geochemistry of these two loci may be distinct from each other in major elements and isotopic ratios (Lassiter *et al.* 1996; Eiler *et al.* 1996), but the geochemistry may also vary systematically in a single locus (Ihinger 1995). Because the composition of such a small

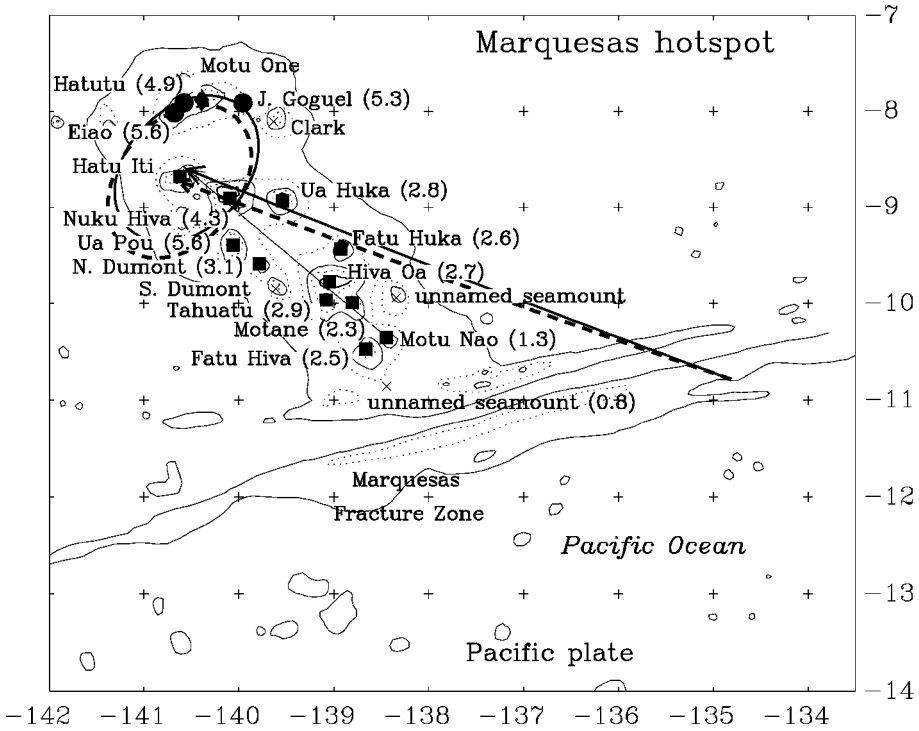

Figure A2. Bathymetric map of the Marquesas islands. Solid squares, volcanoes with ages of roughly 5 Ma and younger that were used to estimate trend; solid circles, volcanoes roughly older than 5 Ma; solid diamond, a likely young island; ×'s, unsampled seamounts and minor sampled seamounts. Thin arrow shows the observed Marquesas trend along its extant length roughly younger than 5 Ma. Other arrows and 2-D 95 per cent confidence ellipses are scaled to show the displacement and corresponding uncertainty over 5.8 Myr. Thick arrow shows motion calculated from HS3-NUVEL1A. Dashed arrow shows motion predicted by removing the Marquesas trend. Bathymetry is from Mammerickx (1992a). Islands are shaded, even 1000 m contours are solid, and odd 1000 m contours are dotted. Mercator projection.

percentage of the volcanic piles have been measured and some measured samples are weathered, whether the two loci have distinct chemical styles is an open question. There are also several ways to 'connect the dots' and not all volcanoes lie along one of the loci as currently drawn (e.g. Niihau Island and Penguin Bank). Thus we base the trend of Hawaii on all volcanoes rather than on that of a particular locus.

Marquesas

The Marquesas Islands lie on the Pacific Plate in northernmost French Polynesia (Fig. A2). The Marquesas archipelago consists of seamounts and islands with a rough, SSE-younging age progression along its short 350 km known length (Duncan & McDougall 1974; Desonie *et al.* 1993). The current location of the Marquesas hotspot is unknown and its track before 7 Ma may (Fleitout & Moriceau 1992) or may not exist. Although most outcrops are alkalic, subaerial tholeiitic flows occur in the most deeply dissected volcanoes and in a 700-m-deep drill hole on Eiao (Duncan *et al.* 1986; Brousse *et al.* 1990; Caroff *et al.* 1995). On Ou Pou there is a 1.6 Myr eruptive hiatus between the alkalic and tholeiitic flows (Duncan *et al.* 1986), while in the Eiao drill hole the change occurs in $<0.34 \pm 0.09$ Myr (Caroff *et al.* 1995). We assign volcano age to be that of the oldest moderately reliable age date, which leads to very scattered ages. When choosing volcanoes for our time windows, we rely most heavily on the youngest tholeiitic ages.

Society

The Society Islands lie on the Pacific Plate in central French Polynesia (Fig. A3). Diffuse volcanism is typical of the Society hotspot throughout its history, a clear record of which exists for only the past 5 Myr (480 km). The volcanic island of Maiao lies 60 km off the main ridge of the Society Archipelago. Tetiaroa, an undated atoll, lies 50 km off the other side of the ridge, although it might be part of another track. The region of active volcanism spans a diameter of 70 km. The tiny island of Mehetia, five large seamounts, and many more smaller seamounts are active (Cheminee *et al.* 1989; Hekinian *et al.* 1991; Binard *et al.* 1991, 1992a). Older low-K tholeiitic rocks have been dredged from two of the larger seamounts, Turoi and Cyana, and from some of the smaller seamounts, including Seismic Volcano 1, indicating that most of their volume formed long ago, perhaps on ridge (Hekinian *et al.* 1991; Binard *et al.* 1992a). We assign volcano age to be the age date of the youngest basalts from the shield stage. To calculate trends we use only those large seamounts from which no low-K tholeiitic rocks have been dredged.

Pitcairn

Pitcairn Island lies on the Pacific Plate in easternmost French Polynesia (Fig. A4). The 1100-km-long Pitcairn–Gambier chain consists of seamounts, atolls and volcanic islands with a well-behaved, SE-younging age progression (Guillou *et al.* 1993). The lineament, although undated, continues to the NW through the Duke of Gloucester Islands. The Mid-Pacific Mountains and some of the Line Islands may be older parts of the track (Gordon & Henderson, unpublished manuscript 1985). The neighbourhood of 0.9 Myr old Pitcairn Island (Duncan *et al.* 1974) is dotted with older atolls of the Oeno-Henderson lineament, which were possibly caused by the

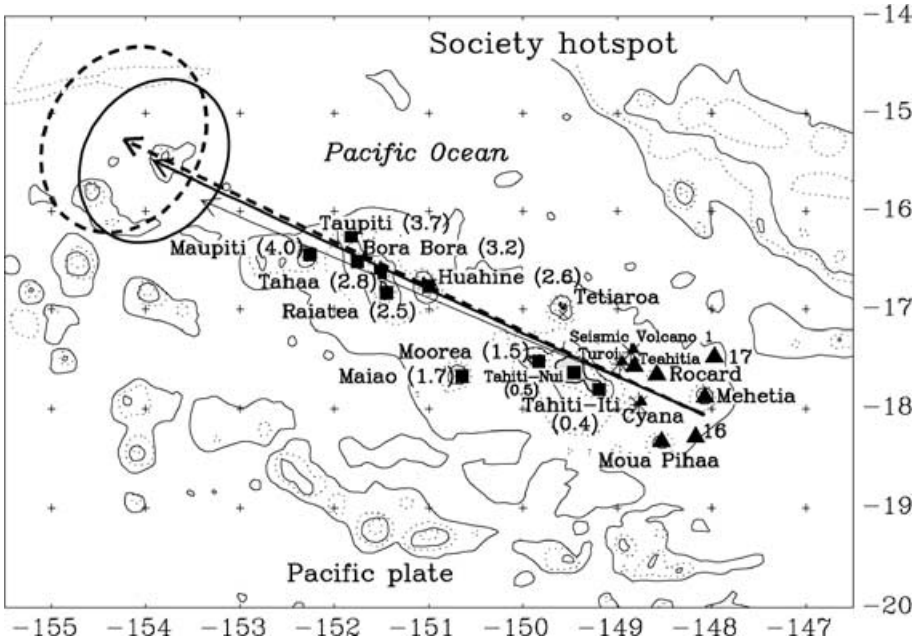

Figure A3. Bathymetric map of the Society islands. Solid triangles, volcanoes with the non-numerical age of active; solid squares, volcanoes that ended their shield building as recently as 5 Ma; ×, unsampled Tetiaroa Atoll; asterisks, seamounts from an earlier episode of volcanism; smaller solid triangles overlying the asterisks, active Society volcanism occurring on the older seamounts. Arrows and 2-D 95 per cent confidence ellipses are scaled to show the displacement and corresponding uncertainty over 5.8 Myr. Thin arrow shows the observed Society trend and volcanic propagation rate. Thick arrow shows motion calculated from HS3-NUVEL1A. Dashed arrow shows motion predicted by removing the Society rate and trend. Bathymetry is from Mammerickx (1992a). Islands are shaded, even 1000 m contours are solid, and odd 1000 m contours are dotted. Mercator projection.

passage of an earlier hotspot (called HS2 by Okal & Cazenave 1985). The present location of the Pitcairn hotspot is marked by two large seamounts with fresh alkalic lavas that lie about 80 km ESE of Pitcairn (Stoffers *et al.* 1990; Binard *et al.* 1992b). Because the width of Pitcairn is small and the plate speed high, we use this short 90-km-long segment.

Macdonald

Macdonald Seamount lies on the Pacific Plate in southernmost French Polynesia (Fig. A5). The Austral–Cook chain consists of seamounts, atolls and islands with a complex age progression along its length of more than 2000 km (Johnson & Malahoff 1971;

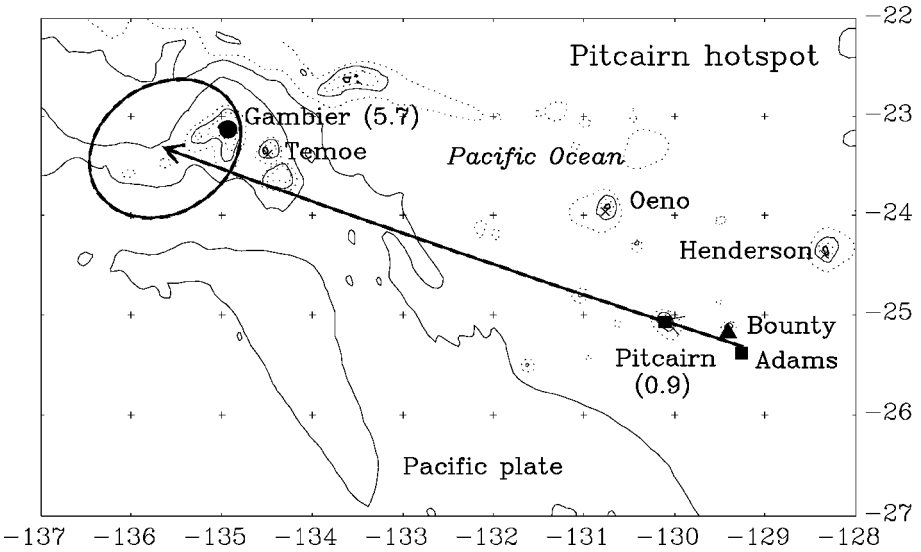

Figure A4. Bathymetric map of the Pitcairn region. Solid triangle, volcano with the non-numerical age of active; solid squares, volcanoes younger than 5 Ma; solid circles, volcanoes older than 5 Ma; ×'s, unsampled Henderson and Oeno atolls that may have formed by the passage of another hotspot. Thin arrow shows the observed Pitcairn trend. Other arrows and 2-D 95 per cent confidence ellipses are scaled to show the displacement and corresponding uncertainty over 5.8 Myr. Thick arrow shows motion calculated from HS3-NUVEL1A. Dashed arrow shows motion predicted by removing the Pitcairn trend. Bathymetry is from Mammerickx (1992a). Islands are shaded, even 1000 m contours are solid, and odd 1000 m contours are dotted. Mercator projection.

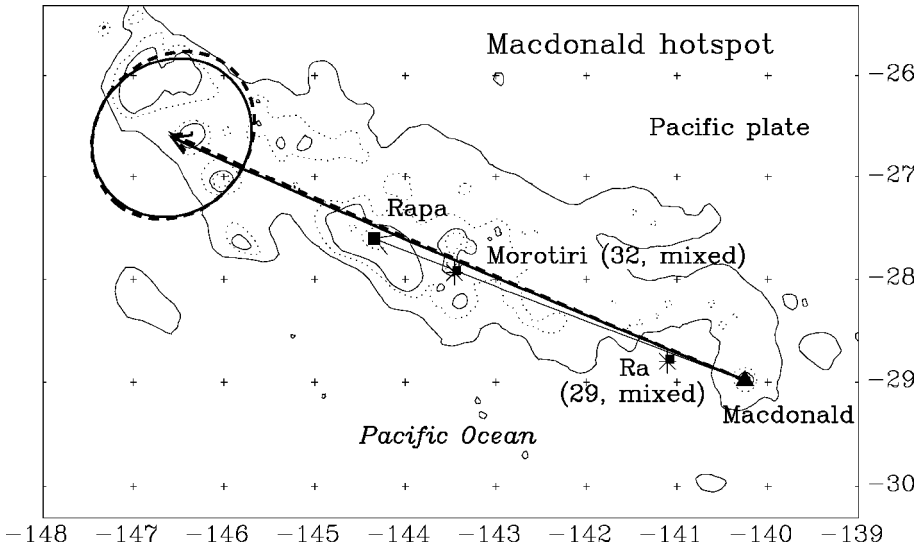

Figure A5. Bathymetric map of the Macdonald hotspot region. Solid triangle, volcano with the non-numerical age of active; solid square, a volcano roughly 5 Myr old; asterisks overlain by the small solid squares, older volcanoes on which Macdonald volcanism has also occurred. Thin arrow shows the observed Macdonald trend. Other arrows and 2-D 95 per cent confidence ellipses are scaled to show the displacement and corresponding uncertainty over 5.8 Myr. Thick arrow shows motion calculated from HS3-NUVEL1A. Dashed arrow shows motion predicted by removing the Macdonald trend. Bathymetry is from Mammerickx (1992a). Islands are shaded, even 1000 m contours are solid, and odd 1000 m contours are dotted. Mercator projection.

Dalrymple *et al.* 1975; Duncan & McDougall 1976; McNutt *et al.* 1997). As early as 1964, Menard noticed the unusual intermixing of guyots and islands (Menard 1964). Some islands show an ESE-younging progression of shield ages with a 0 Ma intercept at Macdonald, but among these are younger and older episodes of shield- and nonshield-building (Turner & Jarrard 1982; McNutt *et al.* 1997). Instead of a single Macdonald hotspot, several additional hotspots, including the Foundation hotspot (O'Connor *et al.* 1998), may have passed through the Tubuai–Cook islands (Diament & Baudry 1987; Baudry *et al.* 1988; Gordon & Henderson, unpublished manuscript, 1985; Fleitout & Moriceau 1992). Bonatti *et al.* (1977), Turner & Jarrard (1982), Mammerickx (1992b) and McNutt *et al.* (1997) proposed or applied the concept of hot lines to ocean-island volcanism that occurs in a line without the monotonic age progression required by the definition of a hotspot. To measure trends we use only volcanoes on which no older rocks have been found. Thus, we discard Ra and Marotiri and keep Macdonald and Rapa, although after this data set was finalized an older seamount was found on the flank of Macdonald (Reynolds & Jordahl, pers. comm. 1999).

Samoa

The Samoa Islands lie on the Pacific Plate just north of the northern corner of the Tonga–Kermadec Trench (Fig. A6). The track of the Samoa hotspot, if it exists, consists of at least 1000 km of volcanic islands and guyots (Duncan 1985) and seamounts. Shield-building ages roughly decrease to the east (at least east from 13.5 Myr-old Combe Bank), although the observed volcanic propagation rate is about 20 km Myr^{-1} slower than that predicted by plate reconstructions (Duncan 1985). Another inconsistency is that shield volcanism has occurred in the past 0.5 Myr in the Wallis Islands (Price *et al.* 1991), which lie one-third of the way from 13.5 Myr old Combe Bank to the Samoa Islands. Natland (1980) suggested that Samoan volcanism may be caused by disturbances in the mantle due to the corner in the Tonga trench, although the He 3/He 4 ratios in shield lavas suggest that primitive mantle is being tapped (Farley *et al.* 1990; Poreda & Farley 1992). On Savai'i, Upolu and possibly Tutuila, posterosional basanites and nephelinites have erupted along a single 110°-striking fissure system that parallels the local strike of the nearby Tonga trench (Natland 1980). This suggests that the stress field caused by the flexure of the subducting Pacific Plate influences the geometry of the posterosional volcanism (Natland 1980) and by analogy may influence the geometry of the volcano locations. While acknowledging the likely influence of the trench, we still consider Samoa to be a hotspot based on its He 3 anomaly, age progression and generally Hawaiian eruptive sequence. After finalizing this data set, Rockne Volcano, which had been known only from an echo-sounding survey (Johnson 1984), was finally sampled and fresh alkalic basalts were found (Hart *et al.* 1999).

Galapagos

The Galapagos Islands lie on the Nazca Plate just south of the Cocos Plate (Fig. A7). The Galapagos hotspot simultaneously created 1000-km-long tracks on these two plates: the westward-younging Carnegie Ridge on the Nazca Plate and the SSW-younging Cocos Ridge on the Cocos Plate (Holden & Dietz 1972; Johnson & Lowrie 1972). By 5 Ma the Galapagos Spreading Centre had shifted to the north and the bulk of the volcanism had switched from on-ridge to near-ridge (Hey 1977). Although the greatest concentration of hotspot volcanism lies 150 to 250 km south of the spreading ridge, the Galapagos Spreading Centre still shows geochemical contamination by the Galapagos hotspot (Schilling *et al.* 1976; Verma *et al.* 1983).

On the Nazca Plate, young volcanoes form a roughly east-west-striking island-dotted ridge (the westernmost Carnegie Ridge) and a NW-striking chain of isolated volcanoes (the Wolf–Darwin lineament). The basalts from the archipelago have variable incompatible elements and isotopic ratios, which range from those similar to the contaminated MORB's of the Galapagos spreading centre to those typical of ocean-island basalt (OIB) (Geist *et al.* 1988;

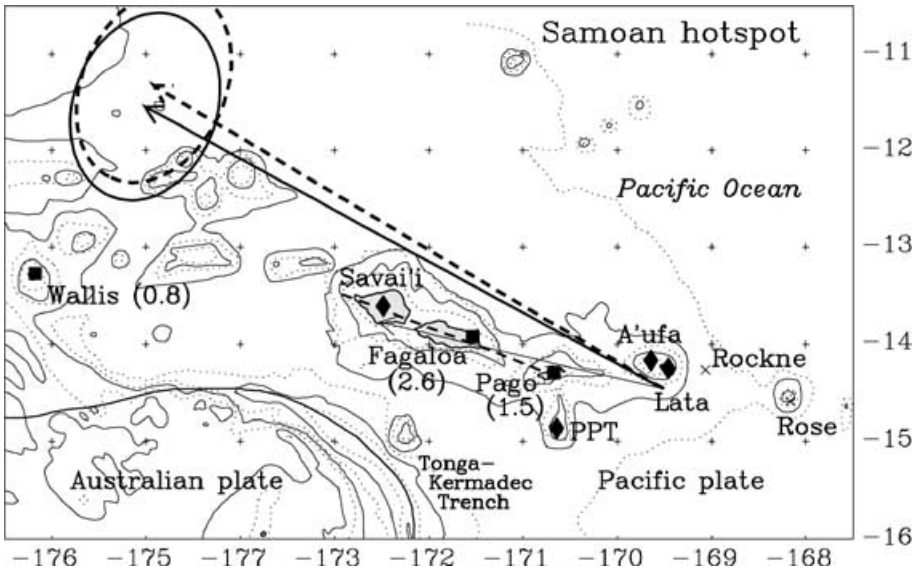

Figure A6. Bathymetric map of the Samoa islands. Solid squares, volcanoes younger than 5 Ma; solid diamonds, young, but undated volcanoes that were used to calculate the trend; ×'s, unsampled Rose Atoll and Rockne Volcano, which was confirmed to be active after this data set was finalized. Thick, solid line is the active plate boundary (Brocher & Holmes 1985). Thick, dashed line is the posterosional fissure system of Natland (1980). Thin arrow shows the observed Samoa trend (although some radiometric dates from the Wallis Islands indicate they are younger than 5 Ma, there were not used to estimate trend). Other arrows and 2-D 95 per cent confidence ellipses are scaled to show the displacement and corresponding uncertainty over 5.8 Myr. Thick arrow shows motion calculated from HS3-NUVEL1A. Dashed arrow shows motion predicted by removing the Samoa trend. Bathymetry is from Mammerickx (1992a). Islands are shaded, even 1000-m contours are solid, and odd 1000-m contours are dotted. Mercator projection.

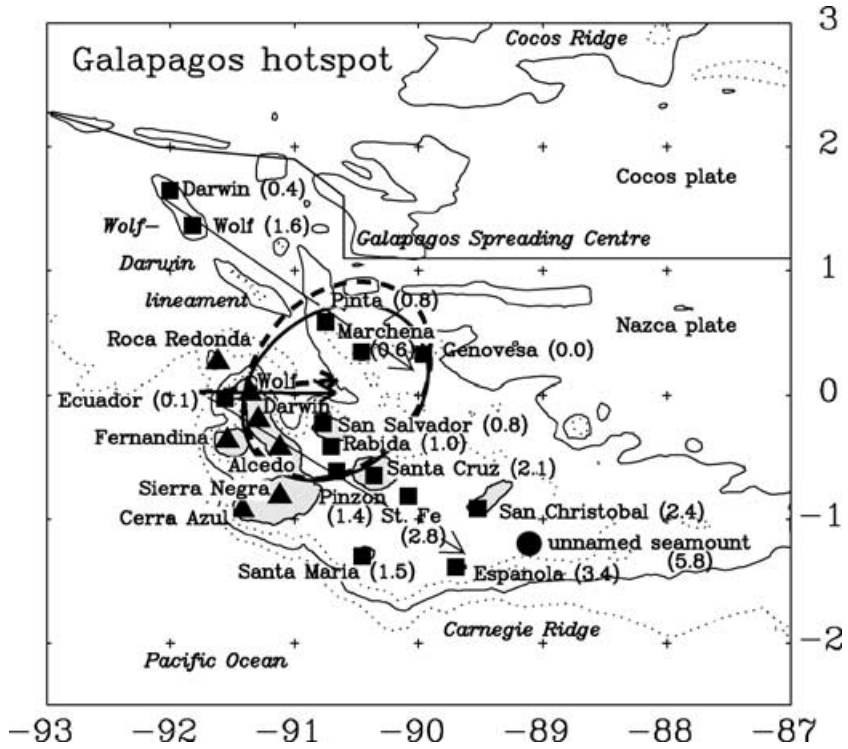

Figure A7. Bathymetric map of the Galapagos islands. Solid triangles, volcanoes with the non-numerical age of active; solid squares, volcanoes younger than 5 Ma; solid circle, a seamount older than 5 Ma. Angular curve is the approximate active plate boundary. Thin arrows show the observed Galapagos trends along the Carnegie Ridge and Wolf–Darwin lineament. Other arrows and 2-D 95 per cent confidence ellipses are scaled to show the displacement and corresponding uncertainty over 5.8 Myr. Thick arrow shows motion calculated from HS3-NUVEL1A. Dashed arrow shows motion predicted by removing the Galapagos trend. Bathymetry is from Mammerickx & Smith (1980). Islands are shaded, even 1000 m contours are solid, and odd 1000 m contours are dotted. Mercator projection.

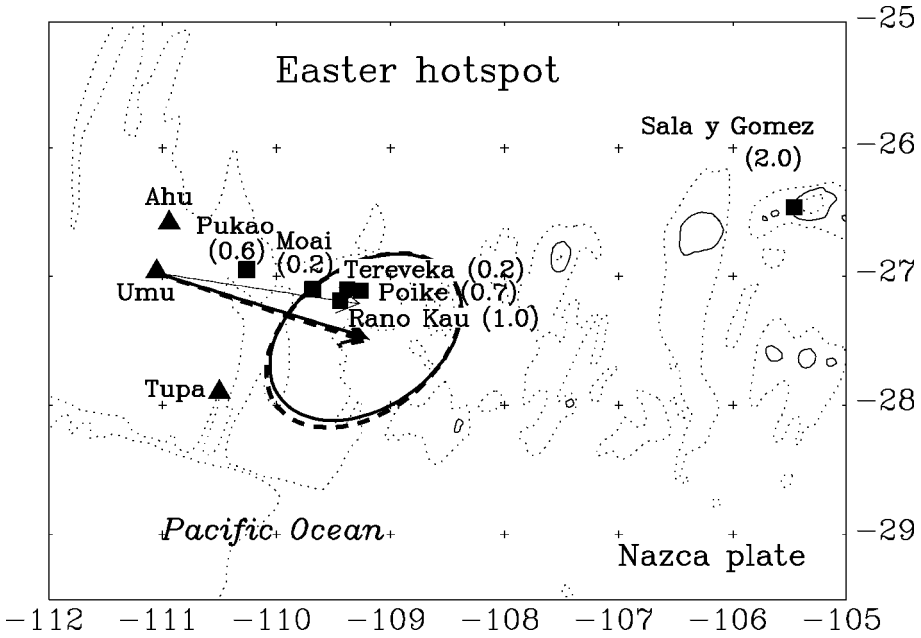

Figure A8. Bathymetric map of the Easter Island region. Solid triangles, volcanoes in the Volcanic Field Group (these have the non-numerical age of active); solid squares, volcanoes with ages of 5 Ma and younger. Thin arrow shows the observed Easter trend (Sala y Gomez was not used to estimate trend). Other arrows and 2-D 95 per cent confidence ellipses are scaled to show the displacement and corresponding uncertainty over 5.8 Myr. Thick arrow shows motion calculated from HS3-NUVEL1A. Dashed arrow shows motion predicted by removing the Easter trend. Island outline is from Hagen *et al.* (1990) and bathymetry is from GEBCO (1982). Islands are shaded, even 1000 m contours are solid, and odd 1000 m contours are dotted. Mercator projection.

Harpp & White 1990; McBirney 1990; White *et al.* 1993). In general the MORB-like basalts occur along the centre of the Carnegie Ridge while those typical of OIB's occur along the periphery of the ridge and along the Wolf–Darwin lineament (Harpp & White 1990; McBirney 1990; Geist 1992; White *et al.* 1993). Based on limited vertical exposures (due to low erosion rates, Standish *et al.* 1998), each island seems to have a different eruptive history (Geist 1992), which may include shield building, fissure eruption, caldera collapse and normal faulting (e.g. Geist *et al.* 1985, 1986; Vicenzi *et al.* 1990). The Wolf–Darwin lineament may form by the sublithospheric channeling of the hotspot source to the spreading ridge (Morgan 1978). Because the Wolf–Darwin volcanoes are isostatically compensated and have ages younger than the seafloor, Feighner & Richards (1994) instead suggest these islands overlie a fault. Volcanism has occurred on most of the islands in the Galapagos archipelago in the past 0.1 Myr (White *et al.* 1993). Based on rocks dredged from the Carnegie Ridge, a broad distribution of volcanism (at least 140 km measured west to east) has been typical of the Galapagos hotspot for at least the past 6 Myr (Sinton *et al.* 1996). Because there is no known consistent eruptive sequence, we assign volcano age to be the oldest age estimate that we judge to be moderately reliable. Although some small young seamounts have been dredged and dated along the Carnegie Ridge (e.g. Sinton *et al.* 1996), to have a uniform data set we only use subaerial volcanoes, except for one submarine feature that is 5.8 Myr old.

Easter-Sala y Gomez

The islands of Easter and Sala y Gomez lie on the Nazca Plate just east of the Easter microplate (Fig. A8). The young volcanism that occurs on these islands as well as that at San Felix and Pitcairn led Bonatti *et al.* (1977) to propose that the extensive volcanism was caused by a hot line. Treated as a single hotspot, the track of the Easter-Sala y Gomez hotspot consists of the older mirror-image northern Tuamotus on the Pacific Plate and the Nazca Ridge on the Nazca Plate and the younger, non-mirrored Sala y Gomez Ridge on the Nazca Plate (Pilger & Handschumacher 1981; Okal & Cazenave 1985). Limited age dates along the Sala y Gomez Ridge show monotonic westward younging (O'Connor *et al.* 1995). On the Pacific Plate the *en echelon* ridges between Crough Seamount and the Easter Microplate might be a weak young Pacific hotspot track (Hekinian *et al.* 1995) or they might be related to the Easter Microplate (Binard *et al.* 1996). The spreading centres of east and west rifts of the Easter Microplate erupt E-MORB, which contains slightly more incompatible elements than normal MORB, with highly radiogenic lead (Hannan & Schilling 1989; Haase *et al.* 1996). Eastward of the microplate, the Nazcan seafloor is barren of recent volcanism for 130 km until the active Ahu and Umu volcanic fields are reached (Hagen *et al.* 1990; Stoffers *et al.* 1994). In the 100 km span between these volcanic fields and Easter Island lie two seamounts having older lavas that are similar to those of the tholeiitic volcanic fields, but having younger lavas that are transitional and similar to many of the older rocks on Easter Island (Haase *et al.* 1997). Using the volcano and ridge geometry and major, trace and unstable elements, Haase *et al.* (1997) divided Easter volcanism into three, possibly time sequential groups: first, the tholeiitic Volcanic Field Group; second, the transitional Main Group; and third, the transitional, but more differentiated Roiho Group. Based on modelling of major, trace, and unstable elements, the deepest and hence hottest mantle temperatures occur beneath the volcanic fields (Haase *et al.* 1996), indicating that the tholeiitic volcanic fields, rather than the islands, best mark the active hotspot. Using an overlapping set of geochemical data, Pan & Batiza (1998) suggest instead that the sublithospheric hotspot source is under Sala y Gomez Island. Neglecting the conflicting petrologic modelling, we prefer the first interpretation because geomorphologically Sala y Gomez volcano is older than Easter Island.

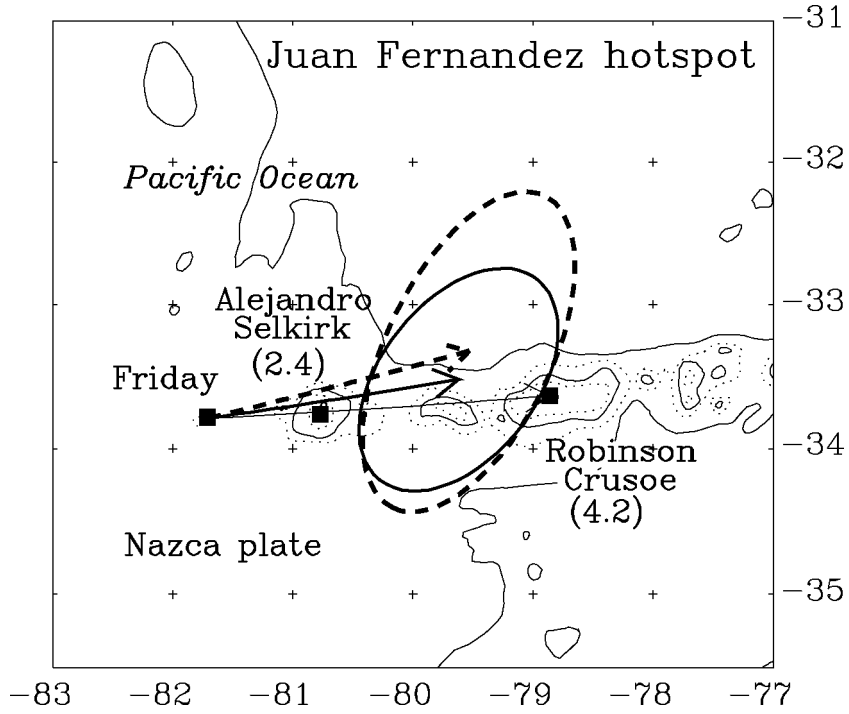

Figure A9. Bathymetric map of the Juan Fernandez region. Solid squares, volcanoes that are likely younger than 5 Ma. Thin arrow shows the observed Juan Fernandez trend. Other arrows and 2-D 95 per cent confidence ellipses are scaled to show the displacement and corresponding uncertainty over 5.8 Myr. Thick arrow shows motion calculated from HS3-NUVEL1A. Dashed arrow shows motion predicted by removing the Juan Fernandez trend. Bathymetry is from GEBCO (1982). Islands are shaded, even 1000 m contours are solid, and odd 1000 m contours are dotted. Mercator projection.

We assign volcano age to be the age of the transition between the Volcanic Fields Group and Main Group. We use only the volcanoes of Easter Island and westward to estimate the observed trend.

Juan Fernandez

The Juan Fernandez Islands lie on the Nazca Plate in the southern Pacific Ocean (Fig. A9). The track consists of two westward-younging main islands and many isolated seamounts that span 800 km and disappear into the Peru–Chile trench (Stuessy *et al.* 1984). Because the stratigraphy of the islands is poorly known and dated, we assign volcano age to be the oldest radiometric date on each island.

Yellowstone

The Yellowstone hotspot lies on the North American Plate and its track spans at least 800 km and 16 Myr (Fig. A10) (Morgan 1972; Armstrong *et al.* 1975; Suppe *et al.* 1975; Pierce & Morgan 1992; Smith & Braile 1994). The track is marked by bimodal volcanism (rhyolites and basalts) at its young, northeast end and thick flood basalts underlain by older bimodal volcanics along the rest of its length (Armstrong *et al.* 1975; Leeman 1982). For the past 2.2 Myr, bimodal eruptive activity has been restricted to the Yellowstone Plateau volcanic field (Armstrong *et al.* 1975; Christiansen 1982). The Yellowstone field consists of three overlapping and partially nested calderas, which formed by the eruption of huge rhyolitic ash-flow sheets, and a much smaller volume of basaltic and rhyolitic flows (Christiansen & Blank 1972). Volcano location of these calderas is the centre of moment of the caldera. Rhyolitic magma for the next catastrophic eruption may be accumulating in the upper crust beneath the northeastern rim of Yellowstone caldera. Evidence for this magma body includes low *P*-wave speed and low gravity, both of which are consistent with a 10–50 per cent partially melted rhyolitic body (Lehman *et al.* 1982; Schilly *et al.* 1982). Because a parabolic zone of normal faulting progresses with the rhyolitic ash flow volcanism (Anders *et al.* 1989), the geometry of the Yellowstone track may poorly reflect the velocity of the North American plate relative to a global hotspot model (Rodgers *et al.* 1990). In HS3-NUVEL1A, however, the misfits of Yellowstone are quite typical, suggesting that whatever complexity is added by the Basin and Range, it is not significantly greater that what is happening at oceanic hotspots. For example, the observed and predicted Yellowstone trends differ only by $11^\circ \pm 52^\circ$ (95 per cent confidence here and below) (Table 16). The observed and predicted Yellowstone rates differ only by 9 ± 32 km Myr^{-1}, which is less than the 16 ± 19 km Myr^{-1} misfit of Hawaii and the 19 ± 21 km Myr^{-1} of Society (Table 16).

Martin Vaz

The island of Trindade and the nearby islands of Martin Vaz lie on the South American Plate in the south Atlantic Ocean about 1400 km east of Rio de Janeiro (Fig. A11). The eastward-younging track of the Martin Vaz hotspot consists of volcanic islands, guyots, conical seamounts and alkalic rocks of the Sao Paulo–Rio de Janeiro littoral belt (Almeida 1961; Burke & Dewey 1973; Baker 1973; Herz 1977). We assign the age of Trindade to be 3.35 ± 0.29 Myr, which is the oldest K–Ar date from one of the less altered samples from the basal complex (Cordani 1968, 1970). The easternmost island group, Ilhas Martin Vaz, has one K–Ar date of 60 Ma, which is inconsistent with

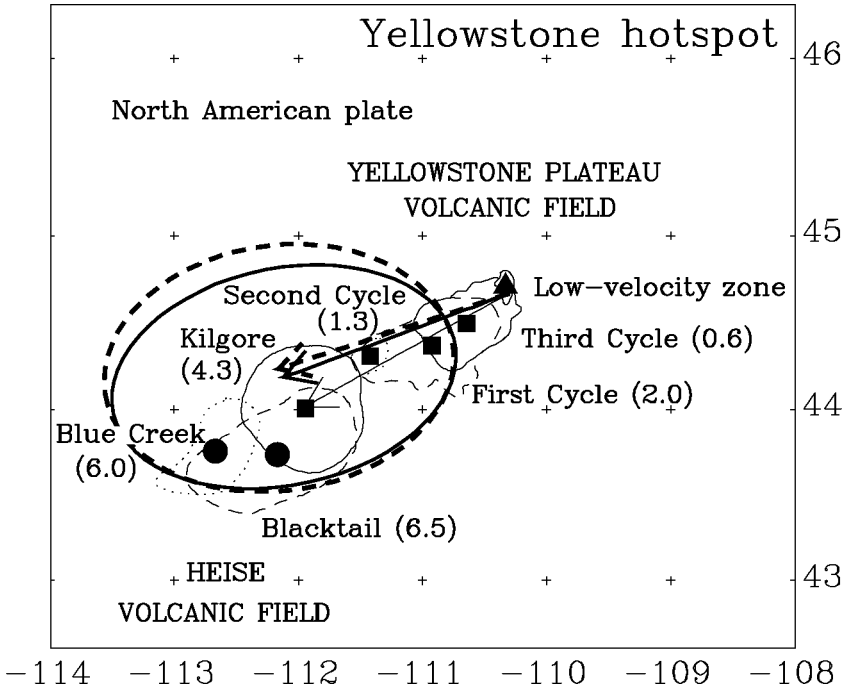

Figure A10. Map of the Yellowstone hotspot region. Solid triangle, the centre of the zone of low wave speed; solid squares, the centres of calderas that erupted huge rhyolitic ash-flow sheets since 5 Ma; solid circles, the centres of calderas that erupted huge rhyolitic ash-flow sheets before 5 Ma. The approximate boundaries of all six calderas are outlined in various patterns (Christiansen 1984; Pierce & Morgan 1992). Thin arrow shows the observed Yellowstone trend. Other arrows and 2-D 95 per cent confidence ellipses are scaled to show the displacement and corresponding uncertainty over 5.8 Myr. Thick arrow shows motion calculated from HS3-NUVEL1A. Dashed arrow shows motion predicted by removing the Yellowstone trend. Mercator projection.

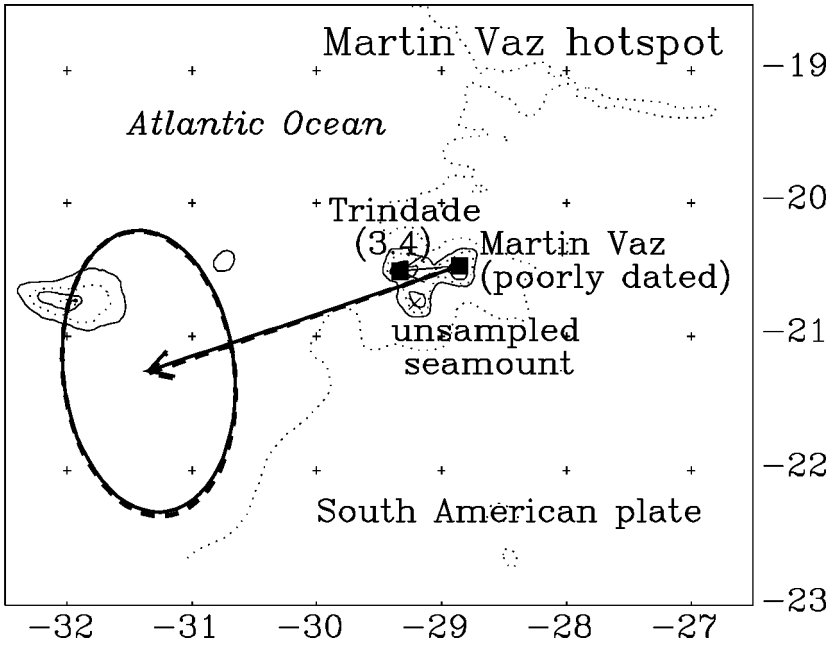

Figure A11. Bathymetric map of the Martin Vaz islands. Solid square, volcanoes that are likely younger than 5 Ma; ×, unsampled nearby seamount. Thin arrow shows the observed Martin Vaz trend. Other arrows and 2-D 95 per cent confidence ellipses are scaled to show the displacement and corresponding uncertainty over 5.8 Myr. Thick arrow shows motion calculated from HS3-NUVEL1A. Dashed arrow shows motion predicted by removing the Martin Vaz trend. Bathymetry is from Cherkis *et al.* (1989). Islands are shaded, even 1000-m contours are solid, and odd 1000-m contours are dotted. Mercator projection.

the young age of Trindade, and another date of <0.73 Ma, which suggests there may have been a mix up in the samples (Cordani 1970). Because the width of Martin Vaz is small and the plate speed moderate, we use the trend from this short (50-km-long) segment.

APPENDIX B: LENGTH OF TIME IT TAKES A VOLCANO TO GROW

Straight-line fits to assigned volcano age vs distance along the Hawaii and Society chains both indicate that it takes 0.7 Myr to build volcanoes in these chains (Table 2). The estimate of 0.7 Myr neglects the time elapsed while 1-km-deep Loihi and 3-km-deep Volcano 16 grew to their current sizes. Hawaiian volcanoes are roughly spaced 35 km apart when projected onto a single trend. If we assume the next Hawaiian volcano is about to erupt 35 km from Loihi and extrapolate from the observed Hawaiian volcanic propagation rate, then this hypothetical volcano would end its shield building 1.1 Myr from now. Prior estimates of the time it takes to grow a Hawaiian volcano through shield building are 0.5–1.5 Myr (Jackson *et al.* 1972), 0.2 Myr (Wright *et al.* 1979), and 0.6 Myr (Moore & Clague 1992). As the duration of the main phase of volcano growth we use 0.8 Myr, which follows from a fit to the Hawaiian rate from volcanoes from Waianae (3.1 Ma) and eastward, which lies between our two estimates (0.7 Myr and 1.1 Myr) above, and is close to the most recent independent estimate (i.e. that of Moore & Clague 1992).